DATA FUSION FOR SYSTEM MODELING, PERFORMANCE ASSESSMENT AND IMPROVEMENT

A Thesis

Presented to

The Academic Faculty

by

Kaibo Liu

In Partial Fulfillment

of the Requirements for the Degree

Doctor of Philosophy in the

School of Industrial and Systems Engineering

Georgia Institute of Technology

December 2013

DATA FUSION FOR SYSTEM MODELING, PERFORMANCE ASSESSMENT AND IMPROVEMENT

Approved by:

Dr. Jianjun Shi, Advisor
School of Industrial and Systems Engineering
Georgia Institute of Technology

Dr. Yajun Mei
School of Industrial and Systems Engineering
Georgia Institute of Technology

Dr. Paul Kvam
School of Industrial and Systems Engineering
Georgia Institute of Technology

Dr. Jing Li
School of Computing, Informatics, and Decision Systems Engineering
Arizona State University

Dr. Nagi Gebraeel
School of Industrial and Systems Engineering
Georgia Institute of Technology

Date Approved: August 27, 2013

To my beloved parents, wife Jiao and son Jiaye.

ACKNOWLEDGEMENTS

I would like to express my sincere gratitude to my advisor and mentor, Professor Jianjun Shi for his devoted supervision, continual encouragement, and insightful guidance. Without his support, this thesis would not have been accomplished. It has been such a memorable and invaluable experience for me to work with and learn from him. His kindness, enthusiasm, and incredible patience have undoubtedly made a significant impact on the developments in my research and personal life, and for that I am grateful.

My gratitude also goes to my thesis committee members, including Professor Nagi Gebraeel, Professor Paul Kvam, Professor Jing Li and Professor Yajun Mei. Their valuable advice, productive discussions, and support have greatly aided me during my Ph.D. study. I would also like to thank them for the assistance and consideration they provided during the process of writing this thesis.

I would like to express my special appreciation for Professor Jean-Philippe P. Richard who highly recommended me to pursue my Ph.D. study at the Georgia Institute of Technology. My special thanks also go to Professor Fugee Tsung and Professor Jiang Wei, who introduced me to quality control and industrial statistics and recommended me to join Professor Jianjun Shi's research group.

Thank you to my professors in the academic society, who have shaped my academic life in various ways. In particular, I would like to recognize both Professor Jionghua Jin and Professor Shiyu Zhou for their kind support and assistance throughout my doctoral study and job search. A special thanks also goes to Professor Jeff Wu for his encouragement and recommendation during my job search. In addition, I would like to

thank Dr. Rong Duan, Mr. Tao Huang, Dr. Shabnam Jain, Professor Ran Jin, Professor Chuck Zhang, Professor Xi Zhang, and all the colleagues in OG Technologies, Inc. for the collaborations and opportunities they have provided me.

My Ph.D. study would have been incomplete without my colleagues and friends whom include but are not limited to: Dr. Shan Ba, Dr. Linkan Bian, Dr. Chia-Jung Chang, Dr. Shuai Huang, Mr. Li Hao, Dr. Kamran Paynabar, Mr. Matthew Plumlee, Dr. Fei Sun, Ms. Yijie Wang, Mr. Hao Yan, Mr. Huan Yan, Ms. Haiyue Yu, Dr. Weidong Zhang and Mr. Cheng Zhou. They have each provided me with both productive and constructive comments, and have given me the valuable gift of friendship. A special thanks goes to Mrs. Shi as well for her tremendous encouragement and care.

I also wish to acknowledge the support from my big family, with my parents in particular, for teaching me the value of knowledge and for always being there for me every step of the way. I am very fortunate to have their love and support.

Last but not least, I want to thank my wife, Jiao Xu for her love, continual support and unflinching faith through this critical stage of my life. She makes it all worthwhile.

TABLE OF CONTENTS

Page

LIST OF TABLES

Page

LIST OF FIGURES

Page

SUMMARY

Due to rapid advancements in sensing and computation technology, multiple types of sensors have been embedded in various applications to online automatically collect massive amounts of production information. Although this data-rich environment provides a great opportunity for a more effective process control, it also raises new research challenges on data analysis and decision making due to the complex data structures, such as large-volume and high-dimensional characteristics and heterogeneous data dependency.

This thesis contributes to the area of *System Informatics and Control* (SIAC) to develop systematic data fusion methodologies for effective quality control and performance improvement in complex systems. These advanced methodologies enable (1) a better handling of the rich data environment communicated by complex engineering systems, (2) a closer monitoring of the system status and (3) a more accurate forecasting of future trends and behaviors. The research bridges the gaps in methodologies among advanced statistics, engineering domain knowledge and operation research. It also forms close linkage to various application areas such as manufacturing, health care, energy and service systems.

This thesis started from investigating the optimal sensor system design and conducting multiple sensor data fusion for process monitoring and diagnosis in different applications. In Chapter 2, we first studied the couplings or interactions between the optimal design of a sensor system in a Bayesian Network and quality management of a manufacturing system, which can improve cost-effectiveness and production yield by

considering sensor cost, process change detection speed and fault diagnosis accuracy in an integrated manner. An algorithm named "Best Allocation Subsets by Intelligent Search" (BASIS) with optimality proof is developed to obtain the optimal sensor allocation design at minimum cost under different user specified detection requirements. Chapter 3 extended this line of research by proposing a novel adaptive sensor allocation framework, which can greatly improve the monitoring and diagnosis capabilities of the previous method. A max-min criterion is developed to manage sensor reallocation and process change detection in an integrated manner. The methodology was tested and validated based on a hot forming process and a cap alignment process. Next in Chapter 4, we proposed a Scalable-Robust-Efficient Adaptive (SERA) sensor allocation strategy for online high-dimensional process monitoring in a general network. A monitoring scheme of using the sum of top-*r* local detection statistics is developed, which is scalable, effective and robust in detecting a wide range of possible shifts in all directions. This research provides a generic guideline for practitioners on determining (1) the appropriate sensor layout; (2) the "ON" and "OFF" states of different sensors; and (3) which part of the acquired data should be transmitted to and analyzed at the fusion center, when only limited resources are available.

To improve the accuracy of the remaining lifetime prediction, Chapter 5 proposed a data-level fusion methodology for degradation modeling and prognostics. When multiple sensors are available to measure the degradation mechanism of the same system, it becomes a high dimensional and challenging problem to determine which sensors to use and how to combine them together for better data analysis. To address this issue, we first defined two essential properties, that if present in a degradation signal, can enhance

the effectiveness for prognostics. Then, we proposed a generic data-level fusion algorithm to construct a composite health index to achieve those two identified properties. The methodology was tested using the degradation signals of aircraft gas turbine engine, which demonstrated a much better prognostic result compared to relying solely on the data from an individual sensor.

In summary, this thesis is the research drawing attention to the area of data fusion for effective employment of the underlying data gathering capabilities for system modeling, performance assessment and improvement. The fundamental data fusion methodologies are developed and further applied to various applications, which can facilitate resources planning, real-time monitoring, diagnosis and prognostics.

CHAPTER 1

INTRODUCTION

1.1 Motivation

The rapid developments of sensor technology, communication network, and computing power have resulted in temporally and spatially dense data-rich environments in a variety of manufacturing and service systems. Although this data-rich environment provides unprecedented opportunities for quality and productivity improvements, it also poses challenges on data analysis and decision making due to the high dimensionality and heterogeneity of the data, the extensive levels of uncertainty in the dynamics of the systems and operational environments, the potential lack of a prior knowledge of the system structure, etc. Since massive data collected from different sources can involve dependent or even redundant information, there is a pressing need to develop advanced methodologies and associated tools that will enable and assist (1) the effective selection and handling of the rich data streams in the complex systems, (2) the extraction of pertinent features to better characterize the data dependences and the system performance, and (3) the integration of the acquired information with engineering domain knowledge for more enhanced process modeling, monitoring, diagnosis, prognosis, and improvement. On the basis of these initiatives, this research focuses on developing systematic data fusion methodologies for effective system modeling, quality control, performance assessment and improvement in complex systems.

1.2 Research Objectives

The objectives of this research are:

1) developing the optimal design of a sensor system in a Bayesian Network at minimum cost under different user specified detection requirements.
2) proposing a novel approach to adaptively reallocate sensor resources in a Bayesian Network with online measurements, which can enhance both monitoring and diagnosis capabilities.
3) generalizing the adaptive sensor allocation strategy for online high-dimensional process monitoring in a general network.
4) and developing a generic data-level fusion methodology for degradation modeling and prognostic analysis with the data collected from multiple sensors.

1.3 State-of-the-art

The advancement in sensor technology facilitates vigorous development in the distributed sensor network (DSN), which has been widely used in industrial and civilian applications such as industrial process monitoring and control, healthcare surveillance, and decision support systems. While a fully deployed sensor system can minimize information loss, the total cost (e.g. installation, maintenance, and operational costs) associated with these sensors can be overwhelming (Edan and Nof 2000). In addition, a fully deployed sensor system can place high demands on bandwidth and energy consumption (Willett et al. 2004). In general, the efficiency of a sensor network can be benchmarked by the sensing cost in achieving customer demand (Ding et al. 2003). Extensive research and practices have shown that the effective use of sensor data with an optimal sensor system design can provide unprecedented opportunities for quality and productivity improvement, such as increasing production throughput, reducing lead time and improving customer demand satisfaction (Ding et al. 2006).

The optimal design of a DSN is a decision making process to determine which variables to measure in order to best detect the change of environment in real time.

Depending on the application domains, the problem of sensor allocation can be conducted with different objectives (Tarabanis et al. 1995; Katenka et al. 2008; Azarbayejani et al. 2008). In quality engineering, the problem of optimal sensor allocation has recently become a promising research topic (Shi 2006). For this area, much research has been done to improve detection delay and root cause diagnosis, with the assumption that certain prior knowledge (i.e. location and distance information of physical variables) is sufficient to quantitatively describe variable relationships involved in the physical system (Khan et al. 1998; Khan and Ceglarek 2000). When such prior information is unavailable, Li and Jin (2010) proposed a sensor allocation method based on a probabilistic model for single mean shift detection using a univariate control chart. A comprehensive overview of the state-of-the-art developments in DSNs for quality and productivity improvements was presented by Ding et al. (2006). Mandroli et al. (2006) further provided a survey of inspection strategy and sensor distribution studies for both quality assurance and fault diagnosis purposes.

Although the aforementioned methods are effective to identify the optimal sensor allocation strategy for different process control applications, they assume that the sensor layout is fixed during online monitoring. This fixed sensor allocation strategy is preferable if we have prior information about potential shifts in variables. Unfortunately, such prior information is usually unknown or unreliable in practice. With this in mind, the adaptive strategy is usually considered to overcome the limitations of the monitoring schemes of the fixed strategy. In quality engineering, there are mainly three types of adaptive strategies: adaptive charting technique, adaptive sampling and adaptive sensor allocation. Adaptive charting techniques are widely used in the quality control area, which adaptively changes control chart philosophy for better process monitoring and diagnosis (Zhu and Jiang 2009; Tsung and Wang 2010). Most adaptive charting techniques assume that the sensor network is fully deployed and thus all variables are measurable. On the other hand, adaptive sampling techniques are mainly used for field

estimation, which aim at exploring the correlation between measured samples to either sequentially add/reduce the amount of acquisitions in the spatial domain or adjust the sampling rate in the time domain (Fiorelli et al. 2006). Finally, the last type of adaptive strategy is called adaptive sensor allocation, which focuses on redistributing scarce resources based on online measurements to maximize capability (e.g. maximize signal to noise ratio) (Hitchings and Castañón 2010). For example, adaptive sensor allocation strategy has been widely used to track object movement (Lim et al. 2006; Zoghi and Kahaei 2010). Although many research efforts have been made on this topic, adaptive sensor allocation strategy is seldom explored in the quality control field for improving monitoring and diagnosis capabilities.

A common question that arises in DSNs is how to develop an effective process control scheme with the objectives of reducing variability and improving the final quality of products (Montgomery 2009). A typical process control problem includes three steps: process monitoring, fault diagnosis, and process recovery. In process monitoring, various methods have been developed, such as univariate statistical process control (Shewhart 1931), multivariate Hotelling T^2 statistical process control (Hotelling 1947), MCUSUM and MEWMA control charts (Woodall and Ncube 1985; Lowry et al. 1992), and some principal component analysis (PCA) based techniques (Bakshi 1998). Regarding the fault diagnosis procedure, one popular technique developed is the MTY T^2 decomposition (Mason et al. 1997). A causation-based T^2 decomposition method is further proposed to improve the diagnosability (Li, Jin, and Shi 2008) in a causal model. On the other hand, the diagnosis problem can be viewed as a task to correctly classify a fault into one of the pre-defined classes. New techniques are developed based on the classification point of view, such as Fisher Discriminant Analysis (Duda et al. 2000) and Support Vector Machine (SVM) (Vapnik 1999). Although the aforementioned methodologies have been successfully applied into different process control applications, they assume that all the variables of interest are available during online monitoring.

On the other hand, with the data collected from multiple sensors, another interesting question is how to combine them together for better degradation modeling and prognostic analysis. The literature pertaining to modeling degradation processes is indeed rich, and contains numerous methods and techniques (Meeker and Escobar 1998; Nelson 1990). However, most of the existing models study only a single measure for degradation. Although it is possible to use multiple sensors and individually analyze the corresponding data, this can often result in significant over or under estimation of the remaining lifetime (Gebraeel 2006). Two key challenges when performing prognostics using multiple sensors are: deciding (1) which specific sensor data to use for modeling degradation; and (2) how to combine/fuse multiple relevant sensor data. Generally, data collected from multiple sensors may contain only partial information about the same degradation process, and thus fusing this information has the potential to provide more accurate and robust prognostic capability. There are three categories of data fusion that are classified based on the level of implementation of the fusion methodology: data-level fusion, feature-level fusion, and decision-level fusion (Hall and Llinas 1997; Volponi et al. 2004). Data-level fusion combines multiple sensor data that measure correlated parameters (Heger and Pandit 2004; Simon and Simon 2005; Kobayashi and Simon 2007; Salahshoor et al. 2008). On the other hand, feature-level fusion integrates feature information that results from independent analysis methods (Goebel and Bonissone 2005; Volponi et al. 2004). Finally, decision-level fusion involves integrating diagnostic actions (e.g. preliminary determination of an entity's location, attributes, and identity) (Sun 2002). A review of some of the literature on multi-sensor data fusion approaches to condition monitoring, fault diagnosis, and prognostics can be found in (Jardine et al. 2006). Although some efforts have focused on developing feature-level and decision-level fusion methodologies for prognostics (Hu et al. 2010; Byington et al. 2007), little research has targeted the development of data-level fusion models.

1.4 Organization of the Thesis

This thesis is organized in a multiple manuscript format. Each of Chapters 2, 3, 4 and 5 are written as a research paper, which has either been accepted or submitted for journal publications. Figure 1.1 outlines the structure of this thesis and also the relationship among these chapters.

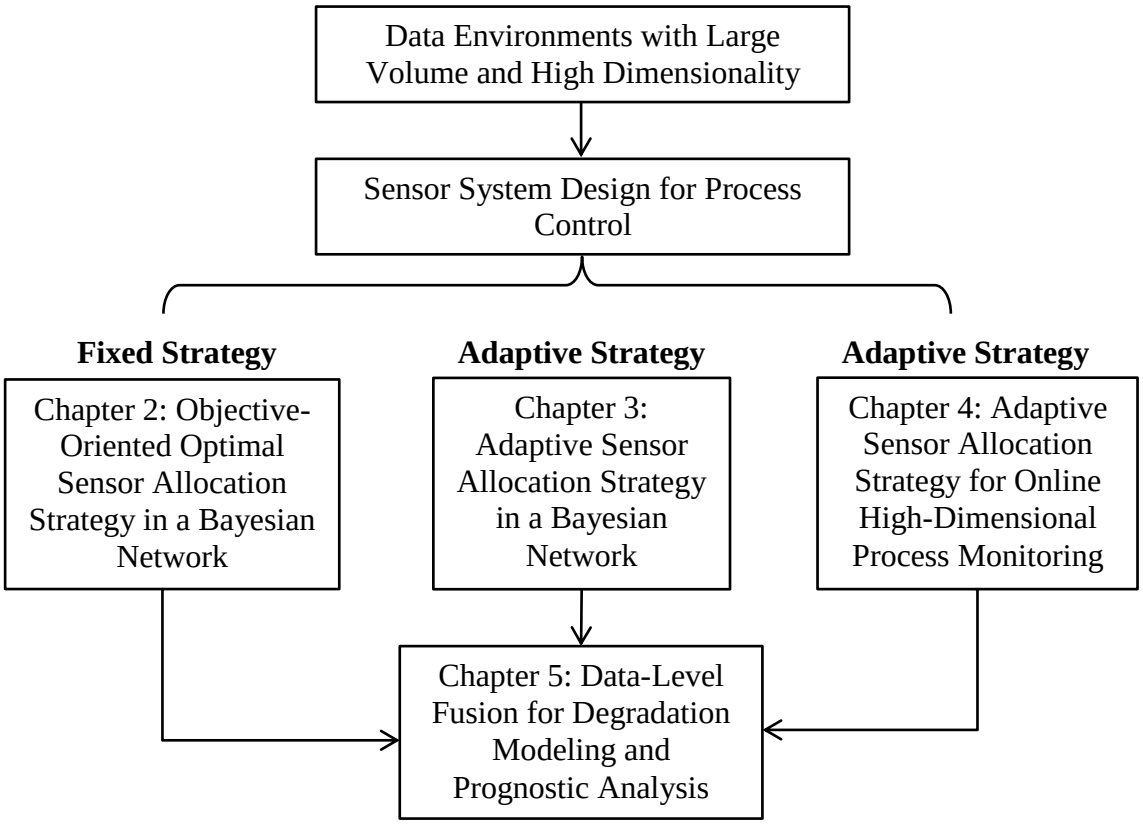

Figure 1.1: Outline of the thesis

In Chapter 2 (Liu and Shi 2012), we study the couplings or interactions between the optimal design of a sensor system in a Bayesian Network and quality management of a manufacturing system, which can improve cost-effectiveness and production yield by considering sensor cost, process change detection speed, and fault diagnosis accuracy in an integrated manner. An algorithm named "Best Allocation Subsets by Intelligent Search" (BASIS) with optimality proof is developed to obtain the optimal sensor

allocation design at minimum cost under different user specified detection requirements. The methodology is tested and validated based on a hot forming process and a cap alignment process.

In Chapter 3 (Liu et al. 2013), we develop a novel approach to adaptively reallocate sensor resources in a Bayesian Network based on online observations. A max-min criterion is proposed to manage sensor reallocation and process change detection in an integrated manner. The proposed method can significantly improve the detection delay and diagnosis accuracy compared with the existing fixed sensor allocation strategies (Liu and Shi 2012).

In Chapter 4 (Liu et al. manuscript), a systematic adaptive sensor allocation strategy is proposed with the purpose of minimizing detection delay in a general network. A monitoring scheme of using the sum of top-r local detection statistics is developed, which is scalable, effective and robust in detecting a wide range of possible shifts in all directions. The methodology is tested with a hot forming process and a real solar flare process. The use of this framework has several advantages over other approaches, which include significant decreases in computational cost (i.e. the complexity is only linear in the number of variables), and extensive savings for physical sensors, data acquisition, transmission and processing time.

In Chapter 5 (Liu et al. 2012), we first define two essential properties, that if present in a degradation signal, can enhance the effectiveness for prognostics. Then, we propose a generic real-time sensor selection and data-level fusion algorithm to construct a composite health index to achieve those two identified properties. This methodology includes data selection, data processing, and data fusion steps that lead to an improved degradation-based prognostic model. Our goal is to identify that the composite health index provides a much better characterization of the condition of a system compared to relying solely on the data from an individual sensor.

In the end, Chapter 6 concludes the thesis and summarizes the original contributions. In addition, future research directions related to this thesis are also discussed.

CHAPTER 2

OBJECTIVE-ORIENTED OPTIMAL SENSOR ALLOCATION STRATEGY FOR PROCESS MONITORING AND DIAGNOSIS IN A BAYESIAN NETWORK

2.1 Introduction

The advancement in sensor technology facilitates vigorous development in the distributed sensor network (DSN), which has been widely used in industrial and civilian applications such as industrial process monitoring and control, healthcare surveillance, and decision support systems.

One of the fundamental issues in a DSN is process control with the objectives of reducing variability and improving the final quality of products (Montgomery 2009). A typical process control problem includes three steps: process monitoring, fault diagnosis and process recovery. In process monitoring, various methods have been developed, such as univariate statistical process control (Shewhart 1931), multivariate Hotelling T^2 statistical process control (Hotelling 1947), MCUSUM and MEWMA control charts (Woodall and Ncube 1985; Lowry et al. 1992), and some principal component analysis (PCA) based techniques (Bakshi 1998). Regarding the fault diagnosis procedure, one popular technique developed is the MTY T^2 decomposition (Mason et al. 1997). While the MTY approach is theoretically sound and appealing, it involves a significant amount of computational issues for high dimensional variables and has inherent deficiencies in identifying the root cause variables in a system. Therefore, a causation-based T^2 decomposition method is proposed to improve the diagnosability (Li, Jin, and Shi 2008) in a causal model. On the other hand, the diagnosis problem can be viewed as a task to

correctly classify a fault into one of the pre-defined classes. New techniques are developed based on the classification point of view, such as Fisher Discriminant Analysis (Duda et al. 2000) and Support Vector Machine (SVM) (Vapnik 1999).

Another critical concern about a DSN is the cost, which includes installation, maintenance, and operational costs (Edan and NOF 2000). While a fully deployed sensor system can minimize information loss, the total cost associated with these sensors can be overwhelming. Moreover, massive data collected from different sensors can involve dependent or redundant information. The efficiency of the sensor network can be benchmarked by the sensing cost in achieving customer demand (Ding et al. 2003). Therefore, it is desirable to quantify the dependencies via a statistical model in order to effectively and efficiently collect sufficient information with minimum cost.

In the past decades, extensive researches and practices have been made for improving manufacturing system design and product quality. In most of cases, manufacturing system design aims at increasing production throughput, reducing lead time and improving customer demand satisfaction. On the other hand, product quality improvement focuses on quick abnormality detection and accurate fault diagnosis (Li et al. 2007). Some efforts have also been made to investigate the couplings or interactions between production system design and product quality (Li, Blumenfeld, and Marin 2008; Li and Meerkov 2009). In general, different system designs may result in different quality performance. In this chapter, we focus on developing an optimal sensor allocation strategy for detecting and diagnosing process variation sources in a timely manner, so that the customer demand can be satisfied economically and efficiently. The effective use of sensor data has provided unprecedented opportunities for quality and productivity improvement (Ding et al. 2006). With the guaranteed customer satisfaction, implementing minimum number of sensors in the system can significantly reduce the cost and time associated with sensor operation and maintenance, so that lead time and inventory level can be reduced. It has been shown that an optimal sensor system enables

manufacturers to improve product quality, and reduce production downtime as well as inventory level (Liu et al. 2005).

The optimal sensor allocation problem is a decision making process that involves the determination of (i) the minimum cost of sensors required to achieve customer demand and (ii) which variables to measure. Most methodologies developed for this type of problem are based on the assumption that certain prior knowledge is sufficient to quantitatively describe the relationship among physical parameters (Khan et al. 1998; Khan and Ceglarek 2000). However, there is a lack of general formulation when such prior knowledge is unknown. Li and Jin (2010) proposed an optimal sensor allocation method by integrating causal models and set-covering algorithms for single mean shift detection using a univariate control chart, which addressed the problem of sensor allocation for process monitoring in causal models. Although the problem is well defined in their paper, the developed method does not take the Bonferroni correction into consideration when searching for the optimal solution. Therefore, the proposed allocation strategy in their paper cannot guarantee to satisfy the specified ARL requirement in certain detection cases. This point will be further elaborated in the case study section of this chapter. In addition, the single mean shift assumption in their paper also leads to limited applications in practice, because there could be cases with multiple mean shifts having different signs and magnitudes in a complex DSN. Although it is possible to build a univariate control chart for each variable, the false alarm rate of the system will raise and the charts will be unable to describe the interrelationships among variables. Thus, multivariate statistical control chart is preferred and adopted.

The objectives of this chapter are to study the optimal sensor allocation strategy that can meet the customer requirement in terms of ARL with minimum sensing cost, and then conduct a generic root cause diagnostic analysis with partial information after implementing the optimal strategy. This research focuses on mean shifts detection and diagnosis with an assumption that the variance of each variable keeps constant.

To conduct the tasks mentioned above, a Bayesian Network (BN) is employed in this chapter to represent the causal relationships among a set of variables in a DSN. The application of BN has recently been successfully demonstrated in fault detection and diagnosis (Verron et al. 2008). The advantages of choosing BN as a framework can be summarized as follows: (1) BN can handle incomplete datasets since the dependency information is embedded visually and numerically. (2) BN provides an effective tool to describe a causal relationship that is mathematically defined in terms of probabilistic independence statements. The causal interpretations facilitate the application of BN to solve real world problems (Pearl and Verma 1991; Li and Shi 2007). (3) BN in conjunction with Bayesian statistical techniques facilitates the combination of domain knowledge and data (Heckerman 1995). Generally speaking, BN can be obtained by integrating engineering knowledge and observational data (Buntine 1994; Koller and Friedman 2009). Li and Shi (2007) presented an example using a BN to describe the causal relationships in a multistage rolling manufacturing process. In this chapter, we assume that the BN has already been correctly acquired, so that no more learning procedures are involved in the following discussions.

The rest of the chapter is organized as follows: Section 2.2 introduces the key terminologies of BN. Section 2.3 presents a concrete formulation for the optimal sensor allocation problem and an intelligent searching algorithm for the optimal solution. Section 2.4 proposes a diagnosis ranking method to find the root cause variables, followed by diagnosability analysis, which includes discussions about diagnosability criteria and minimum diagnosable class. Section 2.5 performs case studies based on a hot forming process and a cap alignment process to illustrate and evaluate the proposed methodologies under different mean shift detection and diagnosis scenarios. Finally, Section 2.6 draws a conclusion.

2.2 BN Representation and Terminology

A BN is a probabilistic graphic model that can be used to represent causal relationships in a system of m physical variables $\boldsymbol{X} = \{X_1, X_2, \dots, X_m\}$. A BN has two components, one qualitative and the other quantitative. The qualitative component is referred to as the *structure* of a BN, which is a directed acyclic graph (DAG). This structure conveys two pieces of information. First, each node corresponds to one physical variable of the system. Second, each directed arc connects two variables and represents their probabilistic dependence. In this chapter, we use an Arabic number to represent each node, and use X_i to represent the physical variable or the numerical value of node, i. The quantitative component, also called the *parameter* of a BN, is a conditional probability annotated on each directed arc of the structure. If there is a directed arc from node i to j, i is the direct cause (called the *parent*) of j and j is the direct effect (also called the *child*) of i, in which "direct" means that the causal influence from i to j is not mediated through any other nodes. A path exists from node i to j if there is one or several directed arcs linking together from i to j, i.e. $i \to \cdots \to j$. In this case, i is an *ancestor* of j and j is a *descendant* of i, respectively. If i does not have any ancestors (descendants), then it is called a *root* (*leaf*) of the system. In this chapter, the sets of *parents*, *children*, *descendants* and *ancestors* of variable X_i or node i are denoted as $\boldsymbol{PA}(i), \boldsymbol{CH}(i), \boldsymbol{DS}(i)$ *and* $\boldsymbol{AN}(i)$, respectively. The sets of *root* and *leaf* nodes of the system are denoted by $\boldsymbol{RO}$ *and* $\boldsymbol{LF}$, respectively. In addition, the kth component of each set is denoted as $PA_k(i), CH_k(i), DS_k(i), AN_k(i), RO_k$ *and* LF_k.

For example, Figure 2.1 shows a linear Gaussian BN to represent the causal relationships involved in a hot forming process (Li and Jin 2010). It has four process variables (X_4: temperature; X_3: material flow stress; X_2: tension in workpiece; X_5: Blank Holding Force (BHF)), and one quality variable (X_1: final dimension of workpiece). A two-dimensional (2-D) physical illustration of the hot forming process is shown in Figure

2.2. According to the definition, nodes 5 and 4 are parents of node 2, and they are the roots of the system; nodes 2 and 3 are the children of node 4; {2, 3, 4, 5} are ancestors of node 1; and {1, 2, 3} are descendants of node 4. There are two distinct paths from node 4 to 1, 4→2→1 and 4→3→1.

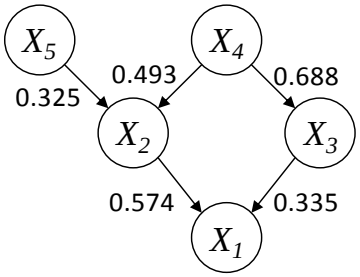

Figure 2.1: BN structure of a hot forming process (Li and Jin 2010)

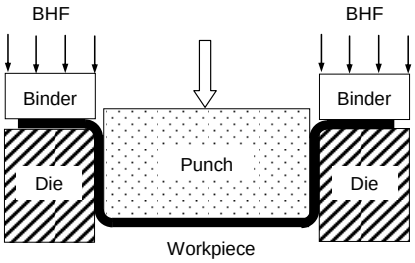

Figure 2.2: 2-D illustration of the hot forming process (Li and Jin 2010)

In this chapter, it is assumed that when the system is under normal operational condition, all variables will follow standard normal distributions, which can be achieved by standardizing all variables. Then, a linear Gaussian parameterization given the BN is represented as (Lauritzen and Wermuth 1989; Li and Jin 2010):

$$X_j = \sum_{k=1}^{card(\boldsymbol{PA}(j))} p(PA_k(j), j) X_{PA_k(j)} + V_j, \tag{2.1}$$

where $p(PA_k(j), j) \in (0,1)$ is called the *path coefficient*, which resembles the conditional probability distribution $p(X_j | X_{PA_k(j)})$ to represent the influence from the kth parent of j to j; $card(\boldsymbol{PA}(j))$ is the cardinality of the set $\boldsymbol{PA}(j)$, the number of parents of j. In addition, we assume that $V_j \sim N(0, \sigma_j^2)$ is independent to $X_{PA_k(j)}$ and V_i $(i \neq j)$, which represents the randomness of variable X_j itself, or the random noise that cannot be described by the linear part of the model. It is used to maintain the unit variance of each variable X_i. Moreover, the *path effect* from i to j is defined to be the product of all path coefficients on that path connecting i to j. Since there may be several paths between i and j, $\tilde{\gamma}(i, j)$ is defined to be the *total effect* of i on j, which equals to the sum of all the path effects from i to j, so that

$$\tilde{\gamma}(i,j) = \begin{cases} \in (0,1) & if\ i \in \boldsymbol{AN}(j) \\ 0 & otherwise \end{cases}. \tag{2.2}$$

$\tilde{\gamma}(i,j)$ represents the regression coefficient when X_j is directly regressed on X_i. For example in Figure 2.1, $\tilde{\gamma}(4,1) = 0.493 * 0.574 + 0.688 * 0.335 = 0.5135$ and $\tilde{\gamma}(1,4) = 0$. Since each variable follows standard normal distributions under regular operational condition, X_5 is equal to V_5 (i.e. $V_5 \sim N(0,1)$), which is not influenced by any other variables, while X_2 is equal to $0.325X_5 + 0.493X_4 + V_2$ (i.e. $V_2 \sim N(0,0.651)$), which is influenced by both variables X_5 and X_4.

To obtain the variance of V_j, we can recursively represent the term $X_{PA_k(j)}$ by equation (2.1) until parameterization on the root nodes of the system. It can be readily shown that equation (2.1) can be transformed into:

$$X_j = \sum_{k=1}^{card(\boldsymbol{AN}(j))} \tilde{\gamma}(AN_k(j), j) V_{AN_k(j)} + V_j. \tag{2.3}$$

Since X_j follows standard normal distribution under normal operational condition and V_j is independent to each other, the variance σ_j^2 can be obtained by:

$$\sigma_j^2 = 1 - \sum_{k=1}^{card(\boldsymbol{AN}(j))} [\tilde{\gamma}(AN_k(j), j)]^2 \sigma_{AN_k(j)}^2. \tag{2.4}$$

At each step, we acquire the variance σ_j^2 if all $\sigma_{AN_k(j)}^2$ $(k = 1, \dots, card(\boldsymbol{AN}(j)))$ are obtained. Then in the end, all variance σ_j^2 $(j \in m)$ can be known sequentially.

2.3 Optimal Sensor Allocation for Quick Mean Shifts Detection

2.3.1 Problem Formulation

The optimal sensor allocation strategy is a "mission-specific" task under given objectives. In this chapter, we investigate the optimal allocation strategy under the requirement that at most p variables in the system may possibly have a mean shift with at least magnitude τ.

Since the graphic representation of a BN has already embedded the numerical relationship among variables, it is possible to monitor the propagation of multiple mean shifts by investigating a multivariate distribution. Although most linear Gaussian Bayesian Networks are represented by equation (2.1) to show the causal influences from parents (Li and Jin 2010; Koller and Friedman 2009), we find that a matrix representation is easier and more compact to illustrate mean shifts propagation within a BN. Specifically, $\boldsymbol{X}$ can be represented by the following forms:

$$\boldsymbol{X} = [\boldsymbol{PC}]\boldsymbol{X} + \boldsymbol{V} + \boldsymbol{\delta}, \tag{2.5}$$

where $\boldsymbol{X} \sim \boldsymbol{N_m}(\boldsymbol{u}, \boldsymbol{\Sigma_X})$, is the measurement value of each physical variable with mean $\boldsymbol{u}$ and the diagonal elements of $\boldsymbol{\Sigma_X}$ are all ones; $[\boldsymbol{PC}]$ is the path coefficient matrix of the BN; $\boldsymbol{V} \sim \boldsymbol{N_m}(\boldsymbol{0}, \boldsymbol{\Sigma_V})$, represents the randomness of $\boldsymbol{X}$ needed to maintain the unit variance of each variable; and $\boldsymbol{\delta}$ indicates the expected mean shift of each variable. For compactness, we define $\boldsymbol{A} = \boldsymbol{I_m} - \boldsymbol{PC}$. According to the definition of $\boldsymbol{PC}$, $\boldsymbol{A}$ is a triangular matrix, whose diagonal elements are all ones. Thus, $\boldsymbol{A}$ is an invertible matrix. The measurement value of a physical variable is available if and only if a sensor is deployed on it, so that only partial elements of $\boldsymbol{X}$ can be obtained during online measurements. Denote the sensor allocation set by $\boldsymbol{s}$, then

$$(\boldsymbol{X} - \boldsymbol{A^{-1}\delta})_{\boldsymbol{s}} = (\boldsymbol{A^{-1}V})_{\boldsymbol{s}}, \tag{2.6}$$

where $(\boldsymbol{X} - \boldsymbol{A^{-1}\delta})_{\boldsymbol{s}}$ represents the sub-vector of $\boldsymbol{X} - \boldsymbol{A^{-1}\delta}$ with rows indexed by $\boldsymbol{s}$. From the definition of $\boldsymbol{V}$, its covariance matrix $\Sigma_{\boldsymbol{V}}$ is a diagonal matrix, where the diagonal elements can be obtained by equation (2.4). $(\boldsymbol{X} - \boldsymbol{A^{-1}\delta})_{\boldsymbol{s}} \sim \boldsymbol{N}_{card(\boldsymbol{s})}(\boldsymbol{0}, [\boldsymbol{A^{-1}\Sigma_V}(\boldsymbol{A^{-1}})^{\boldsymbol{T}}]_{\boldsymbol{s}})$, where $[\boldsymbol{A^{-1}\Sigma_V}(\boldsymbol{A^{-1}})^{\boldsymbol{T}}]_{\boldsymbol{s}}$ is a sub-block matrix of $\boldsymbol{A^{-1}\Sigma_V}(\boldsymbol{A^{-1}})^{\boldsymbol{T}}$ with rows and columns indexed by $\boldsymbol{s}$.

Considering the null hypothesis H_0: $\boldsymbol{\delta} = \boldsymbol{0}$ against the alternative hypothesis H_a: $\boldsymbol{\delta} \neq \boldsymbol{0}$, the chi-square control chart based on individual observation rejects H_0 if

$$\boldsymbol{X_s}^{\boldsymbol{T}}\{[\boldsymbol{A^{-1}\Sigma_V}(\boldsymbol{A^{-1}})^{\boldsymbol{T}}]_{\boldsymbol{s}}\}^{-\boldsymbol{1}}\boldsymbol{X_s} > \mathcal{X}_{\alpha}^{2}(card(\boldsymbol{s})), \tag{2.7}$$

where $\mathcal{X}_{\alpha}^{2}(card(\boldsymbol{s}))$ is the upper control limit, the $(1-\alpha)th$ quantile of the chi-square distribution with degree of freedom $card(\boldsymbol{s})$. When the system becomes abnormal and has a mean shift, the type two error β of the test is

$$\beta = Pr\{\boldsymbol{X_s}^{\boldsymbol{T}}\{[\boldsymbol{A^{-1}\Sigma_V}(\boldsymbol{A^{-1}})^{\boldsymbol{T}}]_{\boldsymbol{s}}\}^{-\mathbf{1}}\boldsymbol{X_s} \leq \mathcal{X}_{\alpha}^{2}(card(\boldsymbol{s}))|\boldsymbol{\delta} \neq \mathbf{0}\}. \tag{2.8}$$

Thus, $ARL_{\boldsymbol{s}}(\boldsymbol{\delta}) = \frac{1}{1-\beta}$ denotes the ARL needed to detect the expected mean shift $\boldsymbol{\delta}$ corresponding to the sensor allocation set $\boldsymbol{s}$. Denote $ARL_U(\tau)$ as the upper bound of the ARL specified by a practitioner to detect the expected mean shift $\boldsymbol{\delta}$ with at least magnitude τ in its nonzero elements. Accordingly, we give a definition about detectable as follows:

Definition 2.1: A mean shift $\boldsymbol{\delta}$ is *detectable* as long as $ARL_{\boldsymbol{s}}(\boldsymbol{\delta}) \leq ARL_U(\tau)$.

According to this definition, the optimal sensor allocation problem can be formulated as a searching problem for the best set of nodes, $\boldsymbol{s}$, which satisfies:

$$min_{\boldsymbol{s}}\ C = \sum_{i\in \boldsymbol{s}} C_i \tag{2.9}$$

$$subject\ to\ ARL_{\boldsymbol{s}}(\boldsymbol{\delta}) \leq ARL_U(\tau),$$

where C_i is the cost of the sensor on node i.

2.3.2 Best Allocation Subsets by Intelligent Search (BASIS)

For a mean shift $\boldsymbol{\delta} \neq \mathbf{0}$, $\boldsymbol{X_s}^{\boldsymbol{T}}\{[\boldsymbol{A^{-1}\Sigma_V}(\boldsymbol{A^{-1}})^{\boldsymbol{T}}]_{\boldsymbol{s}}\}^{-\mathbf{1}}\boldsymbol{X_s} \sim \mathcal{X}'^{2}_{card(\boldsymbol{s})}(\Delta(\boldsymbol{s}))$, where $\mathcal{X}'^{2}_{card(\boldsymbol{s})}(\Delta(\boldsymbol{s}))$ represents a noncentral chi-square distribution with noncentrality parameter $\Delta(\boldsymbol{s}) = (\boldsymbol{A^{-1}\delta})_{\boldsymbol{s}}^{\boldsymbol{T}}\{[\boldsymbol{A^{-1}\Sigma_V}(\boldsymbol{A^{-1}})^{\boldsymbol{T}}]_{\boldsymbol{s}}\}^{-\mathbf{1}}(\boldsymbol{A^{-1}\delta})_{\boldsymbol{s}}$ and degree of freedom $card(\boldsymbol{s})$. According to the analysis in Section 2.3.1, $\boldsymbol{\delta}$ is detectable if and only if

$$\beta = ncx2cdf(\mathcal{X}_{\alpha}^{2}(card(\boldsymbol{s})), card(\boldsymbol{s}), \Delta(\boldsymbol{s})) \leq 1 - \frac{1}{ARL_U(\tau)}, \tag{2.10}$$

where $ncx2cdf(\mathcal{X}_{\alpha}^{2}(card(\boldsymbol{s})), card(\boldsymbol{s}), \Delta(\boldsymbol{s}))$ is a build-in function in Matlab computing the noncentral chi-square cumulative probability at the value $\mathcal{X}_{\alpha}^{2}(card(\boldsymbol{s}))$ with the corresponding degrees of freedom $card(\boldsymbol{s})$ and noncentrality parameter $\Delta(\boldsymbol{s})$.

Assume equation (2.10) achieves equality at $\Delta(\boldsymbol{s}) = \tilde{\Delta}(card(\boldsymbol{s}))$ given the cardinality of the set $\boldsymbol{s}$. Since $ncx2cdf$ is a decreasing function in terms of noncentrality parameter given the degree of freedom parameter, a definition about feasible solution is presented as follows:

Definition 2.2: An allocation set $\boldsymbol{s}$ is a *feasible solution* to detect the mean shift $\boldsymbol{\delta}$ if and only if $\Delta(\boldsymbol{s}) \geq \tilde{\Delta}\big(card(\boldsymbol{s})\big)$.

In other words, equation (2.9) is simplified into the following problem:

$$min_{\boldsymbol{s}}\ C = \sum_{i \in \boldsymbol{s}} C_i \qquad (2.11)$$

$$\textit{subject to } \Delta(\boldsymbol{s}) \geq\ \tilde{\Delta}\big(card(\boldsymbol{s})\big).$$

Since the optimal solution depends on the cardinality of the set $\boldsymbol{s}$, in this chapter we propose an algorithm named "BASIS" in terms of $card(\boldsymbol{s})$ to intelligently search the optimal sensor allocation solution. The BASIS algorithm resembles the idea of the "best" subsets algorithm for model selection in regression (Hocking and Leslie 1967). In the "best" subsets algorithm, several "good" candidate sets are identified for each possible number of predictors, which provide additional information for the investigator in making final selection of predictors for the regression model. Similarly, several feasible solution sets can be identified in terms of different number of sensors allocated in the system. The "intelligent" here means the optimal sensor allocation solution can be derived exhaustively without conducting complex simulation studies. The BASIS algorithm is illustrated in Figure 2.3 and all of the feasible solutions are recorded in the set *"**Opt**"*. Accordingly, the optimal solution can be achieved by choosing the one from *"**Opt**"* with the lowest sensor cost. It can be shown that the computation intensity of the BASIS algorithm is $\Theta(2^m)$. In fact, it is impossible to detect the mean shift that occurs from *leaf* nodes without allocating sensors on them. Therefore, the total number of sensors needed in the system is at least $card(\boldsymbol{LF})$ and all of the *leaf* nodes are required to deploy sensors.

After taking this fact into consideration, the running time of the proposed algorithm is shortened to be $\Theta\{2^{m-card(\boldsymbol{LF})}\}$.

1. *For i=m:-1:1, Compute* $\tilde{\Delta}(i)$ *, where* $ncx2cdf\left(\mathcal{X}_{\alpha}^{2}(i), i, \tilde{\Delta}(i)\right) = 1 - \frac{1}{ARL_U(\tau)}$.
2. *List all searching sets with cardinality i. The number of sets is* $n_i = \binom{m}{i}$ *and each set is denoted as* $\boldsymbol{s}_i(j), j = 1,2, \dots, n_i$. *Denote flagsol=0.*
   a) *For j=1:* n_i,
   b) *Compare* $\Delta\left(\boldsymbol{s}_i(j)\right) = (\boldsymbol{A}^{-1}\boldsymbol{\delta})_{\boldsymbol{s}_i(j)}^{T}\{[\boldsymbol{A}^{-1}\boldsymbol{\Sigma_V}(\boldsymbol{A}^{-1})^{T}]_{\boldsymbol{s}_i(j)}\}^{-1}(\boldsymbol{A}^{-1}\boldsymbol{\delta})_{\boldsymbol{s}_i(j)}$ *with* $\tilde{\Delta}(i)$.
   c) *If* $\Delta\left(\boldsymbol{s}_i(j)\right) \geq \tilde{\Delta}(i)$,
   d) $\boldsymbol{s}_i(j)$ *is a feasible solution and record* $\boldsymbol{s}_i(j)$ *into set* ***Opt****. flagsol=1;*
   e) *End.*

   If (flagsol==0), break.
3. *End.*

Figure 2.3: BASIS algorithm for optimal sensor allocation solution

2.3.3 Solution to Optimal Sensor Allocation

2.3.3.1 Single Mean Shift Case

We start by investigating the simplest case in which our interested detection scenario is that at most one variable in the system may possibly have a mean shift with at least magnitude τ. Denote all of our interested detection scenarios of $\boldsymbol{\delta}$ in Figure 2.3 as $\overline{\boldsymbol{\delta}}$, which form a space as R_1 (i.e. $\boldsymbol{\delta} \in R_1$). In addition, denote the space specified by the kth mean shift scenario as R_1^k. Let $\boldsymbol{\delta}(k) \in R_1^k$ be the single mean shift case with the kth element equal to τ $(k = 1,2, \dots, m)$. Then $\overline{\boldsymbol{\delta}}$ can be summarized as a countable set which

only contains m elements, $\overline{\boldsymbol{\delta}} = \{\boldsymbol{\delta}(1), \boldsymbol{\delta}(2), \ldots, \boldsymbol{\delta}(m)\}$. Modifying $\Delta\left(\boldsymbol{s}_i(j)\right)$ in Figure 2.3 to be:

$$\min_{\boldsymbol{\delta}(k)} \left\{ \left(\boldsymbol{A^{-1}\delta}(k)\right)^{\boldsymbol{T}}_{\boldsymbol{s}_i(j)} \{[\boldsymbol{A^{-1}\Sigma_V}(\boldsymbol{A^{-1}})^{\boldsymbol{T}}]_{\boldsymbol{s}_i(j)}\}^{-1} \left(\boldsymbol{A^{-1}\delta}(k)\right)_{\boldsymbol{s}_i(j)} \right\}, k = 1,2,\ldots,m, \quad (2.12)$$

we get the following proposition:

Proposition 2.1: For single mean shift detection, if $\boldsymbol{s}$ is a feasible solution obtained from the BASIS algorithm, then any $\widetilde{\boldsymbol{\delta}} \in R_1$ is detectable.

Proof: see Appendix A.1.

It can be shown that the running time of the BASIS algorithm for single mean shift case is bounded by $\Theta\left\{\left(2^{m-card(\boldsymbol{LF})}\right) * m\right\}$.

2.3.3.2 Multiple Mean Shifts Case

The BASIS algorithm proposed in Figure 2.3 can also be generalized for detection of multiple mean shifts where at most p variables in the system may possibly have a mean shift with at least magnitude τ. Denote the space of our interested detection scenarios by R_p. Given that at most p variables may possibly have a mean shift, the total number of faulty scenarios is $\sum_{l=1}^{p}\binom{m}{l}$. Denote the space defined by the kth mean shift scenario as R_p^k, so that $R_p = \bigcup_{k=1}^{\sum_{l=1}^{p}\binom{m}{l}} R_p^k$. In the single mean shift case, all of our interested detection scenarios $\overline{\boldsymbol{\delta}}$ can be treated as a finite countable set, of which the cardinality equals the total number of variables in the system. In addition, each element of the set $\overline{\boldsymbol{\delta}}$, has exactly one nonzero entry that equals to τ. However, in the multiple mean shifts case, since positive and negative mean shifts mitigate each other, the cumulative mean shift propagated to the descendant node can be indiscernible though the magnitudes of mean shifts from ancestors are significant. Thus, $\overline{\boldsymbol{\delta}}$ cannot be easily expressed as a countable set as in the single mean shift case.

In order to address the problem of optimal sensor allocation for multiple mean shifts detection by BASIS algorithm in Figure 2.3, we rewrite $\Delta(\boldsymbol{s}_i(j))$ to be a quadric optimization function with the following form:

$$\Delta(\boldsymbol{s}_i(j)) = \min_{k}\left\{\min_{\boldsymbol{\delta}(k)}\left\{\boldsymbol{\delta}(k)^T(\boldsymbol{A^{-1}})^{\boldsymbol{T}}_{\boldsymbol{s}_i^r(j)}\{[\boldsymbol{A^{-1}\Sigma_V}(\boldsymbol{A^{-1}})^{\boldsymbol{T}}]_{\boldsymbol{s}_i(j)}\}^{-\mathbf{1}}(\boldsymbol{A^{-1}})_{\boldsymbol{s}_i^r(j)}\boldsymbol{\delta}(k)\right\}\right\} \quad (2.13)$$

$$\textit{subject to } \boldsymbol{\delta}(k) \in R_p^k, k = 1,2,\dots,\sum_{l=1}^{p}\binom{m}{l},$$

where $(\boldsymbol{A^{-1}})_{\boldsymbol{s}_i^r(j)}$ is the sub-block matrix of $\boldsymbol{A^{-1}}$ with only rows indexed by $\boldsymbol{s}_i(j)$; $\boldsymbol{\delta}(k) \in R_p^k$ is any mean shift case that belongs to the kth faulty scenario ($k = 1,2,\dots,\sum_{l=1}^{p}\binom{m}{l}$). Since $(\boldsymbol{A^{-1}})^{\boldsymbol{T}}_{\boldsymbol{s}_i^r(j)}\{[\boldsymbol{A^{-1}\Sigma_V}(\boldsymbol{A^{-1}})^{\boldsymbol{T}}]_{\boldsymbol{s}_i(j)}\}^{-\mathbf{1}}(\boldsymbol{A^{-1}})_{\boldsymbol{s}_i^r(j)}$ has already been proved to be a positive semidefinite (P.S.D.) matrix (in Appendix A.1), the objective function is bounded below on the feasible region and the global minimizer exists as long as the problem has a feasible solution. In addition, it can be shown that the running time of the BASIS algorithm for multiple mean shifts case is bounded by $\Theta\left\{\left(2^{m-card(\boldsymbol{LF})}\right) * \sum_{l=1}^{p}\binom{m}{l}\right\}$.

Intuitively, when the interested maximum number of mean shift variables p increases, or when the interested smallest magnitude of mean shift τ reduces, or when the interested maximum average run length requirement $ARL_U(\tau)$ decreases, the final number of sensors needed to satisfy the specified requirement will be increased. In other words, the higher the uncertainty about the system, the more the number of sensors is required. Therefore, choosing the allocation strategy is a trade-off problem in practice, and the final solution depends on how to allocate priorities on cost and detection.

In reality, the practitioner can determine the interested minimum magnitude of mean shifts for detection, the maximum number of simultaneous mean shift variables and the upper bound of the specified ARL based on engineering domain knowledge to ensure production yield. The engineering knowledge includes, but not limited to: the tolerance specifications for each variable specified in product/process design (related to the

interested minimum magnitude of mean shifts, τ), the probability of a fault occurred at each variable (related to the maximum number of simultaneous mean shift variables, p), and the cost of defective products produced (related to the specified ARL requirement, $ARL_U(\tau)$).

2.4 Diagnosis Ranking for Multiple Mean Shifts

2.4.1 Problem Formulation

After implementing the optimal allocation strategy, the next topic would be how to diagnose the root cause variables if an out-of-control signal is detected by the control chart. The existing methodologies, such as MTY T^2 decomposition (Mason et al. 1997) or causation-based T^2 decomposition (Li, Jin and Shi 2008), cannot be applied here since it requires the measurements of all variables are available. Therefore, it is desirable to develop a new diagnosis method for the case when only partial information is at hand. The difficulties of this problem arise from two aspects: (1) it is challenging to diagnose mean shifts from m nodes by fewer numbers of sensors, since only the variables with a sensor deployment are measurable; (2) it becomes more complicated when different combinations of the signs and magnitudes of the mean shifts are taken into consideration. To solve the aforementioned problem, we propose a diagnosis ranking method, which can be regarded as an extension to the LASSO-based variable selection method (Wang and Jiang 2009). Recall that we investigate the optimal allocation strategy subjected to the requirements that at most p variables in the system may possibly have a mean shift before an out-of-control signal is triggered, and the diagnosis procedure is conducted after implementing the optimal sensor allocation strategy. Therefore, we further assume that the number of true mean shift variables are bounded by p. As a result, the total number of faulty scenarios is $\sum_{l=1}^{p}\binom{m}{l}$ and the space defined by the kth mean shift scenario is

denoted as R_p^k. Similarly, $\boldsymbol{\delta}(k) \in R_p^k$ is any mean shift case that belongs to the kth faulty scenario ($k = 1,2, \dots, \sum_{l=1}^{p} \binom{m}{l}$).

Constrained to the space defined by each mean shift scenario, the constrained maximum likelihood approach can be implemented to rank the possibility of each mean shift given the out-of-control sample. It is aware that the constrained maximum likelihood approach is equivalent to solve the following problem given the out-of-control signal $\boldsymbol{X_s}$:

$$\min_{\boldsymbol{\delta}(k)} (\boldsymbol{X} - \boldsymbol{A^{-1}\delta}(k))_{\boldsymbol{s}}^{\boldsymbol{T}} \{[\boldsymbol{A^{-1}\Sigma_V}(\boldsymbol{A^{-1}})^{\boldsymbol{T}}]_{\boldsymbol{s}}\}^{-\mathbf{1}} (\boldsymbol{X} - \boldsymbol{A^{-1}\delta}(k))_{\boldsymbol{s}} \tag{2.14}$$

$$\textit{subject to } \boldsymbol{\delta}(k) \in R_p^k.$$

Again, equation (2.14) can be transformed into a quadratic optimization problem as follows:

$$\min_{\boldsymbol{\delta}(k)} \left\{ \boldsymbol{\delta}(k)^{\boldsymbol{T}} (\boldsymbol{A^{-1}})_{\boldsymbol{s}^r}^{\boldsymbol{T}} \boldsymbol{M} (\boldsymbol{A^{-1}})_{\boldsymbol{s}^r} \boldsymbol{\delta}(k) - 2\boldsymbol{X_s^T M} (\boldsymbol{A^{-1}})_{\boldsymbol{s}^r} \boldsymbol{\delta}(k) \right\} \tag{2.15}$$

$$\textit{subject to } \boldsymbol{\delta}(k) \in R_p^k,$$

where $\{[\boldsymbol{A^{-1}\Sigma_V}(\boldsymbol{A^{-1}})^{\boldsymbol{T}}]_{\boldsymbol{s}}\}^{-\mathbf{1}}$ is defined as $\boldsymbol{M}$ for compactness. If the minimized objective value is larger than or equal to the critical value $\mathcal{X}_\alpha^2(card(\boldsymbol{s})) - \boldsymbol{X_s^T M X_s}$, then we have at least $(1-\alpha)\%$ confidence to say that the kth faulty scenario is unlikely to be the true root cause. The proposed diagnosis ranking method is illustrated in Figure 2.4, where the final ranked solutions are recorded in the set $\widetilde{\boldsymbol{RD}}$. Assume there are q ranked solutions included in $\widetilde{\boldsymbol{RD}}$ and the kth one is denoted as $\widetilde{\boldsymbol{RD}}^k$. Therefore, the final conclusion about the mean shift variables is identified in $\widetilde{\boldsymbol{RD}}^1$.

The idea behind Figure 2.4 is inspired by the LASSO-based variable selection method (Wang and Jiang 2009). The LASSO-based variable selection method assumes that not all variables would shift simultaneously and there is an upper bound for the total number of nonzero mean shift variables. This upper bound can be set to be p as discussed in the beginning of this section. The original LASSO-based variable selection algorithm

assumes all variables are measurable, and here, we extend this diagnosis method into the case where only partial observations are available. Due to this extension, new issues (e.g. fault diagnosability and minimal diagnosable class) will be illustrated and discussed in the following sections. One problem associated with the proposed diagnosis ranking method is that the faulty scenarios with the number of p true mean shift variables always obtain the first few ranks in $\widetilde{\boldsymbol{RD}}$ since more degrees of freedom are available for those cases in the quadratic optimization function. Recall that the procedure suggested by classic SPC design recommends the investigator to stop the machine and take the out-of-control action plan immediately when certain out-of-control sample occurs. Therefore, it is more desirable that some in control variables are false positives than the case that certain true mean shift variables are excluded from $\widetilde{\boldsymbol{RD}}^1$. Accordingly, the definition for correct diagnosis is given as follows:

Definition 2.3: A diagnosis result is called *correct* if all true mean shift variables are in $\widetilde{\boldsymbol{RD}}^1$.

For k=1: $\sum_{l=1}^{p}\binom{m}{l}$,

Solve $obj(k) = \underset{\boldsymbol{\delta}(k)}{min}\{\boldsymbol{\delta}(k)^{\boldsymbol{T}}(\boldsymbol{A^{-1}})_{\boldsymbol{s}^r}^{\boldsymbol{T}}\boldsymbol{M}(\boldsymbol{A^{-1}})_{\boldsymbol{s}^r}\boldsymbol{\delta}(k) - 2\boldsymbol{X}_{\boldsymbol{s}}^{\boldsymbol{T}}\boldsymbol{M}(\boldsymbol{A^{-1}})_{\boldsymbol{s}^r}\boldsymbol{\delta}(k)\}$, *subjected to* $\boldsymbol{\delta}(k) \in R_p^k$.

If $obj(k) \leq \mathcal{X}_{\alpha}^2(card(\boldsymbol{s})) - \boldsymbol{X}_{\boldsymbol{s}}^{\boldsymbol{T}}\boldsymbol{M}\boldsymbol{X}_{\boldsymbol{s}}$,

Add $obj(k)$ *into* $\boldsymbol{RD}$.

End.

Sort $\boldsymbol{RD}$ *according to obj values and record into* $\widetilde{\boldsymbol{RD}}$.

Figure 2.4 Diagnosis ranking method for multiple mean shifts

2.4.2 Fault Diagnosability and Minimal Diagnosable Class

One problem for diagnosis with partial information is that certain faulty scenario might be aliases of others. Given that the total number of faulty scenarios is $\sum_{l=1}^{p}\binom{m}{l}$ and the space defined by the kth fault is denoted as R_p^k, we get the following definition for *diagnosable*:

Definition 2.4: The diagnosis problem is said to be *diagnosable* if for any nonzero $\boldsymbol{\delta}_1 \in R_p^{k_i}, \boldsymbol{\delta}_2 \in R_p^{k_j}$, such that $(\boldsymbol{A^{-1}\delta}_1)_{\boldsymbol{s}} = (\boldsymbol{A^{-1}\delta}_2)_{\boldsymbol{s}}$, then $i = j$ $(i, j \in \{1,2, \dots, \sum_{l=1}^{p}\binom{m}{l}\})$.

The intuition behind this definition is that if two mean shift cases are from different faulty scenarios, we can see distinct measurement values on sensors. In other words, we should be able to distinguish different mean shift scenarios in order to uniquely identify the root cause variables. According to the definition of diagnosable, we introduce the definition of minimal diagnosable class. The concept of minimal diagnosable class was first discussed in (Zhou et al. 2003; Shi 2006) and the definition was given based on a state space model. The minimal diagnosable class reveals the interrelationship among different faults. A minimal diagnosable class is a group of faults that cannot be further distinguished. The definition of minimal diagnosable class is represented as follows:

Definition 2.5: A set of faults $\{k_i, \dots, k_j\}$ $\left(i, j \in \{1,2, \dots, \sum_{l=1}^{p}\binom{m}{l}\}\right)$ forms a *minimal diagnosable class*, if there exists nonzero $\boldsymbol{\delta}_i \in R_p^{k_i}, \dots, \boldsymbol{\delta}_j \in R_p^{k_j}$ such that $(\boldsymbol{A^{-1}\delta}_i)_{\boldsymbol{s}} = \cdots = (\boldsymbol{A^{-1}\delta}_j)_{\boldsymbol{s}}$.

2.4.3 Analysis to Diagnosis Ranking Method and Diagnosability

2.4.3.1 Single Mean Shift Case

We start by investigating the simplest case where a single variable in the system may possibly have a mean shift. By implementing the algorithm as shown in Figure 2.4

where $p = 1$, the group of faults in a minimal diagnosable class will achieve the same objective value by the diagnosis ranking method. Therefore, if one of the faults in a minimal diagnosable class is identified in $\widetilde{\boldsymbol{RD}}^1$, the root cause cannot be further distinguished. Given a sensor allocation set $\boldsymbol{s}$, the minimal diagnosable class can be identified in the single mean shift scenario by the following proposition:

Proposition 2.2: Given a single mean shift diagnosis case with m faults $\boldsymbol{\theta} = \{k_1, k_2, \dots, k_m\}$ and k_i is the ith mean shift fault, the fault set $\boldsymbol{\theta}[\boldsymbol{v}] \subseteq \boldsymbol{\theta}$ is a minimal diagnosable class if the nonzero column vector $\boldsymbol{\tau}(i)$ of the reduced row echelon form (RREF) of $(\boldsymbol{A}^{-1})_{\boldsymbol{s}^r}$ can be expressed as $\boldsymbol{\tau}(i) = a\boldsymbol{\tau}(j)$ for $\forall v(i), v(j) \in \boldsymbol{\theta}[\boldsymbol{v}]$, where $v(i)$ is a column index for $\boldsymbol{\tau}(i)$ and a is a constant number.

Proof: see Appendix A.2.

2.4.3.2 Multiple Mean Shifts Case

To extend the single mean shift case to the multiple mean shifts case, we consider the framework where the number of true mean shift variables is bounded by p. Similarly to the single mean shift case, the group of faults in a minimal diagnosable class will achieve the same objective value by implementing the diagnosis ranking method in Figure 2.4. The minimal diagnosable class can be identified in terms of the number of out-of-control variables g from the following proposition, where $1 \le g \le p$.

Proposition 2.3: Given g $(1 \le g \le p)$ out-of-control variables with $\binom{m}{g}$ faults $\boldsymbol{\theta} = \{k_1, k_2, \dots, k_{\binom{m}{g}}\}$ and k_i is the ith mean shift fault, the fault set $\boldsymbol{\theta}[\boldsymbol{v}] \subseteq \boldsymbol{\theta}$ is a minimal diagnosable class if the nonzero column vector $\boldsymbol{\tau}(i)$ of the RREF of $(\boldsymbol{A}^{-1})_{\boldsymbol{s}^r}$ can be expressed as $\sum_{l=1}^{g}[\boldsymbol{\tau}(i)]_l = \sum_{l=1}^{g} a_l[\boldsymbol{\tau}(j)]_l$ for $\forall \boldsymbol{v}(i), \boldsymbol{v}(j) \in \boldsymbol{\theta}[\boldsymbol{v}]$, where $\boldsymbol{v}(i)$ is the column index for $\boldsymbol{\tau}(i)$, $[\boldsymbol{\tau}(i)]_l$ is the lth element of $\boldsymbol{\tau}(i)$, and a_l is a constant number.

Proof for proposition 2.3 follows the same logic as proposition 2.2 and thus is omitted here.

An example is provided here to illustrate this proposition. We consider a sensor allocation strategy for the hot forming problem in Figure 2.1. Sensors are allocated on {1, 3, 5} to monitor the system where at most two variables ($p = 2$) have a mean shift until an out-of-control signal is detected. Then the RREF of $(\boldsymbol{A^{-1}})_{\boldsymbol{s}^r}$ is as follows:

$$\begin{pmatrix} 1.000 & 0.574 & 0 & 0.283 & 0 \\ 0 & 0 & 1.000 & 0.688 & 0 \\ 0 & 0 & 0 & 0 & 1.000 \end{pmatrix}$$

From proposition 2.2, when only one mean shift occurs ($g = 1$), $\boldsymbol{\theta}$ ={{1}, {2}, {3}, {4}, {5}}. $\boldsymbol{\theta}[\boldsymbol{v}]$ ={{1}, {2}} forms a minimum diagnosable class and the total minimal diagnosable classes are {{1}, {2}}, {{3}}, {{4}}, {{5}}. Similarly, when two mean shifts occur ($g = 2$), the total minimal diagnosable classes are {{1, 3}, {2, 3}, {1, 4}, {2, 4}, {3, 4}}, {{1, 5}, {2, 5}}, {{1, 2}}, {{3, 5}}, {{4, 5}}.

2.5 Case Studies

In this section, we revisit the hot forming process introduced in Section 2.2 to evaluate the performance of the proposed BASIS algorithm in Figure 2.3 and the diagnosis ranking method in Figure 2.4 under different specified objectives for mean shift detection and diagnosis. The parameters selected in the case studies are within the typical ranges of actual systems, and thus the case studies could represent the characteristics of the actual systems. In addition, in order to demonstrate the effectiveness of the BASIS algorithm, a cap alignment process is also considered. The cost of each sensor is assumed same in the following case studies.

2.5.1 Optimal Sensor Allocation Strategy in the Hot Forming Process

2.5.1.1 Single Mean Shift Case

Table 2.1 shows the feasible solutions obtained by the BASIS algorithm for a single mean shift fault subjected to different specified objectives (different combinations

of τ and $ARL_U(\tau)$). These different objectives reflect the specific needs in practice. In the study, α is chosen to be 0.01. The optimal solution is the allocation strategy that has the smallest cardinality among all feasible solutions under each specified objective. As expected, the proposed BASIS algorithm is able to provide all feasible solutions in terms of the number of sensors needed in the system.

Table 2.1: BASIS algorithm solutions for single mean shift case under different specified objectives

$ARL_U(\tau)$	τ			
	1.5	2	2.5	3
10	No solution	**{1,2,3,4,5}**[2]	**{1,3,5}**[4] {1,2,3,5},{1,3,4,5} {1,2,3,4,5}	{1,3,5} {1,2,3,5},{1,3,4,5} {1,2,3,4,5}
15	No solution	{1,2,3,4,5}	{1,3,5} {1,2,3,5},{1,3,4,5} {1,2,3,4,5}	{1,3,5} {1,2,3,5},{1,3,4,5} {1,2,3,4,5}
20	**{1,2,3,4,5}**[1]	**{1,3,5}**[3] {1,2,3,5},{1,3,4,5} {1,2,3,4,5}	{1,3,5} {1,2,3,5},{1,3,4,5} {1,2,3,4,5}	**{1,2,5}**[5],{1,3,5} {1,2,3,5},{1,2,4,5} {1,3,4,5},{1,2,3,4,5}

2.5.1.2 Simulation Evaluation and Comparison With the Integrated Causal Models and Set-Covering Algorithms (Li and Jin 2010)

This section will evaluate the performance of the sensor allocation solutions proposed by the BASIS algorithm. There are five scenarios for a potential single mean shift, where each mean shift magnitude is equal to or greater than τ. However, it is sufficient for us to consider the case with mean shift magnitude τ, since a larger magnitude of mean shift is more notable by sensors under the single mean shift case. Moreover, it is sufficient to evaluate the boundary cases which either have a lesser number of sensors proposed as τ increases given the same $ARL_U(\tau)$ requirement, or has a lesser number of sensors proposed as $ARL_U(\tau)$ increases given the same magnitude τ. As a result, there are in total five boundary cases identified (bold font) and the case number

is denoted in superscript in Table 2.1. In fact, the algorithms (Li and Jin 2010) choose to allocate sensors on the bold entries or the subsets of bold entries in the five boundary cases of Table 2.1. Recall that the more the variables to be measured, the quicker the mean shift can be detected. Thus, comparing the ARL result with sensors deployed on the bold entries could provide a clearer demonstration about the advantages of the BASIS algorithm over the integrated causal models and set-covering algorithms. The comparison performances of the five boundary cases by these two algorithms are shown in Table 2.2.

The evaluation process involves the following steps:

1) In each selected boundary case, a mean shift τ to each variable X_i ($i \in \{1,2,3,4,5\}$) is introduced.

2) A $M\ (= 5000)$ samples dataset of $\boldsymbol{X} = \{X_1, X_2, X_3, X_4, X_5\}$ in terms of their distributions with the introduced mean shift at the first sample of each X_i is simulated.

3) For each sample, testing statistics $\boldsymbol{X_s^T}\{[\boldsymbol{A^{-1}\Sigma_V}(\boldsymbol{A^{-1}})^{\boldsymbol{T}}]_{\boldsymbol{s}}\}^{\boldsymbol{-1}}\boldsymbol{X_s}$ is plotted on a chi-square control chart with upper control limit $\mathcal{X}_{\alpha}^2(card(\boldsymbol{s}))$ and lower control limit 0. On the other hand, each univariate X_j ($j \in \boldsymbol{s}$) is plotted on a Shewhart control chart with control limits $\pm z_{\frac{\alpha}{2*card(\boldsymbol{s})}}$, where the Bonferroni correction method is implemented to maintain system type one error as in the integrated causal models and set-covering algorithms.

4) Indices of the first out-of-control sample on the control charts proposed by these two methods are recorded as RL_{1,X_i} and RL_{2,X_i}, respectively.

5) Repeat steps 1)-4) for $N\ (= 10000)$ times. The average of RL_{k,X_i} $(k = 1,2)$, $\overline{RL}_{k,X_i}$ of the introduced mean shift on each variable X_i for these two methods are computed and presented in Table 2.2.

Table 2.2: Estimated ARL for the BASIS algorithm and the integrated causal models and set-covering algorithms

α=0.01	BASIS Algorithm (1)					Integrated causal models and set-covering algorithms (2)				
Mean shift in	X_1	X_2	X_3	X_4	X_5	X_1	X_2	X_3	X_4	X_5
Case 1: $\overline{RL}_{k_i}$	5.65	10.14	7.49	17.44	17.47	16.21	15.59	16.04	12.86	15.29
Case 2: $\overline{RL}_{k_i}$	2.48	4.45	3.30	8.29	8.28	7.03	6.73	6.84	6.03	6.92
Case 3: $\overline{RL}_{k_i}$	3.68	15.42	5.66	14.90	6.06	5.62	23.38	5.55	12.44	5.57
Case 4: $\overline{RL}_{k_i}$	2.04	8.99	3.08	8.31	3.31	2.99	13.87	2.93	7.14	3.02
Case 5: $\overline{RL}_{k_i}$	1.18	1.80	15.61	9.45	2.10	1.92	1.89	31.45	8.14	1.89

According to the evaluation studies in Table 2.2, the following conclusions can be inferred: (1) The BASIS algorithm outperforms the algorithms (Li and Jin 2010) in the sense of meeting ARL requirement. It is aware that all the solutions proposed by the BASIS algorithm can satisfy ARL requirement under each scenario, while the algorithms (Li and Jin 2010) cannot guarantee that, as shown in cases 3, 4 and 5. The reason is that the algorithms (Li and Jin 2010) do not take the Bonferroni correction method into consideration during the searching procedure for the optimal solution. However, it is not a problem for the BASIS algorithm since it is conducted in terms of the number of sensors deployed. (2) It is guaranteed that there is no other better allocation solution beyond the ones indicated by the BASIS algorithm due to the exhaustive property of the proposed method. For example, when $\tau = 2$ and $ARL_U(\tau) = 15$, $\{1, 3, 5\}$ is not identified as a feasible solution, which can be verified by case 3 in Table 2.2 since the ARL needed to detect a mean shift happened from X_2 is greater than 15. (3) The mean shift occurred from a variable with sensor deployment is straightforwardly shown to be able to be detected faster than the one without sensor deployment. This phenomenon is consistent with the one in the algorithms (Li and Jin 2010).

2.5.1.3 Multiple Mean Shifts Case

As discussed in Section 2.3.3.2, the BASIS algorithm can be extended to multiple mean shifts case where at most p variables in the system may have a mean shift with at least magnitude τ. In this case study, p is chosen to be two. Similar to the single mean shift case, different specified objectives for detection (different combinations of τ and $ARL_U(\tau)$) are considered. By replacing the objective function in Figure 2.3 3b) with equation (2.13) as discussed in Section 2.3.3.2, the feasible solutions are shown in Table 2.3. The evaluation process is similar to the single mean shift case as shown in Section 2.5.1.2, and thus it is omitted here.

Table 2.3: BASIS algorithm solutions for multiple (two) mean shifts under different specified objectives

$ARL_U(\tau)$	τ			
	1.5	2	2.5	3
10	No solution	{1,2,3,4,5}	{1,2,3,5} {1,2,3,4,5}	{1,2,3,5} {1,2,3,4,5}
15	No solution	{1,2,3,4,5}	{1,2,3,5} {1,2,3,4,5}	{1,2,3,5} {1,2,3,4,5}
20	{1,2,3,4,5}	{1,2,3,5} {1,2,3,4,5}	{1,2,3,5} {1,2,3,4,5}	{1,2,3,5} {1,2,3,4,5}

2.5.2 Diagnosis Ranking Method for the Hot Forming Process

2.5.2.1 Single Mean Shift Case

Since there are five variables in the hot forming process, five potential single mean shift faults are of interest. Specifically, we conduct the evaluation process based on the allocation solution {1, 3, 5}, which is a feasible solution under most of the specified objectives in Table 2.1. Furthermore, the minimum diagnosable class can be shown as {{1}, {2}}, {{3}}, {{4}}, {{5}} by proposition 2.2. Therefore, the mean shift scenarios from X_1 and X_2 are indiscernible and these two faults will achieve the same objective value by the diagnosis ranking method. Table 2.4 provides the correct diagnosis rate in

terms of definition 2.3 by the diagnosis ranking method in Figure 2.4, where the single mean shift scenarios with different mean shift values are studied.

Table 2.4: Single mean shift scenarios and correct diagnosis rates for solution {1, 3, 5}

	Mean Shift in					$\tau = 1.5$	$\tau = 2.0$	$\tau = 2.5$	$\tau = 3.0$
Sce.	X_1	X_2	X_3	X_4	X_5	Corr. Prob	Corr. Prob	Corr. Prob	Corr. Prob
1	τ					0.852	0.923	0.962	0.981
2		τ				0.665	0.766	0.838	0.889
3			τ			0.600	0.684	0.739	0.780
4				τ		0.485	0.577	0.641	0.700
5					τ	0.832	0.913	0.947	0.974

It can be seen from Table 2.4 that the correct diagnosis rate increases as the mean shift magnitude gets larger, which is consistent with our intuition since the chi-square control chart is insensitive in detecting small mean shifts. Moreover, when the mean shift happens on variable X_4, the correct diagnosis rate is the lowest. Since no sensor is allocated on X_4, the mean shift happened on X_4 is likely to be mistakenly identified as either a mean shift from X_3 or X_5.

2.5.2.2 Multiple Mean Shifts Case

As discussed in Section 2.4.3.2, the diagnosis ranking method can also be generalized for multiple mean shifts case. According to the result in Table 2.3, we implement the sensor allocation solution {1, 2, 3, 5} and then continue the diagnosis procedure. Furthermore, p, the maximum number of true mean shift variables is chosen to be two. The minimum diagnosable classes are identified as {{1}}, {{2}}, {{3}}, {{4}}, {{5}}, {{1, 2}}, {{1, 3}}, {{1, 4}}, {{1, 5}}, {{2, 3}, {2, 4}, {3, 4}}, {{2, 5}}, {{3, 5}}, {{4, 5}} by proposition 2.3. To make a thorough study of the diagnosis performance in response to different faults, a set of 25 experiments is designed to cover three general groups of possible mean shift patterns as shown in Table 2.5. The first

group (cases 1-5) represents the single mean shift fault on each variable. The second and third groups (cases 6-15 and 16-25) represent the situations in which two variables simultaneously have an identical shift magnitude but in the same and opposite directions. Different magnitudes of mean shift in each fault scenario are also studied.

Table 2.5: Multiple mean shifts and correct diagnosis rates for solution {1, 2, 3, 5}

	Mean Shift in					$\tau = 1.5$	$\tau = 2.0$	$\tau = 2.5$	$\tau = 3.0$
Sce.	X_1	X_2	X_3	X_4	X_5	Corr. Prob	Corr. Prob	Corr. Prob	Corr. Prob
1	τ					0.987	0.997	0.999	1.000
2		τ				0.825	0.882	0.914	0.923
3			τ			0.631	0.688	0.729	0.762
4				τ		0.555	0.631	0.681	0.713
5					τ	0.942	0.978	0.992	0.998
6	τ	τ				0.632	0.778	0.999	0.931
7	τ		τ			0.546	0.667	0.751	0.837
8	τ			τ		0.428	0.507	0.587	0.670
9	τ				τ	0.662	0.778	0.875	0.937
10		τ	τ			0.301	0.377	0.426	0.465
11		τ		τ		0.440	0.566	0.673	0.768
12		τ			τ	0.576	0.719	0.827	0.907
13			τ	τ		0.273	0.355	0.442	0.550
14			τ		τ	0.501	0.640	0.740	0.818
15				τ	τ	0.408	0.507	0.605	0.673
16	τ	$-\tau$				0.646	0.774	0.869	0.933
17	τ		$-\tau$			0.538	0.651	0.746	0.834
18	τ			$-\tau$		0.410	0.507	0.580	0.662
19	τ				$-\tau$	0.665	0.788	0.870	0.935
20		τ	$-\tau$			0.547	0.693	0.814	0.904
21		τ		$-\tau$		0.339	0.430	0.526	0.622
22		τ			$-\tau$	0.589	0.727	0.831	0.907
23			τ	$-\tau$		0.242	0.315	0.364	0.422
24			τ		$-\tau$	0.505	0.634	0.732	0.822
25				τ	$-\tau$	0.408	0.508	0.601	0.673

According to the result in Table 2.5, a similar pattern exists here as in the single mean shift diagnosis case: the larger the mean shift magnitude, the higher the correct diagnosis rate. Moreover, there are no significant differences in the correct diagnosis

rates comparing cases 6-15 and cases 16-25. Generally speaking, the diagnosis accuracy is poor when the mean shift variable contains X_4, since X_4 has no sensor allocated.

2.5.3 Computational Time Analysis of the BASIS Algorithm

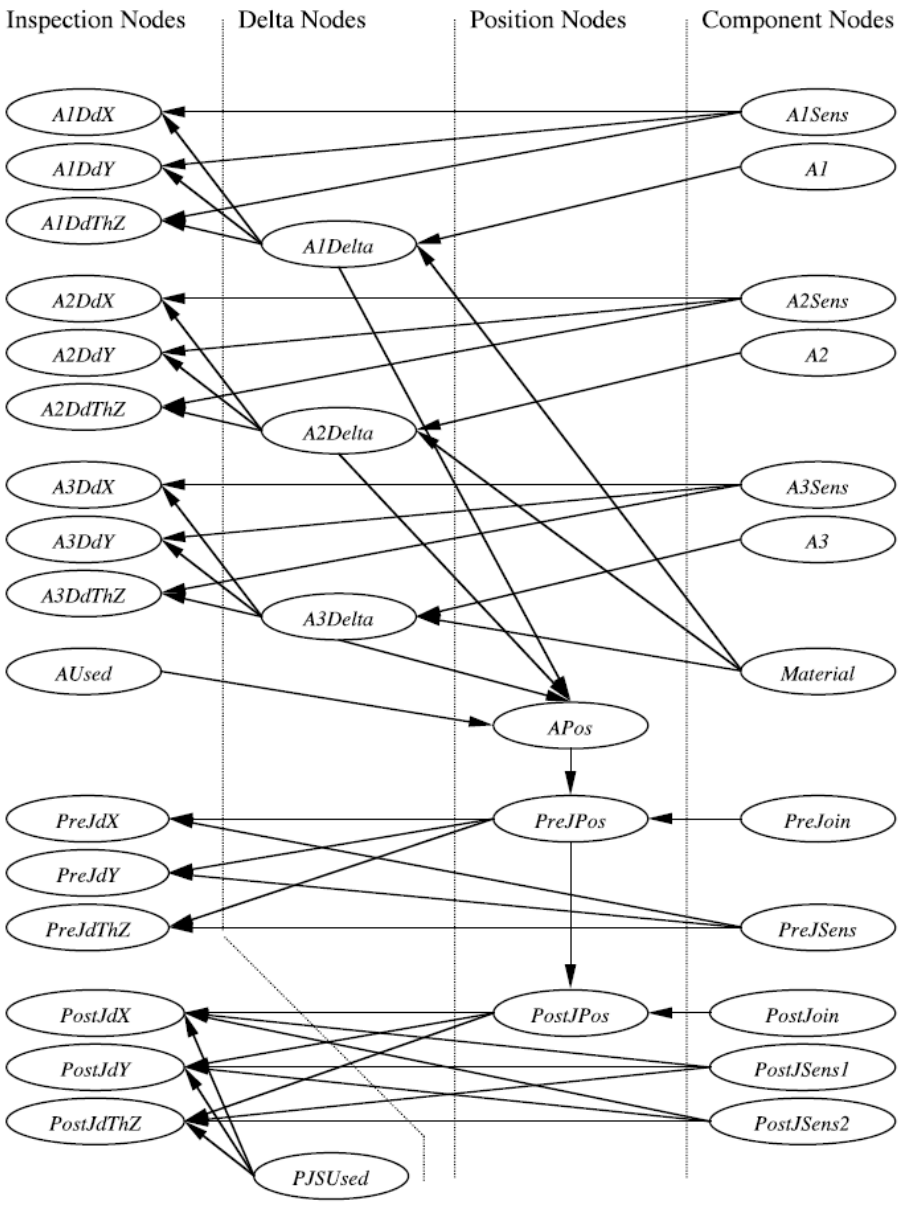

Figure 2.5: BN of a cap alignment process (Wolbrecht et al. 2000)

To demonstrate the effectiveness of the proposed BASIS algorithm, we further conduct the optimal sensor allocation study in a large-scale manufacturing process under the same combinations of τ and $ARL_U(\tau)$ requirements as shown in Table 2.1. Specifically, a BN with 35 variables involved in a cap alignment process at Hewlett Packard is considered (Wolbrecht et al. 2000; Li and Jin 2010), which is shown in Figure 2.5. Due to the page limits, we only focus on the computational time of the BASIS algorithm in this case study.

All experimental studies were performed using MATLAB V7.9 in Windows 7 operating system with two Intel Core i7-2820QM 2.30 GHz processors and 8 GB RAM. The average computational time to derive the optimal sensor allocation solution in a single mean shift case is about 75 seconds, while the average computational in a multiple mean shifts case ($p = 2$) is about 495 seconds.

2.6 Conclusion

Mean shift monitoring and diagnosis are fundamental problems in multivariate process control. While numerous methodologies have been developed with adequate performance when all the variables are measurable, it usually requires excessive cost of sensors in practice. Therefore, this chapter studies the problems of (1) how to optimally allocate sensors with minimum cost under different detection requirements, and (2) how to identify the process root cause with only partial information measurable.

In this chapter, a BN model is assumed available to represent the causal relationships among variables. The BASIS algorithm is proposed to find the optimal solution for process monitoring and then a diagnosis ranking method is developed to identify the root cause. The developed methodologies are successfully demonstrated on a hot forming process and a cap alignment process. The proposed BASIS algorithm is conducted in a systematic and intelligent way, such that for any potential solution $\boldsymbol{s}$, we

only need to compare its noncentrality parameter $\Delta(\boldsymbol{s})$ with the benchmark value $\tilde{\Delta}\big(card(\boldsymbol{s})\big)$ in order to determine its feasibility. Without the BASIS algorithm, in order to derive the optimal solution, expensive Monte Carlo simulations have to be implemented to evaluate the ARL performance of each potential sensor allocation solution under each objective, which is nearly inapplicable in real practice. We would also like to point out that the sensor allocation problem is an off-line effort made in the system design stage. Thus, it is critically important to generate the best sensor placement strategy under given requirement in the design stage. As a result, the computation time spent in searching for the optimal solution is less concern in this situation comparing with real-time applications.

This study has revealed that a trade-off problem occurs when detection speed, fault diagnosis accuracy and cost saving are taken into consideration. The monitoring and diagnosis capabilities that a DSN is able to provide depend strongly on the sensor deployment strategy in the system. Although an allocation design with fewer sensors can lower the running cost, fewer sensors can also prolong detecting time and cause a loss in diagnosability. In contrast, although an allocation plan with many sensors is able to expedite the detection for a mean shift and identify faulty variables more accurately, the cost associated with these sensors can be overwhelming. The final optimal strategy requires integrating the analysis of cost and product quality, which therefore is contingent, objective-oriented, and will ultimately depend on how the practitioner allocates the priorities towards cost, detection, and diagnosis. With the guaranteed customer satisfaction by optimally designing sensor allocation strategy, the average cycle time and cost associated with sensors and inventory can be eventually cut down.

CHAPTER 3

ADAPTIVE SENSOR ALLOCATION STRATEGY FOR PROCESS MONITORING AND DIAGNOSIS IN A BAYESIAN NETWORK

3.1 Introduction

As discussed in Chapter 2, the literature pertaining to sensor system design in quality engineering is indeed rich; however, most existing studies assume that the sensor layout is fixed once sensors are deployed in the network. The fixed sensor allocation strategy is preferable if the probability of a shift occurs at each variable is known, so that the sensor network can be centralized to monitor the shift variables. Unfortunately, such prior information is usually unknown or unreliable in practice. Due to the stochastic nature of the system in practice, different types of faults can occur at any time during production, which can result in a large detection delay and poor diagnosis accuracy. In fact, both Li and Jin (2010), and Liu and Shi (2012) have shown that the detection delay will be longer and the fault diagnosis accuracy will be deteriorated if the root cause variable is not directly measured, since a shift will be propagated and diluted in the downstream variables.

To address this problem, the adaptive strategy can be considered to compensate for the unresponsiveness of the monitoring schemes provided by the fixed strategy. There are mainly three types of adaptive strategies related to process control: adaptive charting techniques, adaptive sampling, and adaptive sensor allocation. Adaptive charting techniques are widely used in the quality control area to achieve certain optimality (e.g. minimize detection delay). Zhu and Jiang (2009) proposed an adaptive T^2 control chart that combined process monitoring and diagnosis in a unified manner. Tsung and Wang

(2010) did a literature review about adaptive charting techniques. They classified adaptive charts into two categories: those with variable sampling parameters and those with variable design parameters. Most adaptive charting techniques assume that the sensor network is fully deployed and thus all variables are measurable. On the other hand, adaptive sampling techniques exploit the correlation between measured samples to timely reduce/add the amount of acquisitions at certain region or adjust the sampling rate, which is mainly used for field estimation. Rahimi et al. (2005) proposed an adaptive sampling method by considering both actuation and sampling costs in an integrated manner for environmental field estimation. Fiorelli et al. (2006) described a methodology for cooperative control of multiple vehicles based on virtual bodies and artificial potentials for missions such as gradient climbing in an environmental field and feature tracking in an uncertain environment. Popa et al. (2006) proposed an extended Kalman filter-based adaptive sampling method to optimally estimate the parameters of distributed variable field models. Finally, adaptive sensor allocation strategy aims to redistribute scarce resources based on online observations to minimize a predefined cost function or maximize capability (e.g. maximize signal to noise ratio) (Hitchings and Castañón 2010). For example, adaptive sensor allocation strategy has been widely used to track object movement (Lim et al. 2006; Zoghi and Kahaei 2010). Although many research efforts have been focused on this topic, adaptive sensor allocation strategy is seldom explored in the quality control field in terms of improving monitoring and diagnosis capabilities. Instead of adaptively changing charting techniques and sampling strategy, this chapter focuses on adaptively reallocating sensors based on online observations to reduce detection delay and also improve fault diagnosis accuracy. Thus, adaptive strategy refers to the adaptive sensor allocation strategy in the remaining of this chapter.

Adaptive strategy for process control is a challenging problem due to the following reasons: (i) the number of potential decisions is large. Assume that there are total of m variables in a system and the number of available sensors is q (e.g. $q \leq m$).

Thus, at each moment, there are $\binom{m}{q}$ ways to redistribute sensors. (ii) The available information is incomplete due to partial deployment of sensors.

To develop the adaptive strategy, a BN is adopted to represent the causal relationships among a set of variables in a DSN. BN has been widely used in fault detection, diagnosis, and prognostic applications (Li, Jin, and Shi 2008; Camci and Chinnam 2010). To limit the scope of the chapter, we assume that a BN has already been obtained, so that no more learning procedures are involved in the following discussions. Under this framework, we focus on single mean shift detection and diagnosis when developing the adaptive sensor allocation strategy. From our experience working with industrial process, this assumption is typically true for a well-maintained manufacturing system, in which a process change can be quickly detected and corrected. As a result, the proposed methodology is more favorable for a relatively robust manufacturing production system, in which it is unlikely to see multiple variables change simultaneously. On the other hand, both the process change detection and the root cause diagnosis will become much more challenging, when multiple shifts occur simultaneously in a system. We decide to leave the change detection and the fault diagnosis of multiple shifts as a future work. We further assume that a shift will remain constant until it is detected and corrected, whereas the variance of each variable stays constant when the system operates in abnormal conditions. In addition, the number of available sensors, q, is assumed to be fixed, which is subjected to the budget constraint.

The objective of this chapter is to study the adaptive sensor allocation strategy, which can enhance process monitoring and diagnosis capabilities compared with the fixed sensor allocation strategy. The adaptive strategy discussed in this chapter can not only be used to update the sensor layout, but also to determine the operating mode of each sensor (i.e. when only q sensors can be in active state in a fully deployed DSN) for online data acquisition and transmission purposes due to the limited bandwidth or energy

constraint. An overview of the proposed adaptive strategy is shown in Figure 3.1. The proposed methodology has three major steps, which include: (i) determining when to reallocate sensors; (ii) estimating the shift variables based on each incoming sample; and (iii) redistributing sensors onto the identified shift variables. Since this procedure also involves automatic fault isolation, the diagnosis accuracy is expected to be boosted.

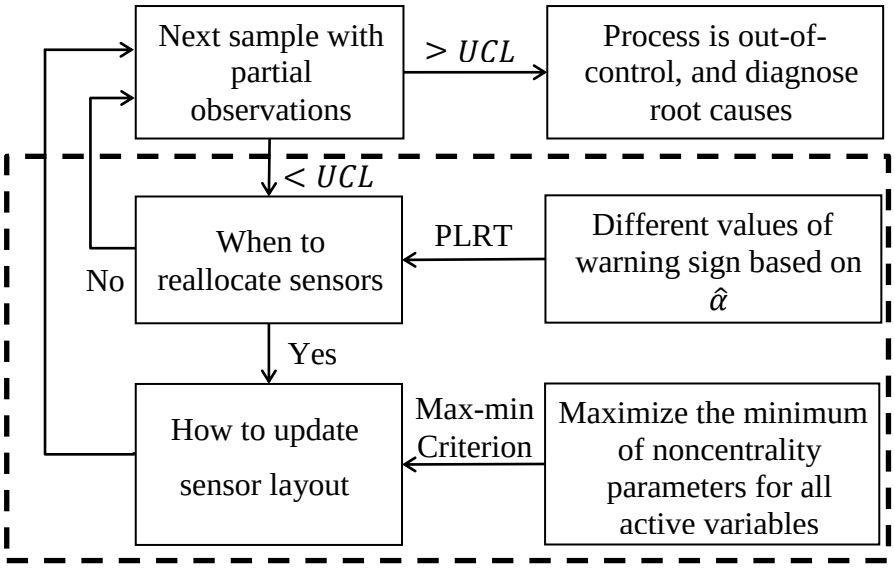

Figure 3.1: The overall flow chart of the proposed adaptive strategy

The rest of the chapter is organized as follows: Section 3.2 proposes an adaptive strategy that can update the sensor layout based on online observations to improve detection delay and fault diagnosis accuracy. Section 3.3 further illustrates and evaluates the proposed methodology based on a hot forming process and a cap alignment process. Finally, Section 3.4 draws a conclusion and discusses future research directions.

3.2 Adaptive Sensor Allocation Strategy in a BN

The proposed adaptive sensor allocation strategy is built upon the fixed sensor allocation strategy (Liu and Shi 2012). For simplicity, the variables notations and

problem formulations will be consistent with (Liu and Shi 2012), and thus are omitted in this chapter. Although the aforementioned monitoring and diagnosis methods are theoretically sound, there are two fundamental limitations: (i) If the root cause variable has no sensor deployed, the detection delay will be much longer than the case when it is directly measured (Li and Jin 2010; Liu and Shi 2012). Since a shift will be propagated and diluted in its downstream variables, this result is consistent with the analysis in (Li, Jin and Shi 2008; Hawkins 1993). (ii) Due to the existence of minimal diagnosable class, the root cause variable cannot be uniquely identified with certain sensor allocation strategy. This phenomenon is more obvious as the number of available sensors becomes smaller. To tackle these two issues, we propose an adaptive sensor allocation strategy which can improve both monitoring and diagnosis capabilities.

Since the adaptive strategy is conducted during online monitoring before an out-of-control signal is triggered, there are two challenging questions: (i) when to reallocate sensors; and (ii) how to update sensor layout. One possibility is to establish two separate tables to record the number of times that incoming samples indicate adding or removing sensors in each variable. Then, reallocation strategy can be implemented once the cumulative counter information crosses a predefined threshold, as the approaches in CUSUM control chart (Page 1954). However, this approach will not only aggravate the workload in the monitoring system design (e.g. determine the optimal value of the threshold), but also require considering where to remove (add) sensors when the criterion for adding (removing) a sensor is satisfied. In addition, the time when an out-of-control sample occurs in a system is usually unknown and unpredictable. Therefore, the cumulative counter information collected during normal operation condition can affect the performance of the adaptive strategy if it is inappropriately used. In order to address these issues, a novel adaptive sensor allocation strategy is proposed as follows.

3.2.1 When to Reallocate Sensors

In this section, we will show that the diagnosis ranking method (Liu and Shi 2012) is equivalent to the penalized likelihood ratio test (PLRT), which can be extended to determine when to reallocate sensors. Since the PLRT is a variant of the generalized likelihood ratio test (GLRT), we first go over the GLRT when examining the following hypothesis $H_0: \boldsymbol{\delta} = \mathbf{0}$ with $H_1: \boldsymbol{\delta} \neq \mathbf{0}$. The statistics for the GLRT can be expressed as:

$$\lambda(\boldsymbol{X_s}) = \frac{max_{\boldsymbol{\delta}=\mathbf{0}}\, L(\boldsymbol{X_s}, \boldsymbol{\delta})}{max_{\boldsymbol{\delta}\neq\mathbf{0}}\, L(\boldsymbol{X_s}, \boldsymbol{\delta})}, \tag{3.1}$$

where $L(\boldsymbol{X_s}, \boldsymbol{\delta})$ is the likelihood when observing $\boldsymbol{X_s}$ with the mean shift $\boldsymbol{\delta}$. The null hypothesis is rejected if $\lambda(\boldsymbol{X_s}) \leq b_1(\boldsymbol{s})$, where $b_1(\boldsymbol{s})$ is a constant number that corresponds to a specific type I error and sensor allocation set $\boldsymbol{s}$. Since

$$L(\boldsymbol{X_s}, \boldsymbol{\delta}) = \frac{1}{(2\pi)^{\frac{card(s)}{2}} |\boldsymbol{M_s}|^{\frac{1}{2}}} e^{-\frac{\left(\boldsymbol{X_s} - \left(\boldsymbol{A^{-1}\delta}\right)_{\boldsymbol{s}}\right)^T \boldsymbol{M_s^{-1}} \left(\boldsymbol{X_s} - \left(\boldsymbol{A^{-1}\delta}\right)_{\boldsymbol{s}}\right)}{2}},$$

the rejection region can be expressed as:

$$\Lambda\left(\lambda(\boldsymbol{X_s})\right) = min_{\boldsymbol{\delta}\neq\mathbf{0}}\left(\boldsymbol{\delta^T} (\boldsymbol{A^{-1}})_{\boldsymbol{s}^r}^{\boldsymbol{T}} \boldsymbol{M_s^{-1}} (\boldsymbol{A^{-1}})_{\boldsymbol{s}^r} \boldsymbol{\delta} - 2\boldsymbol{X_s^T M_s^{-1}} (\boldsymbol{A^{-1}})_{\boldsymbol{s}^r} \boldsymbol{\delta}\right) \leq b_2(\boldsymbol{s}), \tag{3.2}$$

where $\Lambda\left(\lambda(\boldsymbol{X_s})\right) = 2log\left(\lambda(\boldsymbol{X_s})\right)$ and $b_2(\boldsymbol{s}) = 2log(b_1(\boldsymbol{s}))$.

It is straightforward to see that equation (3.2) will be minimized when $(\boldsymbol{A^{-1}})_{\boldsymbol{s}^r} \boldsymbol{\delta} = \boldsymbol{X_s}$. However, since $\boldsymbol{X}$ is contaminated by noise $\boldsymbol{V}$, this solution needs to be revised to consider the noise factors. To address this problem, we introduce the PLRT with a L_0 penalty norm, $\sum_k I(|\delta_k| \neq 0)$, where $|\delta_k|$ is the absolute value of the k^{th} element of $\boldsymbol{\delta}$. Since we only focus on single mean shift detection and diagnosis, the rejection region can be transformed into:

$$\Lambda\left(\lambda(\boldsymbol{X_s})\right) = min_{\boldsymbol{\delta}\neq\mathbf{0}}\left(\boldsymbol{\delta^T} (\boldsymbol{A^{-1}})_{\boldsymbol{s}^r}^{\boldsymbol{T}} \boldsymbol{M_s^{-1}} (\boldsymbol{A^{-1}})_{\boldsymbol{s}^r} \boldsymbol{\delta} - 2\boldsymbol{X_s^T M_s^{-1}} (\boldsymbol{A^{-1}})_{\boldsymbol{s}^r} \boldsymbol{\delta}\right) \leq b_2(\boldsymbol{s})$$

$$\textit{subject to } \sum_k I(|\delta_k| \neq 0) \leq 1. \tag{3.3}$$

Because increasing the number of nonzero elements in $\boldsymbol{\delta}$ will always decrease $\Lambda\left(\lambda(\boldsymbol{X_s})\right)$, the inequality constraint in equation (3.3) will be deterministically achieved. Thus, the rejection region can be rewritten as:

$$\Lambda\big(\lambda(\boldsymbol{X_s})\big) = min_k\big\{min_{\boldsymbol{\delta}(k)}\big\{\boldsymbol{\delta}(k)^{\boldsymbol{T}}(\boldsymbol{A^{-1}})_{\boldsymbol{s}^r}^{\boldsymbol{T}}\boldsymbol{M_s^{-1}}(\boldsymbol{A^{-1}})_{\boldsymbol{s}^r}\boldsymbol{\delta}(k) - 2\boldsymbol{X_s^T}\boldsymbol{M_s^{-1}}(\boldsymbol{A^{-1}})_{\boldsymbol{s}^r}\boldsymbol{\delta}(k)\big\}\big\} \le b_2(\boldsymbol{s})$$

$$\textit{subject to } \boldsymbol{\delta}(k) \in R^k, \tag{3.4}$$

where the left hand side of the inequality is consistent with equation (2.15). The PLRT formulation can force small mean shifts to zero and automatically leave out the most significant shift variable. Thus, equation (3.4) can be used to identify the root cause variable if we assume a mean shift will be propagated and diluted along the directed arcs towards the descendants in a BN. Let

$$C_{\boldsymbol{s}}(k) = max_{\boldsymbol{\delta}(k)}\{-\boldsymbol{\delta}(k)^{\boldsymbol{T}}(\boldsymbol{A^{-1}})_{\boldsymbol{s}^r}^{\boldsymbol{T}}\boldsymbol{M_s^{-1}}(\boldsymbol{A^{-1}})_{\boldsymbol{s}^r}\boldsymbol{\delta}(k) + 2\boldsymbol{X_s^T}\boldsymbol{M_s^{-1}}(\boldsymbol{A^{-1}})_{\boldsymbol{s}^r}\boldsymbol{\delta}(k)\} \text{ and}$$

$$C_{\boldsymbol{s}} = max_k\, C_{\boldsymbol{s}}(k),$$

$$\textit{subject to } \boldsymbol{\delta}(k) \in R^k. \tag{3.5}$$

Then, the rejection region can be expressed as follows for better interpretation:

$$C_{\boldsymbol{s}} \ge B(\boldsymbol{s}), \tag{3.6}$$

where $B(\boldsymbol{s}) = -b_2(\boldsymbol{s})$ and can be considered as a warning sign to determine when to reallocate sensors. Note that the boundary point $B(\boldsymbol{s})$ is a function of $\boldsymbol{s}$, which corresponds to a specific type I error $\hat{\alpha}$. To determine the value of $B(\boldsymbol{s})$, for each given $\boldsymbol{s}$, we can implement the Monte Carlo simulation to estimate the empirical distribution of $C_{\boldsymbol{s}}$, $F_{n(\boldsymbol{s})}(t)$ given $\boldsymbol{\delta} = \boldsymbol{0}$ (see Appendix A.3 for details). Depending on the different values of warning signs (i.e. associated with different values of $\hat{\alpha}$), $B(\boldsymbol{s})$ can be set as $D_{\hat{\alpha}}(\boldsymbol{s}) = F_{n(\boldsymbol{s})}^{\boldsymbol{-1}}(1-\hat{\alpha})$, where $F_{n(\boldsymbol{s})}^{\boldsymbol{-1}}(1-\hat{\alpha})$ is the inverse of the empirical distribution function of $F_{n(\boldsymbol{s})}(t)$ at percentile $100 * (1-\hat{\alpha})$.

3.2.2 How to Update Sensor Layout

Once the condition of reallocating sensors is satisfied (i.e. $C_{\boldsymbol{s}} \ge D_{\hat{\alpha}}(\boldsymbol{s})$), the next question is how to update sensor layout. Hawkins (1993) and Li, Jin and Shi (2008) have shown that a mean shift will be propagated and diluted in its downstream variables, and

thus it is desirable to add a sensor onto the root cause variable that identified by the PLRT. Although this approach sounds straightforward, there are two open questions to be addressed: (i) since the number of available sensors is fixed, one sensor needs to be removed first in order to be redeployed onto the identified variable; however, which sensor should be removed is hard to determine. (ii) Due to the existence of minimal diagnosable class, the PLRT can only identify the class of variables that are equally likely to be responsible for the shift. In other words, variables within the same minimal diagnosable class will achieve the same objective value in equation (3.4). To address these two problems, we will first give a definition about *active adding variable* and *active adding set*:

Definition 3.1: The i^{th} variable is said to be *active adding* if $i = argmax_k(C_{\boldsymbol{s}}(k))$ and $C_{\boldsymbol{s}} > D_{\widehat{\alpha}}(\boldsymbol{s})$. The set that consists of all the *active adding variables* is defined as *active adding set*, which is denoted as $\boldsymbol{H}$.

Since the monitoring statistics $T^2 = \boldsymbol{X_s^T M_s^{-1} X_s}$ follows a noncentral chi-square distribution $\mathcal{X}'^2_{card(\boldsymbol{s})}(\Delta(\boldsymbol{s}))$ with noncentrality parameter $\Delta(\boldsymbol{s}) = (\boldsymbol{A^{-1}\delta})_{\boldsymbol{s}}^{\boldsymbol{T}} \boldsymbol{M_s^{-1}} (\boldsymbol{A^{-1}\delta})_{\boldsymbol{s}} = \boldsymbol{\delta} (\boldsymbol{A^{-1}})_{\boldsymbol{s}^r}^{\boldsymbol{T}} \boldsymbol{M_s^{-1}} (\boldsymbol{A^{-1}})_{\boldsymbol{s}^r} \boldsymbol{\delta}$, the reallocation strategy $\boldsymbol{s}'$ should maximize $\Delta(\boldsymbol{s}')$ in order to enhance monitoring capability. Let ${}^{i}\Delta(\boldsymbol{s}) = \boldsymbol{e_i^T} (\boldsymbol{A^{-1}})_{\boldsymbol{s}^r}^{\boldsymbol{T}} \boldsymbol{M_s^{-1}} (\boldsymbol{A^{-1}})_{\boldsymbol{s}^r} \boldsymbol{e_i}$, where $\boldsymbol{e}_i = [0 \ \dots 1 \ \dots 0]^T$ with the i^{th} element equal to one. Therefore, ${}^{i}\Delta(\boldsymbol{s})$ can be treated as a benchmark value to evaluate the performance of the sensor allocation strategy $\boldsymbol{s}$ to detect the mean shift that occurs at variable X_i. In other words, when a mean shift occurs at variable X_i, the larger the value of ${}^{i}\Delta(\boldsymbol{s})$ is, the smaller the out-of-control ARL will be. Since all variables within the active adding set are equally likely to be responsible for the shift, we propose a max-min criterion, in which the reallocation strategy will maximize the minimum of ${}^{i}\Delta(\boldsymbol{s})$ for any variable X_i that belongs to the active adding set, $\boldsymbol{H}$. Mathematically,

$$\boldsymbol{s}' = argmax_{\boldsymbol{s}}\{min_{i \in \boldsymbol{H}}\left({}^{i}\Delta(\boldsymbol{s})\right)\}. \tag{3.7}$$

In certain cases, there may be multiple reallocation strategies that can achieve the same optimum in equation (3.7). Then, the max-min criterion can be implemented again based on the variables from the set $\boldsymbol{H}^C = \{1, \dots, m\} \backslash \boldsymbol{H}$, where $\boldsymbol{H}^C$ represents the set of elements in $\{1, \dots, m\}$ but not in $\boldsymbol{H}$. The motivation behind this approach is that if the solution is not unique by implementing the max-min criterion running on the active adding set, considering a reallocation strategy which optimizes the max-min criterion based on the remaining variables can further enhance monitoring capability, in case the root cause variable is not identified in the active adding set. Mathematically,

$$\boldsymbol{s}'' = argmax_{\boldsymbol{s} \in \boldsymbol{s}'} \{min_{j \in \boldsymbol{H}^C} \left({}^{j}\Delta(\boldsymbol{s}) \right)\}$$

$$\text{if } \boldsymbol{s}' = argmax_{\boldsymbol{s}} \{min_{i \in \boldsymbol{H}} \left({}^{i}\Delta(\boldsymbol{s}) \right)\} \text{ is not unique.} \tag{3.8}$$

It is worth mentioning that once the sensor on any leaf node is removed, it cannot be added back. Thus, all leaf nodes are required to have sensors deployed all the time (i.e. q is required to be larger than $card(\boldsymbol{LF})$). On the other hand, since the adaptive strategy is implemented online, the computational time is critical. We can offline calculate the value of ${}^{i}\Delta(\boldsymbol{s})$ for $\forall i \in \{1, \dots, m\}$ and $\forall \boldsymbol{s}$, where the computational complexity is $O(m \cdot \binom{m - card(\boldsymbol{LF})}{q - card(\boldsymbol{LF})})$. In this way, the computational complexity for implementing the max-min criterion online is O(the number of potential different active adding sets).

Because the PLRT can automatically identify the variable that is most likely to be responsible for the mean shift and the max-min criterion can maximize the noncentrality parameter, both the type II error of T^2 control chart and the out-of-control ARL are expected to be decreased after reallocating sensors each time. In addition, since the procedure of the adaptive strategy automatically involves fault isolation by redistributing sensors to concentrate on monitoring the shift variables, the fault diagnosis accuracy is expected to be boosted. Another advantage of this proposed adaptive strategy is that the in-control ARL will not be affected, since it only depends on the type I error α of T^2

control chart (i.e. $UCL = \mathcal{X}_{\alpha}^{2}(card(\boldsymbol{s}))$), but is independent to the value of warning sign (i.e. associated with $\hat{\alpha}$) and how sensors are redeployed during online monitoring.

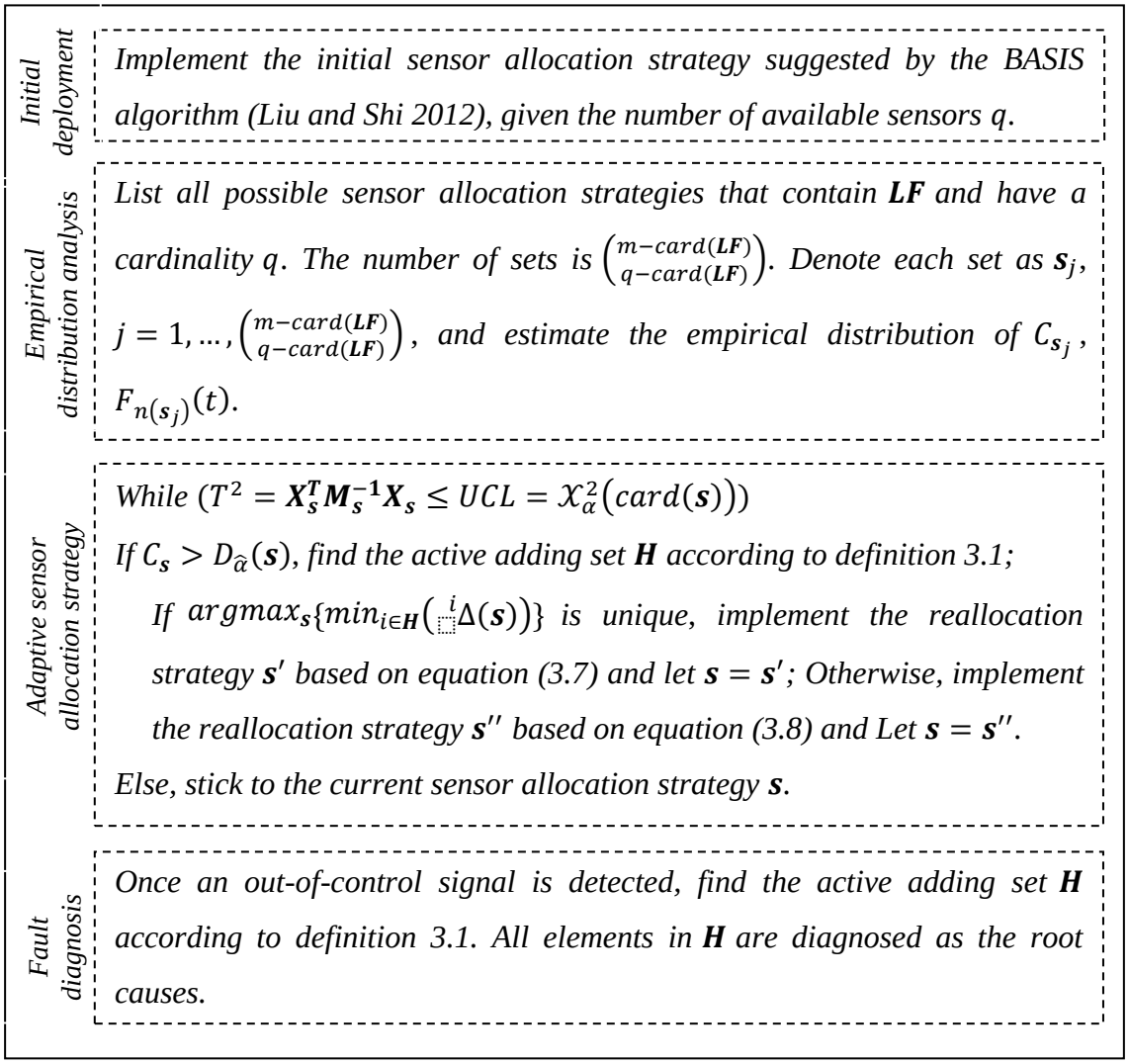

Figure 3.2: Adaptive sensor allocation strategy for single mean shift detection and diagnosis

The initial sensor allocation strategy is not crucial since the adaptive strategy will be updated based on online observations; however, we can implement the BASIS algorithm (Liu and Shi 2012), which can provide the optimal solution when the fixed strategy is considered. This sensor deployment strategy can ensure a fast response to an

initial out-of-control situation. The idea of our proposed adaptive sensor allocation strategy is summarized in Figure 3.2.

3.2.3 An Illustration Example

Consider the hot forming process in Figure 2.1 with initial sensor deployment as $\boldsymbol{s} = \{1, 3, 5\}$. A series of sample points with 1.5 mean shifts at the first sample of X_2 are generated until an out-of-control sample is detected by the T^2 control chart with $\alpha = 0.01$ (i.e. $UCL = \mathcal{X}^2_{0.01}(3) = 11.345$). Table 3.1 shows the value of each ${}^{i}\Delta(\boldsymbol{s})$ for all six (i.e. $\binom{5-1}{3-1}$) potential sensor allocation strategies, where a "+" represents a sensor is deployed on the variable. Table 3.2 illustrates how the adaptive sensor allocation strategy evolves over time based on the online measurements. $\hat{\alpha}$ is chosen to be 1.0 for illustration, which indicates sensor layout is updated after each sample. The second to the sixth columns (i.e. the columns associated with the headers "X_i") record the sensor measurement; the seventh to the eleventh columns illustrate the $C_{\boldsymbol{s}}(i)$ value; the twelfth column shows the active adding set given by definition 3.1; and the last column lists the updated sensor layout based on the max-min criterion after each sample. In this example, the T^2 control chart signals at the fourth sample. With sensor placement on nodes {1, 2, 4}, {2, 5} forms a minimum diagnosable class and thus the final conclusion about the root cause variable is either X_2 or X_5.

The initial allocation strategy {1, 3, 5} is suggested by the BASIS algorithm (Liu and Shi 2012) which is the optimal solution when fixed sensor allocation strategy is considered. However, {1, 3, 5} is not effective to detect the mean shift that occurs at variable X_2 or X_4, since the value of ${}^{2}\Delta(\boldsymbol{s})$ or ${}^{4}\Delta(\boldsymbol{s})$ ($\boldsymbol{s}$ ={1, 3, 5}) is relatively small compared to other allocation strategies. Thus, this example illustrates how the adaptive strategy can be favorable to mean shift detection via timely self-adjusted sensor redeployment.

Table 3.1: The value of each ${}^{i}\Delta(\boldsymbol{s})$ for all potential sensor allocation strategies ("+" represents a sensor is deployed on the variable)

X_1	X_2	X_3	X_4	X_5	${}^{1}\Delta(\boldsymbol{s})$	${}^{2}\Delta(\boldsymbol{s})$	${}^{3}\Delta(\boldsymbol{s})$	${}^{4}\Delta(\boldsymbol{s})$	${}^{5}\Delta(\boldsymbol{s})$
+	+	+			2.337	1.13	1.13	0.55	0.119
+	+		+		2.054	1.321	0.23	1	0.14
+	+			+	1.902	1.149	0.213	0.325	1
+		+	+		1.477	0.486	1.899	1	0.051
+		+		+	1.461	0.481	1.055	0.506	1
+			+	+	1.425	0.47	0.16	1	1

Table 3.2: Evolutions of sensor layout by implementing the adaptive strategy when 1.5 mean shifts occur at X_2

No.	X_1	X_2	X_3	X_4	X_5	$C_{\boldsymbol{s}}(1)$	$C_s(2)$	$C_s(3)$	$C_s(4)$	$C_s(5)$	Active adding set	Updated $\boldsymbol{s}'$
1	2.71		1.30		0.49	5.456	5.456	0.533	3.419	0.243	{1, 2}	{1, 2, 4}
2	1.26	2.07		-0.11		0.019	5.925	0.019	0.011	5.925	{2, 5}	{1, 2, 5}
3	-0.07	1.00			0.19	1.111	1.336	1.111	0.233	0.035	{2}	{1, 2, 4}
4	1.06	3.15		-1.03		0.533	17.638	0.533	1.051	17.638	{2, 5}	

3.3 Case Studies

3.3.1 Hot Forming Process

3.3.1.1 Simulation Setup

This study will evaluate the performance of the proposed adaptive sensor allocation strategy (Figure 3.2) based on the hot forming process (Figure 2.1). There are five variables in the hot forming process. Thus, five potential single mean shift scenarios with different shift magnitudes will be discussed in this study. In addition, different number of available sensors q with different combinations of $\hat{\alpha}$ values will be implemented in the system to thoroughly compare the performance of the adaptive and the fixed strategy. It is aware that the fixed strategy corresponds to the case when $\hat{\alpha}$ equals to 0. The parameters selected in the case study are based on the characteristics of the actual system.

The adaptive strategy is conducted during online monitoring no matter when the system is in-control or out-of-control. Therefore, at the moment when a mean shift occurs, the sensor layout is not unique in reality, but it can affect the monitoring performance. In order to address this issue, we consider the least favorable sensor layout for mean shift detection, which is called the worst initial sensor deployment (WISD), when a mean shift occurs. In other words, when a mean shift occurs at variable X_i, we assume that sensors are deployed right on the variables that result in the smallest ${}^{i}\Delta(\boldsymbol{s})$ value based on Table 3.1, no matter how sensor layout has evolved before the mean shift occurs. In this way, we can get the most conservative comparisons between the adaptive and the fixed strategy. For example, if $q = 3$, sensors are deployed on nodes $\{1, 3, 4\}$ when a mean shift occurs at variable X_5, whereas sensors are deployed on nodes $\{1, 2, 5\}$ when a mean shift occurs at variable X_4.

To evaluate the monitoring capability, we will focus on two metrics for ARL performance evaluation: (i) the maximum out-of-control ARL to detect the same amount of mean shift that occurs at each variable; and (ii) the average out-of-control ARL to detect the same amount of mean shift that occurs at each variable. Both metrics have practical meanings. The first metric is intended to show the maximum ARL needed in the worst detection case, which can provide a benchmark value to satisfy customer requirements (i.e. how fast an out-of-control status can be detected if a mean shift is possible to occur at any variable), whereas the second metric assesses the overall detection delay. On the other hand, to evaluate the fault diagnosis capability, we give two definitions about *correct diagnosis* and *uniquely correct diagnosis*:

Definition 3.2: A diagnosis result is called *correct* if the root cause variable belongs to the active adding set.

Definition 3.3: A diagnosis result is called *uniquely correct* if the root cause variable belongs to the active adding set and the cardinality of the set is one.

Specifically, we focus on the rates of these two metrics: (i) the rate of correct diagnosis divided by the average cardinality of the active adding set; and (ii) the rate of uniquely correct diagnosis. The first metric measures the overall capability of the fault diagnosis accuracy, which is insensitive to the number of solutions identified in the active adding set. For example, if the random guess algorithm is implemented in the fault diagnosis step, then the result of the first metric will always be $1/m$ (recall m is the total number of variables), no matter how many solutions are identified in the active adding set. In other words, the first metric evaluates on average, the probability that a solution in the active adding set will be the root cause variable. On the other hand, the second metric measures the probability that the mean shift variable can be uniquely and correctly diagnosed. The detailed simulation steps can be found in Appendix A.4.

3.3.1.2 Performance Evaluations and Comparisons

Tables 3.3, 3.4 and 3.5 summarize the performance comparisons between the adaptive and the fixed strategy under different combinations of mean shift magnitudes τ, number of available sensors q and $\hat{\alpha}$ values. Seven metrics RL_{max}, $\overline{\overline{RL}}$, F_{min}, UF_{min}, $\bar{\bar{F}}$, $\overline{\overline{UF}}$ and $\overline{\overline{AS}}$ are considered for performance evaluations (see Appendix A.4 for details). According to the definitions of these metrics, RL_{max} and $\overline{\overline{RL}}$ are desired to be as small as possible, which measure the monitoring capability, whereas F_{min}, UF_{min}, $\bar{\bar{F}}$ and $\overline{\overline{UF}}$ are desired to be as large as possible, which measure the fault diagnosis capability. There is one additional column called "Impv.", which shows the percentage of improvement (i.e. positive value) or deterioration (i.e. negative value) by implementing the adaptive strategy ($\hat{\alpha} = 1$) over the fixed strategy ($\hat{\alpha} = 0$).

According to the results in Tables 3.3, 3.4 and 3.5, the following conclusions can be drawn:

(i) The adaptive strategy outperforms the fixed strategy in terms of detection delay and fault diagnosis accuracy. Generally speaking, the adaptive strategy significantly improves the monitoring capability (which is measured by RL_{max} and $\overline{\overline{RL}}$ metrics) and the diagnosis capability (which is measured by F_{min}, $\bar{\bar{F}}$, UF_{min} and $\overline{\overline{UF}}$ metrics) under different fault scenarios. This enhanced monitoring capability ensures that the mean shift abnormality can be detected in a timely manner, and thus less defective products can be produced. In addition, the enhanced diagnosis capability ensures that less effort spent in investigating the assignable causes, and thus production downtime and inventory level can be reduced.

(ii) As $\hat{\alpha}$ increases from 0 to 1, the advantages of the adaptive strategy over the fixed strategy become more significant. Both monitoring and diagnosis capabilities achieve the best at $\hat{\alpha} = 1$, where sensors are reallocated after each sample. However, the side effect is the increased number of times of sensor redeployment. If we assume that it is costless to change sensor layout or minimizing detection delay is the first priority, the adaptive strategy with $\hat{\alpha} = 1$ is preferred. In this way, the computational time spent in estimating the appropriate value for the warning sign can be saved. Otherwise, the best $\hat{\alpha}$ value should be determined by considering the detection delay, the fault diagnosis accuracy and the cost of reallocating sensors in an integrated manner. Another interesting phenomenon is that as $\hat{\alpha}$ increases from 0 to 1, the amount of improvement in the monitoring and diagnosis capabilities becomes less significant. For example, in the case of $q = 2$ and $\tau = 1.5$ in Table 3.3, the amount of reductions in $\overline{\overline{RL}}$ is [9.602, 1.377, 0.621, 0.406, 0.357] as $\hat{\alpha}$ increases from 0 to 1 with equal interval of 0.2.

(iii) As τ becomes larger, the mean shift abnormality is easier to be detected by the control chart, which is consistent with our intuition. However, the diagnosis accuracy is not guaranteed to be always increased. For example in Table 3.4, all the metrics

associated with the diagnosis capability, F_{min}, $\bar{\bar{F}}$, UF_{min} and $\overline{\overline{UF}}$ are deteriorated as τ increases from 2.5 to 3. There are three reasons for these observations: (a) As the mean shift becomes significant, it is more noticeable and can be detected even with a poorly deployed sensor strategy. Thus, the sensor layout may not be able to update to the one that is most favorable to fault diagnosis when an out-of-control signal is triggered. (b) The WISD in Tables 3.3-3.5 only shows the most conservative comparisons between the adaptive and the fixed strategy. (c) The adaptive strategy with the max-min criterion is proposed primarily to minimize detection delay instead of maximizing diagnosis accuracy, and thus it is not guaranteed to outperform the fixed strategy in term of diagnosis capability in any fault scenario. Due to the aforementioned reasons, in certain cases, the metrics associated with the diagnosis capability in the "Impv." column can even be negative, especially when q and τ are relatively large.

(iv) As q increases, the advantages of the adaptive strategy over the fixed strategy become less pronounced. This is because the sensor network gets closer to the fully deployed network as the number of available sensors increases. Thus, there is less number of candidate allocation strategies when redeploying sensors. At the extreme case when $q = m$ (i.e. a fully deployed sensor network), the adaptive strategy is the same as the fixed strategy.

Table 3.3: Performance comparisons between the adaptive and the fixed strategy under different mean shift magnitudes when the number of available sensors is 2

	Fixed	**Adaptive with WISD**						**Fixed**	**Adaptive with WISD**					
	$q = 2$ and $\tau = 1.5$							$q = 2$ and $\tau = 2$						
$\hat{\alpha} =$	0	0.2	0.4	0.6	0.8	1.0	Impv.	0	0.2	0.4	0.6	0.8	1.0	Impv.
RL_{max}	62.16	27.76	27.58	27.42	27.32	27.24	0.56	44.97	15.35	15.29	15.24	15.19	15.15	0.66
$\overline{\overline{RL}}$	30.03	20.42	19.05	18.43	18.02	17.66	0.41	19.02	11.33	10.12	9.58	9.26	9.06	0.52
F_{min}	0.22	0.26	0.26	0.26	0.26	0.26	0.16	0.23	0.27	0.27	0.27	0.27	0.27	0.18
$\bar{\bar{F}}$	0.33	0.39	0.4	0.41	0.41	0.42	0.28	0.36	0.44	0.46	0.47	0.48	0.48	0.36
UF_{min}	0	0	0	0	0	0	0	0	0	0	0	0	0	0
$\overline{\overline{UF}}$	0.18	0.36	0.38	0.39	0.4	0.4	1.2	0.19	0.41	0.43	0.44	0.45	0.45	1.37
$\overline{\overline{AS}}$	0	3.78	5.76	7.28	8.55	9.57	-	0	2.46	3.36	3.95	4.38	4.72	-
	$q = 2$ and $\tau = 2.5$							$q = 2$ and $\tau = 3$						
RL_{max}	33.52	9.26	9.19	9.17	9.16	9.16	0.73	23.85	7.34	5.74	5.72	5.7	5.69	0.76
$\overline{\overline{RL}}$	12.81	7.11	6.16	5.77	5.53	5.38	0.58	8.65	4.97	4.25	3.94	3.76	3.66	0.58
F_{min}	0.23	0.27	0.27	0.27	0.27	0.27	0.17	0.24	0.27	0.27	0.27	0.27	0.27	0.15
$\bar{\bar{F}}$	0.37	0.46	0.49	0.5	0.51	0.52	0.38	0.39	0.47	0.5	0.52	0.52	0.53	0.37
UF_{min}	0	0	0	0	0	0	0	0	0	0	0	0	0	0
$\overline{\overline{UF}}$	0.2	0.43	0.45	0.46	0.47	0.47	1.42	0.2	0.43	0.46	0.47	0.48	0.48	1.42
$\overline{\overline{AS}}$	0	1.74	2.17	2.43	2.59	2.71	-	0	1.29	1.52	1.63	1.7	1.75	-

Table 3.4: Performance comparisons between the adaptive and the fixed strategy under different mean shift magnitudes when the number of available sensors is 3

	Fixed	**Adaptive with WISD**						**Fixed**	**Adaptive with WISD**					
	$q = 3$ and $\tau = 1.5$							$q = 3$ and $\tau = 2$						
$\hat{\alpha} =$	0	0.2	0.4	0.6	0.8	1.0	Impv.	0	0.2	0.4	0.6	0.8	1.0	Impv.
RL_{max}	28.41	21.78	19.5	18.77	18.26	17.75	0.38	15.84	12.85	10.54	9.57	9	8.67	0.45
$\overline{\overline{RL}}$	17.79	15.04	13.87	13.47	13.21	13.03	0.27	9.2	8.13	7.09	6.64	6.4	6.26	0.32
F_{min}	0.4	0.42	0.43	0.43	0.43	0.44	0.08	0.44	0.45	0.47	0.47	0.48	0.48	0.1
$\bar{\bar{F}}$	0.53	0.59	0.61	0.61	0.61	0.62	0.16	0.6	0.65	0.68	0.69	0.7	0.7	0.17
UF_{min}	0	0.19	0.19	0.2	0.2	0.2	-	0	0.2	0.22	0.22	0.23	0.23	-
$\overline{\overline{UF}}$	0.39	0.59	0.6	0.61	0.61	0.61	0.57	0.44	0.64	0.67	0.68	0.68	0.69	0.57
$\overline{\overline{AS}}$	0	3.39	5.05	6.37	7.43	8.25	-	0	2.03	2.63	3	3.28	3.48	-
	$q = 3$ and $\tau = 2.5$							$q = 3$ and $\tau = 3$						
RL_{max}	9.22	9.01	6.83	5.9	5.39	5.06	0.45	5.46	6.86	4.92	4.19	3.77	3.5	0.36
$\overline{\overline{RL}}$	5.21	5.29	4.44	4.08	3.88	3.76	0.28	3.22	3.87	3.19	2.93	2.78	2.68	0.17
F_{min}	0.46	0.46	0.48	0.48	0.49	0.49	0.07	0.47	0.41	0.42	0.42	0.42	0.42	-0.12
$\bar{\bar{F}}$	0.64	0.67	0.69	0.7	0.71	0.71	0.12	0.68	0.66	0.68	0.69	0.7	0.7	0.04
UF_{min}	0	0.2	0.21	0.21	0.22	0.22	-	0	0.15	0.17	0.18	0.18	0.18	-
$\overline{\overline{UF}}$	0.46	0.64	0.66	0.67	0.68	0.68	0.47	0.49	0.6	0.62	0.63	0.64	0.64	0.3
$\overline{\overline{AS}}$	0	1.42	1.66	1.78	1.86	1.91	-	0	1.06	1.17	1.22	1.25	1.27	-

Table 3.5: Performance comparisons between the adaptive and the fixed strategy under different mean shift magnitudes when the number of available sensors is 4

	Fixed	**Adaptive with WISD**						**Fixed**	**Adaptive with WISD**					
	$q = 4$ and $\tau = 1.5$							$q = 4$ and $\tau = 2$						
$\hat{\alpha} =$	0	0.2	0.4	0.6	0.8	1.0	Impv.	0	0.2	0.4	0.6	0.8	1.0	Impv.
RL_{max}	28.33	18.62	17.59	17.49	17.46	17.44	0.39	15.56	10.42	9.06	8.58	8.39	8.35	0.46
$\overline{\overline{RL}}$	14.62	13.48	12.63	12.38	12.19	12.08	0.17	7.18	7.07	6.36	6.09	5.94	5.86	0.19
F_{min}	0.52	0.63	0.66	0.67	0.67	0.67	0.3	0.62	0.6	0.61	0.62	0.62	0.63	0.01
$\bar{\bar{F}}$	0.73	0.71	0.72	0.73	0.73	0.73	0.01	0.82	0.77	0.79	0.8	0.81	0.81	-0.01
UF_{min}	0.52	0.48	0.53	0.55	0.56	0.56	0.08	0.62	0.36	0.39	0.41	0.42	0.42	-0.32
$\overline{\overline{UF}}$	0.73	0.69	0.71	0.72	0.72	0.72	-0.01	0.82	0.72	0.75	0.76	0.77	0.77	-0.06
$\overline{\overline{AS}}$	0	1.28	1.68	1.98	2.22	2.42	-	0	0.97	1.11	1.2	1.26	1.31	-
	$q = 4$ and $\tau = 2.5$							$q = 4$ and $\tau = 3$						
RL_{max}	8.67	6.76	5.56	5.09	4.86	4.7	0.46	5.27	4.98	4	3.6	3.39	3.27	0.38
$\overline{\overline{RL}}$	3.95	4.42	3.87	3.65	3.53	3.46	0.13	2.48	3.17	2.77	2.61	2.52	2.47	0.01
F_{min}	0.72	0.54	0.55	0.55	0.55	0.55	-0.23	0.77	0.51	0.51	0.51	0.51	0.51	-0.34
$\bar{\bar{F}}$	0.88	0.79	0.81	0.82	0.82	0.82	-0.07	0.92	0.78	0.8	0.81	0.82	0.82	-0.11
UF_{min}	0.72	0.16	0.18	0.19	0.19	0.2	-0.73	0.77	0.05	0.05	0.05	0.05	0.05	-0.93
$\overline{\overline{UF}}$	0.88	0.7	0.73	0.74	0.75	0.75	-0.15	0.92	0.67	0.7	0.71	0.72	0.72	-0.21
$\overline{\overline{AS}}$	0	0.81	0.88	0.92	0.94	0.95	-	0	0.69	0.74	0.76	0.77	0.77	-

In addition, we have also studied the random initial sensor deployment (RISD) approach, in which we will randomly distribute q sensors when the mean shift just occurs in the system. Similar results can be achieved as shown in Tables 3.3-3.5, though the RISD approach can provide a smaller detection delay and a better fault diagnosis accuracy. However, the difference between the WISD and the RISD approach in terms of the number of times of sensor redeployment (i.e. $\overline{\overline{AS}}$) is smaller than one in almost all scenarios. Thus, the sensor layout at the moment when a mean shift occurs in the system has little effect on the monitoring and diagnosis capabilities, and the proposed method is able to timely update the sensor layout for process change detection. Due to the page limits, the detailed results are omitted here.

3.3.2 Cap Alignment Process

Since the adaptive strategy is implemented during online monitoring, the computational time taken by the adaptive strategy is another critical concern, which is required to be at least less than the cycle time (i.e. the amount of time between two consecutive products). In order to demonstrate the feasibility and effectiveness of our proposed adaptive strategy in real time, a cap alignment process (Liu and Shi 2012; Wolbrecht et al. 2000) with 35 variables in Figure 2.5 is considered. For demonstration, in this study, we choose $q = 28$ and $\alpha = 0.01$ when establishing the T^2 control chart.

Experimental studies were conducted based on MATLAB V7.9 in Windows 7 operating system with two Intel Core i7-2820QM 2.30 GHz processors and 8 GB RAM. The average computational time taken by the adaptive strategy is about 0.0083 seconds at each time, which can satisfy the requirement of most real production systems.

Table 3.6 further summarizes the performance comparisons between the adaptive strategy with WISD and the fixed strategy when 1.5 mean shifts are possible to occur at any single variable. It clearly shows that the adaptive strategy is superior to the fixed strategy in terms of both monitoring and diagnosis capabilities.

Table 3.6: Performance comparisons between the adaptive and the fixed strategy with 28 available sensors and 1.5 mean shifts

$q = 28$ and $\tau = 1.5$	**Fixed** ($\hat{\alpha} = 0$)	**Adaptive WISD** ($\hat{\alpha} = 1$)	Impv.
RL_{max}	71.451	53.49	0.251
$\overline{\overline{RL}}$	38.966	35.99	0.076
F_{min}	0.113	0.217	0.92
$\bar{\bar{F}}$	0.391	0.441	0.128
UF_{min}	0.113	0.222	0.965
$\overline{\overline{UF}}$	0.391	0.442	0.13
$\overline{\overline{AS}}$	0	24.461	-

3.4 Discussion and Conclusion

Process control with only partial observations is a common and challenging problem in most production systems. This chapter proposes a novel adaptive sensor allocation strategy, which can enhance both monitoring and diagnosis capabilities compared with the fixed strategy (Liu and Shi 2012). Unlike the fixed strategy, which is conducted offline to minimize the detection delay of an overall system, the adaptive strategy is performed during online monitoring, which aims at reallocating sensors to concentrate on monitoring the shift variables. To develop the adaptive strategy, a BN model is assumed available to represent the causal relationships among a set of variables. The experimental results, which are demonstrated on a hot forming process and a cap alignment process, have shown that the adaptive strategy can significantly improve the detection delay and fault diagnosis accuracy while maintaining the same in-control ARL.

This fundamental investigation establishes a new research question that focuses on adaptively reallocating sensors for abnormality detection during online monitoring. This study also reveals that a trade-off problem occurs when the cost of reallocating sensors, the monitoring capability (associated with the cost of producing defective products), and the diagnosis capability (associated with the cost spent in investigating root causes) of a sensor system are taken into consideration. The optimal adaptive strategy should be the one that can minimize the total cost. When it is costless to reallocate sensors or minimizing detection delay is the first priority, sensor layout should be updated after each sample. In this way, the computational time spent in estimating the appropriate value for the warning sign can be saved.

This chapter assumes that only a single mean shift may occur at any variable and a BN model exists in a DSN. However, these two assumptions may be invalid in some applications. Thus, our further research will focus on proposing an efficient adaptive strategy that enables to detect and diagnose a wide range of possible shifts with all directions in a general DSN.

CHAPTER 4

SCALABLE-EFFICIENT-ROBUST ADAPTIVE (SERA) SENSOR ALLOCATION STRATEGY FOR ONLINE HIGH-DIMENSIONAL PROCESS MONITORING

4.1 Introduction

In the last chapter, we introduced an adaptive algorithm for process control, which was proposed in Liu et al. (2013) by investigating the multivariate T^2 control chart and causal structures. Although the algorithm (Liu et al. 2013) is better in the sense of reducing detection delay and increasing diagnosis accuracy as compared with the fixed sensor allocation strategy, it has four limitations when applied in practice. First, it assumes that a prior knowledge about the BN for the system is always available. Second, it assumes that only a single mean shift may occur in the system until it is detected by the control chart. Third, it only takes the spatial relationship of measurements into consideration, but ignores the temporal relationship when detecting process changes. Hence, it still results in a relatively long detection delay. Fourth, the computational cost is exponential in the total number of variables (i.e. m), which makes it difficult to be implemented online, especially for large-volume and high-dimensional datasets.

To address the aforementioned issues, this chapter proposes an improved novel adaptive sensor allocation strategy to further minimize detection delay while maintaining a pre-specified false alarm rate in a general network. The proposed method is *scalable*, *efficient* and *robust* in detecting a wide range of possible shifts in all directions. We name the new algorithm as Scalable-Efficient-Robust Adaptive (SERA) sensor allocation strategy. Here, *scalable* means that the proposed algorithm can be easily implemented

online for large-volume and high-dimensional datasets, since its computational cost is only linear in the total number of variables (i.e. m). *Efficient* means that the proposed algorithm can significantly improve the detection delay, compared with the adaptive strategy proposed by Liu et al. (2013). *Robust* means that the proposed algorithm is able to detect a wide range of possible shifts in all directions without making the single mean shift and the BN assumptions. Our approach is inspired by the monitoring scheme in (Mei 2011), which is based on investigating the sum of top-r local CUSUM statistics. However, our approach is different to the one in (Mei 2011) because the monitoring scheme proposed by Mei (2011) assumes that all variables are measurable and independent. Therefore, it cannot be directly employed to the adaptive sensor allocation topic.

The adaptive sensor allocation strategy discussed here includes a broad scope of applications: (1) when only a limited number of sensors is available during online monitoring; (2) when only a limited number of sensors can be in "ON" state in a fully deployed DSN at any moment for data acquisition and transmission purposes; and (3) when only partially acquired data sources can be analyzed at the fusion center due to limited transmission and processing capabilities (i.e. those partially analyzed data can be considered to have sensor deployed while others do not). For example, in the area of structure health monitoring, one major problem is the availability of responses. Due to budget constraint or practical reasons such as the inaccessibility of some degrees of freedom, the number of sensors is usually smaller than the total number of degrees of freedom of the structure (Limongelli 2003). Another example is in the area of volcanic earthquake detection, in which only a limited number of sensors can be selected in "ON" state for online data processing and communication due to bandwidth or energy constraint (Tan et al. 2012). Last but not least, when analyzing large-volume and high-dimensional datasets (e.g. video stream data), especially in fast and transient processes, one major problem is that the transmission and processing time by taking into account of

the full data frame may not satisfy the detection requirement in real-time monitoring. Thus, the challenging question here is how to adaptively determine which part of the data is to be transmitted and processed at each acquisition time for quick change detection.

The chapter is organized as follows: In Section 4.2, we will state our problem formulation and then review the CUSUM-based methodologies. Section 4.3 proposes an improved adaptive sensor allocation strategy with only partial information available for online process monitoring and further provides two properties with the developed method. Parameter settings involved in the algorithm will also be discussed. Section 4.4 first conducts a case study based on a hot forming process and then compares the performance with the one in (Liu et al. 2013). A real solar flare process is also implemented to test and validate our proposed algorithm in practice. Finally, Section 4.5 draws a conclusion.

4.2 Problem Formulation and CUSUM-Based Methodology Review

This section describes the problem of adaptive sensor allocation in the quality control field, and introduces the notations and assumptions used in the chapter. Since our approach is derived on the basis of the CUSUM philosophy, we also review the CUSUM-based methodologies, especially focusing on the monitoring technique proposed by Mei (2011).

4.2.1 Problem Formulation

In a standard quality control setup, there are m variables $\boldsymbol{X} = \{X_1, \dots, X_m\}$ of interest and $\boldsymbol{X_t} = \{X_{1,t}, \dots, X_{m,t}\}$ is the observed value of each variable at time t. When the process is in-control, $\boldsymbol{X_t}$ is independently and identically distributed (i.i.d.) across different time t with a joint distribution function $F(\boldsymbol{X})$, where each variable k has a probability density function $f(X_k)$. In this chapter, the in-control mean vector $\boldsymbol{u_F}$ and the covariance matrix $\boldsymbol{\Sigma_F}$ of $F(\boldsymbol{X})$ are assumed to be known (Hawkins 1993). In practice,

these parameters can be estimated from a sufficiently large sample of measurements on the process or known from engineering specifications when designing the process. Without losing generality, a preliminary transformation has been applied to the data, so that each variable has a mean of 0 and a standard deviation of 1.

In this chapter, we are interested in developing a monitoring scheme when only q out of m measurements are available at each acquisition time. The number of sensors, q, is assumed to be a fixed number and it is costless to change the sensor locations. In addition, we assume that sensor redeployment can be timely conducted at each time t, so that the measurements taken at time $t+1$ will be based on the updated sensor layout. Moreover, we only focus on the possible shifts in the mean vector of $\boldsymbol{X_t}$ and assume that covariance matrix $\boldsymbol{\Sigma_F}$ is unchanged after the shift. Specifically, we assume that at some unknown finite time, different mean shifts with unknown magnitudes and directions occur at certain variables and remain constant in the process until they are detected and corrected. The shifts will affect an unknown subset of data streams, and thus a variable that deviates from normal condition does not necessarily indicate the root cause (Zhou et al. 2003). For example, in a multistage manufacturing process, a mean shift will be propagated to its downstream variables and reflect different shifts in multiple channels. We denote the distribution after process changes as $G(\boldsymbol{X})$, where each variable k has a probability density function $g(X_k)$ with mean u_k and variance 1. While this study only focuses on mean shift detection, it can be extended to detect shifts in both mean and variance.

The objective of this article is to develop a novel adaptive sensor allocation strategy with only partial information available in a general network, which can quickly detect the process changes while under a false alarm constraint. The proposed method simultaneously manages sensor relocation and process change detection.

4.2.2 CUSUM-Based Methodology Review

CUSUM-based methodologies are a set of sequential procedures to calculate cumulative sums based on likelihood ratios, which can be used for detecting a shift in a process. The CUSUM procedure was first developed by Page (1954), who proposed to monitor a univariate variable (i.e. $m = 1$) with CUSUM statistic $W_{1,t}$ at time t:

$$W_{1,t} = max\left(W_{1,t-1} + log\frac{g(X_{1,t})}{f(X_{1,t})}, 0\right), W_{1,0} = 0. \quad (4.1)$$

In the case that $f(X_1)$ and $g(X_1)$ are normal distribution density functions with variances all 1 and means 0 and u_1, respectively, equation (4.1) can be simplified as:

$$W_{1,t} = max\left(W_{1,t-1} + u_1X_{1,t} - \frac{u_1^2}{2}, 0\right), W_{1,0} = 0. \quad (4.2)$$

When the post-change mean (i.e. u_1) is unknown, the standard approach is to estimate it by the maximum likelihood method (Lorden 1971; Tsui at el. 2012) or replace it with a constant parameter, which represents the interested-smallest magnitude of mean shift for detection, u_{min}. When $u_{min} \geq 0$, the CUSUM control chart is only able to detect a positive mean shift. In order to detect the mean shift in both positive and negative directions, the two-sided CUSUM procedures are suggested (Page 1954). In addition, several efforts have been made to combine the two-sided procedures into a single control chart (see Crosier 1986; Cheng and Thaga 2005a).

Since the univariate CUSUM control chart was proposed, numerous contributions have been made to study the CUSUM control chart for the multivariate case. Woodall and Ncube (1985) suggested monitoring CUSUMs of individual measurements simultaneously and raised an out-of-control alarm whenever any of the univariate CUSUM charts indicates out-of-control. Healy (1987) viewed the CUSUM procedures as a series of sequential probability ratio tests and proposed a method for detecting a shift in both the mean vector and the covariance matrix based on a linear combination of individual measurements. Crosier (1988) suggested two multivariate CUSUM procedures, in which the first one is based on the square root of T^2 statistics and the second one is based on a vector-valued CUSUM scheme. Pignatiello and Runger (1990) proposed two

similar multivariate CUSUM schemes, which are simpler but have a better average run length (ARL) performance than the ones in (Crosier 1988). Hawkins (1993) introduced CUSUM procedures based on a set of regression-adjusted variables. Ngai and Zhang (2001) considered a two-sided CUSUM chart for monitoring process mean via projection pursuit method. Chan and Zhang (2001) further extended the method for monitoring the covariance matrix. Qiu and Hawkins (2001, 2003) proposed a rank-based multivariate CUSUM procedure, which is distribution free. Cheng and Thaga (2005b) developed a multivariate max-CUSUM chart to simultaneously monitor the shifts in both mean vector and covariance structure with different directions.

On the other hand, a different approach of using CUSUM for the multivariate case is to combine local procedure together into a single global scheme. One is a CUSUM scheme based on the maximum of local CUSUM statistics (see Tartakovsky 2006). Specifically, an alarm will be raised at time t:

$$N_{max}(b) = inf\{t \geq 1: max_k\, W_{k,t} \geq b\}, \tag{4.3}$$

where b is a constant number that determines the operating characteristics of the procedure (i.e. maintain a pre-specified false alarm rate requirement). The approach of using the maximum of local CUSUM statistics is preferable when the number of root cause variable is one. Another monitoring scheme was proposed by Mei (2010), which is based on the sum of all local CUSUM statistics. The proposed stopping time is:

$$N_{sum}(c) = inf\{t \geq 1: \sum_{k=1}^{m} W_{k,t} \geq c\}, \tag{4.4}$$

where c is a suitable constant number like b in equation (4.3). This procedure is most effective when multiple variables simultaneously shift. Recently, Mei (2011) further proposed a generalized CUSUM procedure based on the sum of top-r local CUSUM statistics with the stopping time:

$$N_{top,r}(d) = inf\{t \geq 1: \sum_{k=1}^{r} W_{(k),t} \geq d\}, \tag{4.5}$$

where $W_{(1),t} \geq \cdots \geq W_{(k),t} \geq \cdots \geq W_{(m),t}$ are the decreasing order statistics of $\{W_{k,t}, k = 1,2, \ldots, m\}$ and d is a suitable constant number like b and c in equations (4.3) and (4.4). The procedures of using the maximum of local CUSUM statistics and the sum of all local CUSUM statistics can be regarded as the special cases of the sum of top-r local CUSUM statistics when $r = 1$ and $r = m$, respectively. Empirical results have shown that using the sum of top-r local CUSUM statistics is robust and efficient with suitable choices of r (Mei 2011). Due to only m local CUSUM statistics are recursively calculated at each time epoch, the computational cost is linear in m. Therefore, the method (Mei 2011) is scalable for online monitoring of a large number of data streams.

4.3 Adaptive Sensor Allocation Strategy

In this chapter, we employ the sum of top-r local CUSUM statistics (Mei 2011) as the baseline method, and further integrate it with the idea of max-CUSUM control chart (Cheng and Thaga 2005a, b). We call the new monitoring statistic as "the sum of top-r local statistics", and it will be used in the adaptive sensor allocation framework. Two properties and parameter settings associated with the developed methodology will be discussed in Sections 4.2 and 4.3, respectively. Unlike the approach in Liu et al. (2013), which only focuses on the spatial relationship of measurements, our approach first look at the temporal domain information to derive individual local statistic for each variable, and then combine the spatial domain information among different local statistics by using the sum of top-r approach (Mei 2011). For simplicity, we assume $f(X_k)$ and $g(X_k)$ follow normal distributions for $k = 1,2, \ldots, m$. However, our method is not limited to this assumption and can be generalized to other distributions.

4.3.1 Methodology Development

There are three fundamental questions when developing the adaptive sensor allocation strategy: (1) how to construct local statistics; (2) when to indicate process is out-of-control; and (3) how to redistribute sensor layout.

4.3.1.1 Local Statistic

In this chapter, our interest is to detect both positive and negative mean shifts. Inspired by the max-CUSUM control chart (Cheng and Thaga 2005a, b), we construct the two-sided local statistic for each variable k at time t as follows:

$$W_{k,t} = max(W_{k,t}^{(1)}, W_{k,t}^{(2)}), \tag{4.6}$$

where $W_{k,t}^{(1)}$ and $W_{k,t}^{(2)}$ are the local statistics for detecting positive and negative mean shifts, respectively.

Depending on whether a sensor is deployed on the variable, there are two approaches to construct the local statistics, $W_{k,t}^{(1)}$ and $W_{k,t}^{(2)}$. When a sensor is deployed on variable k at time t, we use the following approach to calculate the local statistics based on equation (4.2):

$$W_{k,t}^{(1)} = max\left(W_{k,t-1}^{(1)} + u_{min}X_{k,t} - \frac{u_{min}^2}{2}, 0\right)$$

$$\text{and } W_{k,t}^{(2)} = max\left(W_{k,t-1}^{(2)} - u_{min}X_{k,t} - \frac{u_{min}^2}{2}, 0\right), \tag{4.7}$$

where $W_{k,0}^{(1)} = W_{k,0}^{(2)} = 0$. Since the post-change mean (i.e. u_k) in equation (4.2) is usually unknown, it has been replaced by a constant parameter u_{min} (i.e. $u_{min} \geq 0$), the interested-smallest magnitude of mean shift for detection, as introduced in Section 4.2.2. (see the guidelines in Section 4.3.3 on how to determine the value for u_{min}).

When a sensor is not deployed on variable k at time t, we use the second approach to construct the local statistics by introducing an incremental parameter Δ (i.e. $\Delta \geq 0$):

$$W_{k,t}^{(1)} = W_{k,t-1}^{(1)} + \Delta \text{ and } W_{k,t}^{(2)} = W_{k,t-1}^{(2)} + \Delta, \tag{4.8}$$

where Δ is a constant tuning parameter and is related to how frequently the sensor recourses will be reallocated (see the guidelines in Section 4.3.3 on how to determine the value for Δ).

It is worth mentioning that the two-sided local statistic $W_{k,t}$ is always nonnegative for $\forall k$ and $\forall t$ based on equations (4.6)-(4.8), and it will be large no matter when the process has a positive or negative mean shift in variable k. In the following study, we will assume the constructed local statistics are all two-sided, unless otherwise specified.

4.3.1.2 Stopping Time and Redistribute Sensor Layout

As discussed in Section 4.2, we employ the approach in (Mei 2011) to determine the stopping time by equation (4.5): $N_{top,r}(d) = inf\{t \geq 1: \sum_{k=1}^{r} W_{(k),t} \geq d\}$ (see the guidelines in Section 4.3.3 on how to determine the values for r and d). Recall that $W_{k,t}$ is the local statistic to detect the mean shift in each variable k, while the sum of top-r local statistics is the monitoring statistic to detect the change in the system.

Denote the variable index of the decreasing order statistic $W_{(k),t}$ as $l_{(k),t}$. Since a larger local statistic indicates the variable is more likely to have a shift, we will redistribute sensor resources onto the variables with the first q largest local statistics after checking the stopping rule at each time t:

$$\boldsymbol{S} = \{l_{(1),t}, \dots, l_{(q),t}\}, \tag{4.9}$$

where $\boldsymbol{S}$ denotes the new sensor layout. In case that there are a non-unique solution for $\boldsymbol{S}$, we will randomly choose one of the solutions to update $\boldsymbol{S}$.

4.3.1.3 Overview of the SERA Algorithm.

The initial sensor layout is not critical since the adaptive sensor allocation strategy will be timely updated according to the online measurements. An overview of the SERA algorithm is illustrated in Figure 4.1.

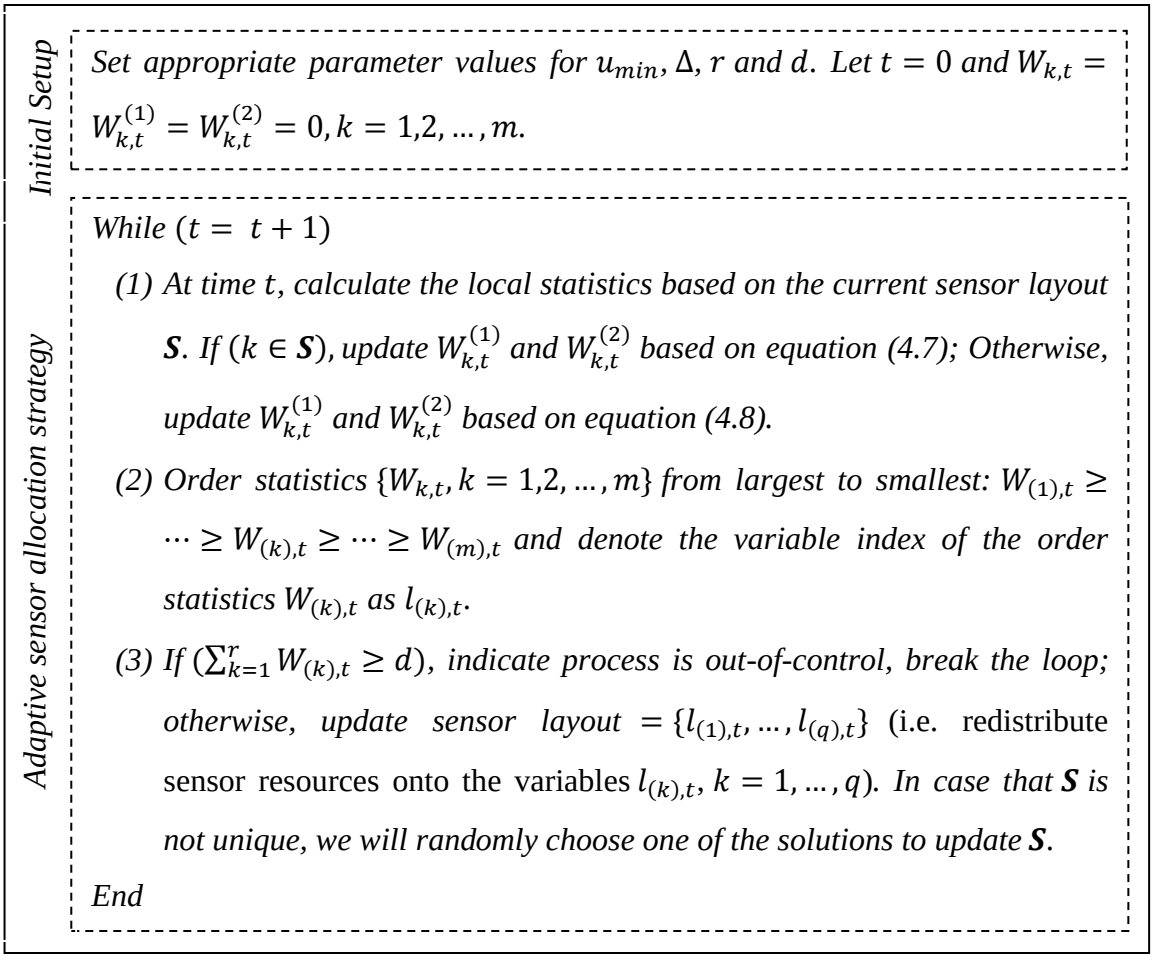

Figure 4.1: The overall flow chart of the SERA algorithm

4.3.2 Properties of SERA Algorithm

In this section, we provide two properties associated with the SERA algorithm. These two properties ensure that the SERA algorithm can not only quickly detect a wide range of possible shifts in all directions, but also identify the shift variables under certain constraints. In the properties, the following variable plays an important role: $\rho_k = u_{min}|E(x_k)| - \frac{u_{min}^2}{2} - \Delta$, which characterizes the difference between the true post-change mean $|E(x_k)|$ and our pre-assigned parameters u_{min} and Δ.

Denote $\boldsymbol{M} = \{1, \dots, m\}$. We first investigate the property when where is no mean shift or only small mean shifts (i.e. $\rho_k \leq 0$ for $\forall k \in \boldsymbol{M}$) occurring in the system.

Property 4.1: Let $d \to \infty$ and $\rho_k \leq 0$ for $\forall k \in \boldsymbol{M}$. Denote $\boldsymbol{S_t}$ as the sensor allocation at time t. For any t_0 and any variable $k \in \boldsymbol{M}$, denote $T_{t,k} = inf\{t \geq 1: k \in \boldsymbol{S_t}, t > t_0\}$, then $P(T_{t,k} < \infty) = 1$ (Proof is given in Appendix A.5).

The first property discusses the randomness of sensor layout when the system is either in-control or only small mean shifts happen. When $\rho_k \leq 0$, sensor resources will not stick to the variable k, but will be redistributed to other variables with infinite number of times as $d \to \infty$. In other words, sensor resources will not stick to a certain layout and any variable will not be left unattended during online monitoring though only limited resources are available for a given time.

Denote $card(*)$ as the cardinality of the set $*$. Next, we investigate the property when modest mean shifts happen (i.e. $\rho_k > 0$, for $\exists k \in \boldsymbol{M}$) in the system.

Property 4.2: Let $d \to \infty$ and $\boldsymbol{B} = \{k \in \boldsymbol{M}: \rho_k > 0\}$. Let event A_t represent the existence of a set $\boldsymbol{B_0} \subset \boldsymbol{B}$ and $card(\boldsymbol{B_0}) = min(card(\boldsymbol{S_t}), card(\boldsymbol{B}))$ at time t, where $k \in \boldsymbol{S_t}$ for all $k \in \boldsymbol{B_0}$. Then $lim_{t\to\infty} P(A_t) = 1$ (Proof is given in Appendix A.6).

The second property indicates that sensor resources will eventually swarm and stick to the set of variables with modest mean shifts. In other words, when $\rho_k > 0$, there is always a nonzero probability that once a sensor is deployed on variable k, it will never be redistributed to other variables. In this way, the sum of top-r local statistics can be significantly large. Thus, this property also shows that the SERA algorithm is able to localize the process changes. However, since the SERA algorithm is developed based on individual local information, it can only identify the shift variables instead of the root causes.

4.3.3 Parameter Settings

In this section, we will discuss how to set the values of four parameters, u_{min}, Δ, r, and d in the SERA algorithm.

(1) The selection of u_{min}: As discussed in Section 4.3.1.1, the parameter u_{min} (i.e. $u_{min} \geq 0$) represents the interested-smallest magnitude of mean shift for detection. In reality, the practitioner can determine the value of u_{min} based on engineering domain knowledge to ensure production yield. For example, in a manufacturing process, the tolerance specifications for each variable specified in product/process design can be used to determine the interested-smallest magnitude of mean shift, u_{min} (Liu and Shi 2012).

(2) The selection of Δ: Δ (i.e. $\Delta \geq 0$) is a tuning parameter, which is associated with how frequently the sensor recourses will be reallocated. In practice, Δ cannot be either too large or too small. If Δ is too large, then the reallocation scheme will be dominated by Δ. As a result, sensors will be redistributed onto the variable that currently does not have sensor deployed after each time no matter whether this variable has a shift or not. By property 4.2, if we want to detect the shift resulted from variable k, then $\rho_k > 0$ or equivalently, $u_{min}|u_k| - \frac{u_{min}^2}{2} > \Delta$. On the other hand, according to property 4.1, if Δ is too small, then the monitoring system may take a longer time to reallocate sensors from the in-control variables onto the shift variables.

(3) The selection of r: At first, r should be smaller than q, the total number of sensors. Otherwise, the sum of top-r local statistics will include unobserved variables when the system is out-of-control, which will degrade the performance of the control chart. Ideally, r should be chosen approximately equal to the total number of root cause variables. On the other hand, Mei (2011) has shown that when the total number of root cause variables is unknown, the monitoring scheme with relatively small r value is more robust to detect a wide range of possible shifts.

(4) The selection of d: d is the threshold to stop the monitoring procedure. The practitioner can determine the optimal d value from sufficiently large in-control measurements or via Monte Carlo simulation with bootstrap technique (Efron and

Tibshirani 1993; Chatterjee and Qiu 2009). The value of d is related to the false alarm rate, α of the monitoring scheme:

$$\alpha = 1/ARL_U, \tag{4.10}$$

where ARL_U is the prescribed in-control ARL when no change occurs in the system.

4.4 Case Studies

4.4.1 Hot Forming Process

In this section, we will evaluate the performance of the proposed SERA algorithm and compare with the existing one in Liu et al. (2013) under different shift scenarios based on a hot forming process. A BN for the hot forming process was identified by Li and Jin (2010) and is shown in Figure 2.1. As mentioned in Section 4.1, the method in Liu et al. (2013) is based on investigating the multivariate T^2 control chart and the causal structures (in the following pages, we denote this algorithm as causation-based adaptive (CBA) algorithm) when only partial information is available during online monitoring. As a result, a BN must be known before conducting this algorithm. In addition, the CBA algorithm can only detect single mean shift. To demonstrate the effectiveness of our proposed SERA algorithm, in the following case studies, we assume that the BN is unknown when implementing the SERA algorithm, whereas the BN is available when implementing the CBA algorithm in phase 2 monitoring and diagnosis.

4.4.1.1 Single Mean Shift Case

In this case study, we focus on comparing the performance of the proposed SERA algorithm with the CBA algorithm when only a single mean shift may occur at any variable in the hot forming process. The following discussions will consider five potential single mean shift scenarios with different shift magnitudes, τ (i.e. $\tau = 1.5, 2, 2.5, 3$) and different number of available sensors, q (i.e $q = 2, 3, 4$). In addition, the false alarm rate,

α is chosen to be 0.01. Since the SERA algorithm can only identify the shift variables, it is not suitable for root cause diagnosis, especially when the causal structure is unknown. However, since only a single mean shift may occur in the system and the shift will propagate and dilute along the BN (e.g. a mean shift in X_2 with $u_2 = 1$ will result in a mean shift in X_1 with $u_1 = 0.574$), we will use a simple rule of root cause diagnosis for the SERA algorithm: the variable with the largest CUSUM statistic. This diagnosis approach can demonstrate how many times the out-of-control alarm is triggered with the largest contribution from the root cause variable. To evaluate the monitoring and the root cause diagnosis capabilities, specifically, we focus on the following metrics when each time the same amount of mean shift occurs at each variable: (1) the maximum out-of-control ARL, RL_{max}; (2) the average out-of-control ARL, $\overline{\overline{RL}}$; (3) the minimum rate of *uniquely correct diagnosis*, UF_{min}; and (4) the average rate of *uniquely correct diagnosis*, $\overline{\overline{UF}}$. A diagnosis result is called *uniquely correct* if the true mean shift variable is uniquely identified. According to the definitions of these metrics, RL_{max} and $\overline{\overline{RL}}$ are desired to be as small as possible, whereas UF_{min} and $\overline{\overline{UF}}$ are desired to be as large as possible. Parameter settings (e.g. values for τ, q and α) and performance evaluation metrics (e.g. RL_{max}, $\overline{\overline{RL}}$, UF_{min} and $\overline{\overline{UF}}$) are selected to be consistent with (Liu et al. 2013).

The SERA algorithm is implemented during online monitoring no matter when the system is in-control or out-of-control. Thus, the sensor layout is not unique at the moment when a mean shift occurs, and thus it can affect the monitoring performance. In order to address this issue, we consider the *worst initial sensor deployment (WISD)*, which will provide the least favorable sensor layout for detection when a mean shift occurs in the system. Define $\{\rho_{(k)}\}$ as the increasing order statistics of $\{\rho_k\}$. In other words, when a mean shift occurs at variable k, we assume that sensors are deployed right on the variables associated with $\{\rho_{(1)}, \dots, \rho_{(q)}\}$, no matter how sensor placement has

evolved before. In this way, we can get the most conservative performance evaluation of the SERA algorithm.

Table 4.1: Performance comparisons between the SERA and the CBA algorithm under different combinations of Δ, τ, and q values for single mean shift case

	CBA	SERA Δ= 0.01	SERA Δ= 0.1	SERA Δ= 0.5	Impv. (%)	CBA	SERA Δ= 0.01	SERA Δ= 0.1	SERA Δ= 0.5	Impv. (%)
	$q = 2$ and $\tau = 1.5$					$q = 2$ and $\tau = 2$				
RL_{max}	27.24	9.03	8.77	10.36	67.80	15.15	6.45	6.19	7.25	59.14
$\overline{\overline{RL}}$	17.66	8.40	8.17	9.93	53.74	9.06	5.98	5.79	6.95	36.09
UF_{min}	0	0.56	0.60	0.75	-	0	0.49	0.54	0.73	-
$\overline{\overline{UF}}$	0.40	0.83	0.84	0.92	110	0.45	0.82	0.84	0.92	86.67
	$q = 2$ and $\tau = 2.5$					$q = 2$ and $\tau = 3$				
RL_{max}	9.16	5.25	5.05	5.83	44.87	5.69	4.67	4.41	5.01	22.50
$\overline{\overline{RL}}$	5.38	4.90	4.74	5.58	11.90	3.66	4.32	4.16	4.81	-13.66
UF_{min}	0	0.41	0.45	0.66	-	0	0.33	0.36	0.54	-
$\overline{\overline{UF}}$	0.47	0.80	0.82	0.91	74.47	0.48	0.77	0.79	0.88	64.58
	$q = 3$ and $\tau = 1.5$					$q = 3$ and $\tau = 2$				
RL_{max}	17.75	7.88	7.72	7.65	56.51	8.67	5.51	5.40	5.33	37.72
$\overline{\overline{RL}}$	13.03	7.27	7.16	7.10	45.05	6.26	5.10	5.01	4.97	19.97
UF_{min}	0.20	0.64	0.67	0.73	235	0.23	0.58	0.62	0.74	169.57
$\overline{\overline{UF}}$	0.61	0.87	0.88	0.90	44.26	0.69	0.87	0.88	0.92	27.54
	$q = 3$ and $\tau = 2.5$					$q = 3$ and $\tau = 3$				
RL_{max}	5.06	4.43	4.36	4.28	13.83	3.50	3.53	3.76	3.69	-7.43
$\overline{\overline{RL}}$	3.76	4.10	4.03	3.99	-7.18	2.68	3.86	3.46	3.42	-29.1
UF_{min}	0.22	0.52	0.55	0.69	150	0.18	0.44	0.46	0.61	155.56
$\overline{\overline{UF}}$	0.68	0.86	0.87	0.92	27.94	0.64	0.84	0.86	0.91	34.38
	$q = 4$ and $\tau = 1.5$					$q = 4$ and $\tau = 2$				
RL_{max}	17.44	7.51	7.36	7.14	57.8	8.35	5.22	5.16	5.03	38.2
$\overline{\overline{RL}}$	12.08	6.85	6.75	6.55	44.12	5.86	4.74	4.69	4.57	19.97
UF_{min}	0.56	0.63	0.65	0.71	16.07	0.42	0.56	0.59	0.67	40.48
$\overline{\overline{UF}}$	0.72	0.86	0.87	0.89	20.83	0.77	0.85	0.86	0.89	11.69
	$q = 4$ and $\tau = 2.5$					$q = 4$ and $\tau = 3$				
RL_{max}	4.70	4.22	4.14	4.03	11.91	3.27	3.59	3.57	3.47	-9.17
$\overline{\overline{RL}}$	3.46	3.76	3.72	3.64	-7.51	2.47	3.17	3.15	3.10	-27.53
UF_{min}	0.20	0.46	0.49	0.59	145	0.05	0.36	0.39	0.48	680
$\overline{\overline{UF}}$	0.75	0.82	0.83	0.87	10.67	0.72	0.79	0.80	0.84	11.11

Table 4.1 summarizes the performance comparisons between the SERA algorithm and the CBA algorithm under different combinations of mean shift magnitude τ, incremental parameter Δ, and number of available sensors q. In this study, we choose $r = 2$ and $u_{min} = 1.5$ according to the characteristics of the actual system. The detailed simulation steps can be found in Appendix A.7. The numbers in the "CBA" column can be referred to (Liu et al. 2013). The column "Impv." shows the percentage of improvement (i.e. positive value) or deterioration (i.e. negative value) in each performance metric by implementing the SERA algorithm ($\Delta = 0.1$) over the CBA algorithm. According to Table 4.1, we can draw the following conclusions:

(1) The SERA algorithm outperforms the CBA algorithm in both monitoring and diagnosis capabilities. In most of the scenarios, the SERA algorithm can significantly improve the detection delay (which is related to RL_{max} and $\overline{\overline{RL}}$ metrics) and also the diagnosis accuracy (which is related to UF_{min} and $\overline{\overline{UF}}$ metrics) compared with the CBA algorithm, although the causal information is unknown when implementing the SERA algorithm. On the other hand, the differences between the RL_{max} and the $\overline{\overline{RL}}$ metrics are much smaller for the SERA algorithm under different mean shift scenarios. This characteristic ensures that a mean shift can be detected in a timely manner no matter where the root cause is. In this way, a more robust monitoring scheme is obtained, and thus less defective products will be produced due to quick detection of process changes.

(2) The performance of the SERA algorithm is relatively stable when Δ changes within a certain range. However, when Δ is set to be a very large number (e.g. $\Delta = 1.5$: in this way, $\rho_k < 0$ for $u_k = 1.5$), the performance of the SERA algorithm deteriorates very fast, especially when the number of available sensors is small (due to page limits, the result is omitted). On the other hand, the system associated with different number of available sensors need different optimal Δ values. For example, when $q = 2$, $\Delta = 0.1$

can provide the best performance compared with $\Delta = 0.01$ or 0.5. On the contrary, when $q = 3$ or 4, $\Delta = 0.5$ can provide the best performance compared with $\Delta = 0.01$ or 0.1. According to the empirical study, as the number of available sensors increases, a larger Δ value is preferred.

(3) As τ increases, the detection delay of both methods decreases, which is consistent with our intuitions; however, the amount of improvement in the "Impv." columns becomes smaller. It is known that the CUSUM-type chart is more efficient for detecting small mean shifts than the Shewhart chart (Montgomery 2009). However, in this example, even with large mean shifts, the detection delay of the SERA algorithm (which is based on the CUSUM statistics) is still comparable to the CBA algorithm (which is based on T^2 statistics). On the other hand, the diagnosis accuracy of both methods becomes smaller as τ increases. This is because as the mean shift becomes significant, the abnormality can be more easily noticed by the system even with a poorly deployed sensor layout.

(4) As q increases, less information is lost in the system, and thus the detection delay of both methods decreases. In addition, the amount of improvements in both the detection delay and the diagnosis accuracy of the SERA algorithm become less pronounced. As a result, the SERA algorithm is more efficient and robust than the CBA algorithm, especially when the number of available sensors is small.

4.4.1.2 Multiple Mean Shifts Case

The CBA algorithm is only able to detect single mean shift, but the SERA algorithm can detect a wide range of possible shifts in all directions. Consequently, in this study, we focus on evaluating the performance of the SERA algorithm when multiple mean shifts occur in the network. In addition, we are interested in studying the effect of sensor layout on the detection delay of the SERA algorithm when the mean shifts right

occur in the system. Specifically, two approaches to the initial sensor deployment are considered in the following analysis. The first one is called the WISD as introduced in Section 4.4.1.1, and the second approach is called *random initial sensor deployment (RISD)*, which will randomly distribute q sensors to the variables when mean shifts right occur in the system. By comparing these two approaches, we can get a thorough study about the robustness of the SERA algorithm to the initial sensor layout.

Similarly to the single mean shift case, different mean shift magnitudes τ and different number of available sensors q are considered. In this study, Δ is chosen to be 0.1. The evaluation process is similar to the single mean shift case as shown in Section 4.4.1.1, and thus it is omitted here. Tables 4.2 and 4.3 elaborate the performance of the SERA algorithm when two variables simultaneously have a mean shift with identical magnitude but in the same and the opposite directions, respectively. According to the results in Tables 4.2 and 4.3, we can get the following conclusions:

(1) As q and τ increase, less information is lost during online monitoring and the mean shift becomes more significant, and thus detection delay decreases. In addition, since mean shifts with different directions will mitigate each other when propagating to downstream variables, the detection delay in Table 4.3 is larger than that in Table 4.2.

(2) Compared with the RISD, the WISD only has a little larger detection delay in both RL_{max} and $\overline{\overline{RL}}$ metrics (the difference is within one ARL in almost all scenarios). Thus, this study shows that the sensor layout at the moment when a mean shift occurs in the system has little effect on the monitoring performance. In other words, the SERA algorithm is able to timely update the sensor layout for detecting process changes.

Table 4.2: Performance evaluations of the SERA algorithm under different combinations of initial sensor layouts, τ and q values for multiple (two) mean shifts with same direction

	SERA (WISD)	SERA (RISD)	SERA (WISD)	SERA (RISD)	SERA (WISD)	SERA (RISD)	SERA (WISD)	SERA (RISD)
$q = 2$	$\tau = 1.5$		$\tau = 2$		$\tau = 2.5$		$\tau = 3$	
RL_{max}	5.98	5.20	4.51	3.61	3.86	2.88	3.45	2.41
$\overline{\overline{RL}}$	5.05	4.24	3.94	3.05	3.39	2.46	3.05	2.10
$q = 3$	$\tau = 1.5$		$\tau = 2$		$\tau = 2.5$		$\tau = 3$	
RL_{max}	5.11	4.43	3.75	3.06	3.13	2.38	2.77	2.01
$\overline{\overline{RL}}$	4.24	3.63	3.20	2.58	2.68	2.05	2.36	1.74
$q = 4$	$\tau = 1.5$		$\tau = 2$		$\tau = 2.5$		$\tau = 3$	
RL_{max}	4.37	4.12	3.04	2.84	2.43	2.21	2.09	1.85
$\overline{\overline{RL}}$	3.75	3.39	2.73	2.39	2.21	1.89	1.90	1.58

Table 4.3: Performance evaluations of the SERA algorithm under different combinations of initial sensor layouts, τ and q values for multiple (two) mean shifts with different directions

	SERA (WISD)	SERA (RISD)	SERA (WISD)	SERA (RISD)	SERA (WISD)	SERA (RISD)	SERA (WISD)	SERA (RISD)
$q = 2$	$\tau = 1.5$		$\tau = 2$		$\tau = 2.5$		$\tau = 3$	
RL_{max}	8.25	7.59	5.83	5.07	4.78	3.97	4.26	3.43
$\overline{\overline{RL}}$	7.00	6.31	5.08	4.26	4.22	3.34	3.76	2.83
$q = 3$	$\tau = 1.5$		$\tau = 2$		$\tau = 2.5$		$\tau = 3$	
RL_{max}	7.13	6.49	4.94	4.27	3.98	3.24	3.45	2.71
$\overline{\overline{RL}}$	5.96	5.33	4.23	3.56	3.44	2.75	3.01	2.30
$q = 4$	$\tau = 1.5$		$\tau = 2$		$\tau = 2.5$		$\tau = 3$	
RL_{max}	6.65	6.01	4.59	3.94	3.61	2.99	3.10	2.44
$\overline{\overline{RL}}$	5.30	4.90	3.68	3.27	2.91	2.52	2.46	2.08

4.4.2 Solar Flare Detection

In this section, we conduct a case study based on a real dataset collected from the solar data observatory, which illustrates the emergences of solar flares. A solar flare is defined as a sudden, transient, and intense variation in brightness, which is usually observed over the Sun's surface. A solar flare can emit large energetic charged particles, which can disturb the Earth's ionosphere and radio communications. Thus, there is a pressing need to detect the solar flare as soon as possible. However, due to the transient

characteristic of the solar flare process and large amount of dataset, traditional methodologies by analyzing the full data stream can usually exceed the transmission and processing capabilities during online monitoring, and thus are incapable of detecting solar flares in real time.

The dataset is recorded in a video format and is publicly available online at http://nislab.ee.duke.edu/MOUSSE/index.html. There are in total 300 frames in the video, each of which contains a size of $232 \times 292 = 67744$ dimensional online data. According to the video, there are at least two obvious transient flares which occur at frames $t = 187{\sim}202$ and $t = 216{\sim}268$, respectively. For monitoring purposes, the background information has been already removed and the remaining data is approximately normal distributed as mentioned in (Xie et al. 2013).

In this study, the parameters are selected as $u_{min} = 3$, $\Delta = 0.1$, $r = 40$ (we have also tried other combinations of the parameters, and achieved a similar result). In addition, we assume that only 2000 out of 67744 pixels are available (i.e. $q = 2000$) at each data frame and can be sent to the fusion center for analysis due to limited transmission and processing capabilities. Figure 4.2 (a) and Figure 4.3 (a) show the snapshots of the video at frames $t = 198$ and $t = 230$, when the first and second solar flare are brightest, respectively. Figure 4.2 (b) and Figure 4.3 (b) illustrate the snapshots at frames $t = 202$ and $t = 268$, when the first and second solar flare are nearly over, respectively. Figure 4.2 (c) is the snapshot at frame $t = 186$, which is the moment right before the first solar flare occurs, and Figure 4.3 (c) shows the snapshot at frame $t = 300$, which is the last frame of this video. Figures 4.2 (d)-(f) and Figures 4.3 (d)-(f) demonstrate the locations of sensors which are marked by white dots at the corresponding frames $t = 198, 202, 186$ and $t = 230, 268, 300$, respectively.

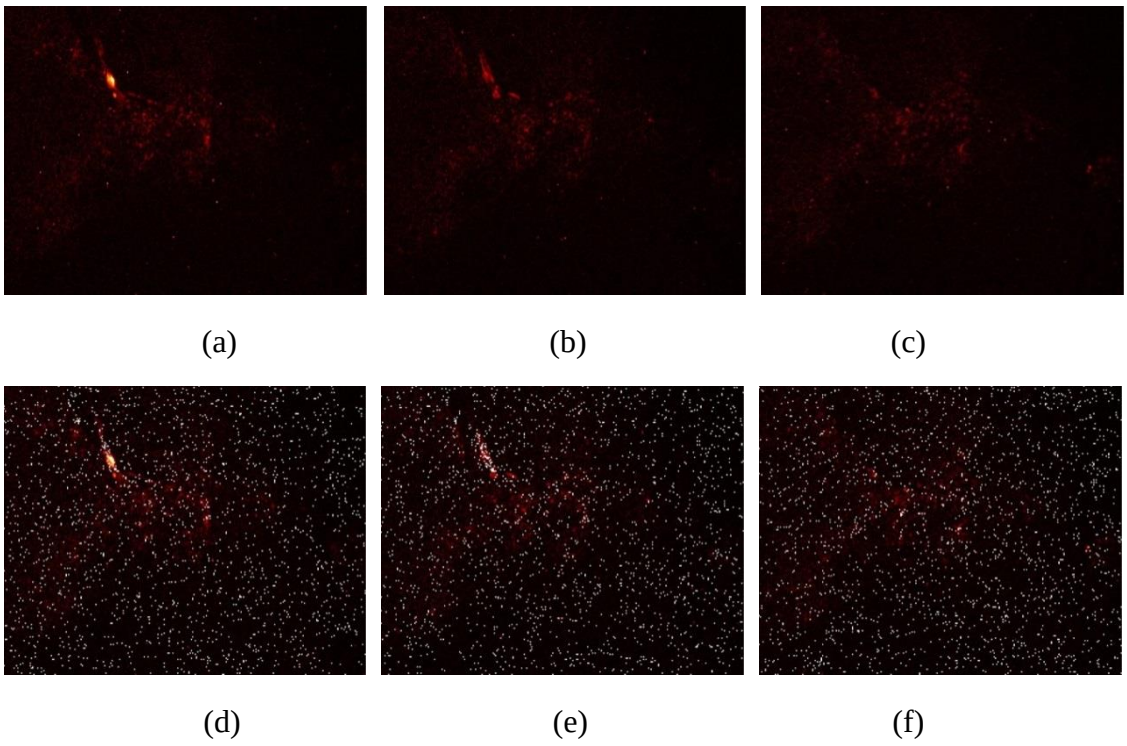

Figure 4.2: Detection of the first solar flare: snapshots of the video (a) at frame $t = 198$, when the first solar flare is brightest; (b) at frame $t = 202$, when the first solar flare is nearly over; and (c) at frame $t = 186$, the moment right before the first solar flare starts. The locations of 2000 sensors are (d) at frame $t = 198$; (e) at frame $t = 202$; and (f) at frame $t = 186$.

Figure 4.2 and Figure 4.3 show that our method can not only detect the emergences of solar flares, but also localize the flares (i.e. sensors clearly swarm to the regions and show the patterns of the solar flare in Figure 4.2 (e) and Figure 4.3 (e)), which is due to property 4.2 of the SERA algorithm. On the other hand, when there is no solar flare happening, locations of sensors are nearly random and do not show any obvious pattern as shown in Figure 4.2 (f). In addition, comparing Figure 4.3 (e) and (f), when the solar enters a normal state after the flare disappears, sensors do not stick to the locations of the previous solar flare and tend to be redistributed to the random pattern again. Therefore, these two phenomena further validate property 4.1 of the SERA algorithm. Due to this characteristic, the SERA algorithm is also able to detect multiple shifts that occur at different time.

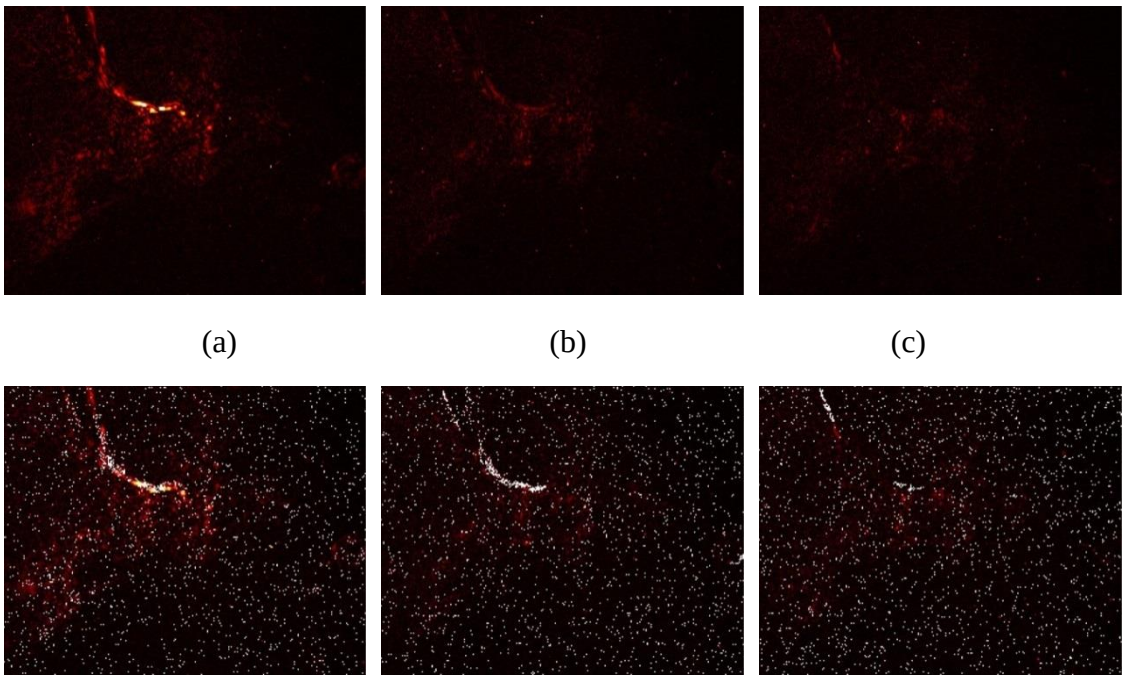

(a) (b) (c)

(d) (e) (f)

Figure 4.3: Detection of the second solar flare: snapshot of the video (a) at frame $t = 230$, when the second solar flare is brightest; (b) at frame $t = 268$, when the second solar flare is nearly over; and (c) at frame $t = 300$, the last frame of this video. The locations of 2000 sensors are (d) at frame $t = 230$; (e) at frame $t = 268$; and (f) at frame $t = 300$.

Figure 4.4 plots the values of the sum of top-r local statistics by implementing the SERA algorithm at frames $t = 101{\sim}300$. Although many methodologies have already been developed to estimate the threshold d, accurately determining its value given any prescribed in-control ARL is still a challenging problem, especially when the training sample is small. In this study, we estimate the value of threshold d based on the data in the first 100 frames with bootstrap technique (The detailed steps can be found in Appendix A.8). In Figure 4.4, the red horizontal line represents $d = 1050$, which corresponds to the false alarm rate of 0.0004. Although 2000 pixels are available, which accounts for only 2.95% of the total information, our method can still quickly detect the two solar flares at frames $t = 190$ and $t = 221$ as shown in Figure 4.4. This is comparable to the results in (Xie et al. 2013), where the two solar flares are detected at

frames $t = 191$ and $t = 217$. However, the method in (Xie et al. 2013) is based on the generalized likelihood ratio procedure (Siegmund and Venkatraman 1995) and assumes that all 67744 pixels in each data frame are available. In addition, there is no recursive formula in (Xie et al. 2013) and thus their method is not suitable for online monitoring applications.

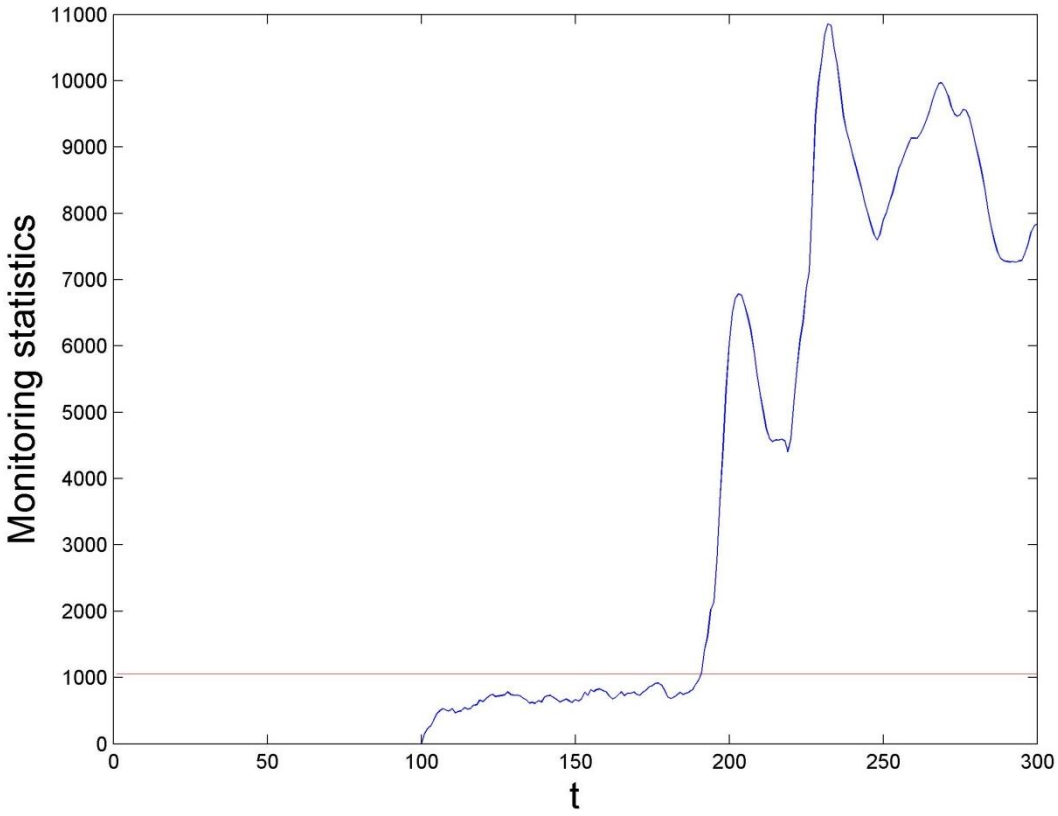

Figure 4.4: The monitoring statistics (i.e. the sum of top-r local statistics) over different acquisition time by implementing the SERA algorithm. The red horizontal line is the threshold $d = 1050$, which corresponds to the false alarm rate of 0.0004.

4.5 Conclusion

Fast process change detection is an important and challenging topic in many industrial and civilian applications. Although efforts have been made in developing the optimal design of DSNs by assuming that sensor deployment is fixed, few studies have

been focused on investigating the adaptive sensor allocation strategy based on online measurements to minimize detection delay. This chapter develops a novel monitoring scheme by using the sum of top-r local statistics for fast process change detection in a general network. The use of this framework has several advantages over other approaches, which include significant decreases in computational cost (i.e. the complexity is only linear in the number of variables), and extensive savings for physical sensors, data acquisition, transmission and processing time. The proposed adaptive algorithm, which is named as SERA, is scalable, efficient, and robust to detect a wide range of possible shifts in all directions, even in large-volume and high-dimensional data environments. Two properties of this algorithm are also given in this chapter. The methodology has been tested and validated on a hot forming process and a real solar flare process. Both studies have demonstrated the capabilities of the SERA algorithm to quickly detect and also localize the process changes (i.e. sensors swarm and stick to the out-of-control region).

CHAPTER 5

A DATA-LEVEL FUSION MODEL FOR DEVELOPING COMPOSITE HEALTH INDICES FOR DEGRADATION MODELING AND PROGNOSTIC ANALYSIS

5.1 Introduction

Unexpected equipment failure often leads to severe economic losses and can sometimes have catastrophic consequences. A typical example that occurs in the industrial sector is unexpected machine failures that result in production downtime, delayed delivery schedule, poor customer satisfaction and safety issues. Condition monitoring and prognostics, which utilize sensor data to assess the health status of equipment and make inferences about the remaining lifetime, play important roles in condition-based maintenance (Mobley 2002). As equipment degrade, sensor data related to the underlying failure processes (such as temperature, vibration, emissions, etc.) evolve in a manner that is related to the severity of degradation process and are typically referred to as degradation signals. Given a predetermined failure threshold, monitoring these degradation signals can provide accurate inferences about the remaining lifetime of each system or unit.

The literature pertaining to modeling degradation processes is indeed rich, and contains numerous methods and techniques (Meeker and Escobar 1998; Nelson 1990). However, most of the existing models study only a single measure for degradation. These approaches are effective when the degradation mechanism is well understood and a single sensor is capable of capturing most of the characteristics of the underlying degradation process. In reality, a single sensor is typically insufficient for characterizing various types

of manifestations that may result from even a single degradation process. Although it is possible to use multiple sensors and individually analyze the corresponding data, this can often result in significant over or under estimation of the remaining lifetime (Gebraeel 2006). In fact, different sensor data may exhibit different signal patterns. Some sensors are highly related to the degradation mechanism, and thus can show a strong degradation trend while others may not. Two key challenges when performing prognostics using multiple sensors are: (1) deciding on which specific sensor data to use for modeling degradation, and (2) how to combine/fuse multiple relevant sensor data. Generally, data collected from multiple sensors may contain only partial information about the same degradation process, and thus fusing this information has the potential to provide more accurate and robust prognostic capability. In addition, the data fusion approach can save cost by identifying and collecting only relevant sensor data for prognostics in future monitoring.

There are three categories of data fusion that are classified based on the level of implementation of the fusion methodology: data-level fusion, feature-level fusion, and decision-level fusion (Hall and Llinas 1997; Volponi et al. 2004). Data-level fusion combines multiple sensor data that measure correlated parameters. Heger and Pandit (2004) applied a data-level fusion approach by using multi-directional illumination and image fusion to generate an image with a high degree of relevant information for grinding tool condition monitoring and fault diagnostic applications. Kalman filter is another common technique applied to multi-sensor fusion (Simon and Simon 2005; Kobayashi and Simon 2007). Salahshoor et al. (2008) presented an integrated design framework based on the extended Kalman filter data fusion algorithm for enhancing the detection and diagnosis of sensor and process faults. On the other hand, feature-level fusion integrates feature information that results from independent analysis methods. Prior knowledge about the degradation mechanism and physical laws are usually implemented to create desired features. For example, Goebel and Bonissone (2005) applied a feature-

level fusion approach to predict industrial web paper breakage using an Adaptive Neuro-Fuzzy Inference System model. Volponi *et al.* (2004) performed information fusion at the feature-level to maximize the amount of meaningful information that can be extracted from separate data sources to obtain comprehensive diagnostic and prognostic knowledge regarding the health of the aircraft gas turbine engine. Finally, decision-level fusion involves integrating diagnostic actions (e.g. preliminary determination of an entity's location, attributes, and identity). Sun (2002) conducted a decision-level fusion analysis for vehicle health monitoring and degradation detection where decisions were made based on each sensor and their features (e.g. power spectrum, wavelets, autoregressive modeling, and entropy spectrum). A review of some of the literature on multi-sensor data fusion approaches to condition monitoring, fault diagnosis, and prognostics can be found in Jardine et al. (2006).

While the aforementioned techniques were effective in different levels of data fusion, most of them aimed at improving monitoring and diagnostic performances. Little literature has discussed how these methodologies can be applied to degradation modeling and prognostics. Some extensions to prognostic applications can be found in feature-level and decision-level fusion models (Hu et al. 2010; Byington et al. 2007), but seldom at data-level fusion. On possible explanation is that feature-level and decision-level fusion models are performed on intermediate results, i.e., after analyzing the original data. In such scenarios, it is usually more flexible to aggregate the information from independent analysis techniques (feature-level) or decisions (decision-level). Nonetheless, these two approaches are highly dependent on the quality of the raw data, and how that data is analyzed and processed. Therefore, there is a significant need to develop a data-level fusion technique that deals with constructing an efficient composite health index that is specific and relevant to degradation modeling and prognostics. This composite health index can be regarded as the key metric for assessing the health status of each unit. Feature-level and decision-level fusion techniques can still be implemented on the basis

of the constructed health index to further improve prognostic results. Figure 5.1 illustrates the flow chart on different levels of data fusion approaches to final prognostic analysis. The contribution of this chapter is highlighted by the dashed rectangle in Figure 5.1.

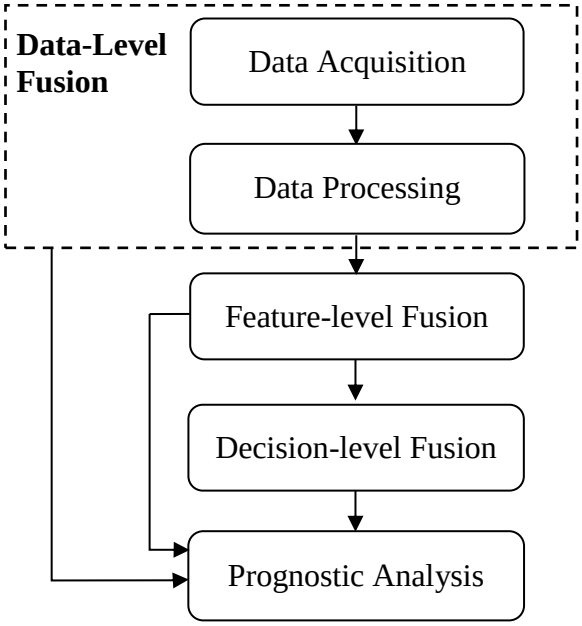

Figure 5.1: Different levels of data fusion approaches to prognostic analysis

The remainder of this chapter is organized as follows. Section 5.2 describes the simulation model developed using the NASA Commercial Modular Aero-Propulsion System Simulation (C-MAPSS) for commercial aircraft gas turbine engines, and provides an overview of the degradation dataset taken from (Saxena, Goebel, Simon, and Eklund 2008). Section 5.3 develops a concrete formulation of constructing an efficient composite health index based on the data-level fusion technique for degradation modeling and prognostics. Key elements related to the problem formulation, which include essential properties for developing degradation signals, algorithm robustness, weight coefficients setting, selection of data-fusion function, and tuning parameter setting, will be addressed. Section 5.4 demonstrates the improved performance of the composite health index when

it is used for model fitting and remaining life prediction based on the dataset introduced in Section 5.2. Section 5.5 draws a conclusion and discusses future research directions.

5.2 Overview of the System and Dataset

5.2.1 System Model Description

This chapter considers the degradation of a simulated turbofan engine that is monitored using multiple sensors. The simulation model of the turbofan engine was developed using C-MAPSS, a simulation tool developed at NASA and widely used in engine health monitoring research for simulating realistic large commercial turbofan engines (Saxena, Goebel, Simon, and Eklund 2008; Sarkar et al. 2011). Figure 5.2 provides a schematic diagram of a commercial aircraft gas turbine engine that was simulated using C-MAPSS. Figure 5.3 presents the main subroutines used in the simulation model.

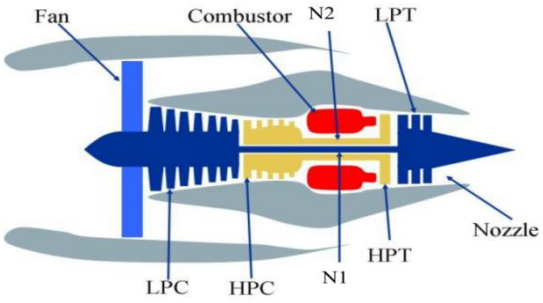

Figure 5.2: Simplified engine diagram simulated in C-MAPSS (Frederick et al. 2008)

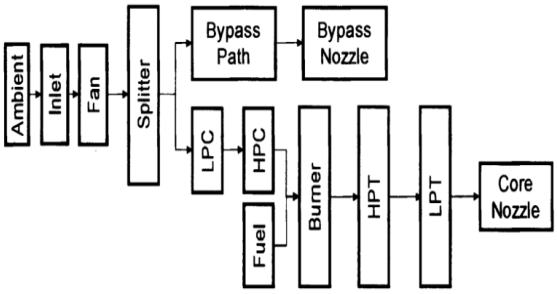

Figure 5.3: A layout of modules and connections in the simulation (Frederick et al. 2008)

A model of a 90,000 lb thrust engine is developed and simulations are run for operations at altitude from 0 to 42,000 ft., Mach number (speed) from 0 to 0.84, and throttle resolver angle (TRA) from 20 to 100. Users can adjust these three conditions: aircraft altitude, Mach number (speed), and TRA to simulate different environmental

conditions. The C-MAPSS simulation model is embedded in a MATLAB Simulink platform. The software allows running in a closed-loop environment, and thus no user input is required during replications. The software has 14 inputs and can generate 21 outputs that are available for analysis. Those 21 outputs are described in Table 5.1.

Table 5.1 Sensors with available data (Saxena, Goebel, Simon, and Eklund 2008)

Symbol	Description	Units
T2	Total temperature at fan inlet	°R
T24	Total temperature at LPC outlet	°R
T30	Total temperature at HPC outlet	°R
T50	Total temperature at LPT outlet	°R
P2	Pressure at fan inlet	psia
P15	Total pressure in bypass-duct	psia
P30	Total pressure at HPC outlet	psia
Nf	Physical fan speed	rpm
Nc	Physical core speed	rpm
epr	Engine pressure ratio (P50/P2)	--
Ps30	Static pressure at HPC outlet	psia
phi	Ratio of fuel flow to Ps30	pps/psi
NRf	Corrected fan speed	rpm
NRc	Corrected core speed	rpm
BPR	Bypass Ratio	--
farB	Burner fuel-air ratio	--
htBleed	Bleed Enthalpy	--
Nf_dmd	Demanded fan speed	rpm
PCNfR_dmd	Demanded corrected fan speed	rpm
W31	HPT coolant bleed	lbm/s
W32	LPT coolant bleed	lbm/s

The basis for developing the simulation model was that damage accumulation will be different for each engine, and thus will not be directly quantifiable based on the flight duration and flight conditions. Consequently, the underlying assumption was users had to rely on sensor data collected during each flight to make decisions regarding the health state of the engine. The simulation model was specifically used to characterize degradation in engine performance due to wear and tear based on the usage pattern of the engines. In order to make it more realistic, an unknown variance in the initial level of

wear and random noise were introduced to represent system variability. In other words, each engine started with different degrees of initial wear and manufacturing variation, which was unknown to the user until the failure threshold was reached. The failure threshold was used to define the EoL (end-of-life) beyond which the unit is considered to have failed. Note that users did not have explicit access to the simulation model and the failure threshold was not announced a priori. A detailed description of the process by which the data was generated is discussed in (Saxena, Goebel, Simon, and Eklund 2008).

5.2.2 Dataset Description

A total of four datasets were generated using this simulation model along with the corresponding failure mode and operational conditions (Saxena, Goebel, Simon, and Eklund 2008). In this chapter, we consider the data pertaining to a single failure mode and a single operating condition. However, our approach can be extended to scenarios with multiple failure modes and multiple operating conditions in future studies. The dataset considered in this work consists of 100 training units, 100 testing units, and a file recording the actual remaining lifetime of the 100 testing units. Each training unit is run to failure, while each testing unit is stopped at some random point prior to its failure. Time is measured in observation epochs, in this case, number of flights. Sensor readings from the 21 outputs are collected after each observation epoch for each unit.

5.3 Development of a Degradation Data-Level Fusion Methodology

We develop a data-level fusion methodology for combining degradation signals from multiple sensors with the objective of constructing a composite health index that accurately characterizes the underlying degradation process and can be used to perform precise prognostic analysis. One critical challenge is how to guarantee that the resulting composite health index is more suitable for degradation modeling and prognostics than

any one of the original sensor signal. To answer this question, we first define a few essential properties that if present in a degradation signal, can enhance its effectiveness when used for prognostics.

5.3.1 Essential Properties for Developing Degradation Signals

Saxena, Celaya, Balaban, Goebel, Saha, Saha, and Schwabacher (2008) pointed out the inconsistencies in the choice of metrics when comparing the performance of various prognostic techniques, and further summarized and suggested several general metrics that can be used for prognostic applications. Although the efforts in (Saxena, Celaya, Balaban, Goebel, Saha, Saha, and Schwabacher 2008) focused on proposing metrics for evaluating performance of prognostic techniques instead of degradation signals, the authors indicated some desirable properties that degradation signals should have for successful prognostic applications.

Property 5.1: Once an initial fault occurs, the trend of the degradation signals should be monotonic.

Property 5.2: Given the same environmental conditions and failure modes, the variance in the failure threshold of different units should be minimal.

Property 5.1 suggests that although raw sensor data may be non-monotonic due to noise, it is important to develop a composite health index that has a clearer monotonic trend. On the other hand, property 5.2 implies that for a given raw sensor data, there may be significant differences among the failure threshold of different units. However, it is important to develop a composite health index that has the least possible variation in its failure threshold. Since we assume that each engine fails due to a single failure mode under a single operating condition, we expect that a composite health index that exhibits a consistent pattern for all units as engine degrades, which can be achieved by jointly maximizing the monotonic property and minimizing the variance in the failure threshold when constructing the health index.

5.3.2 Problem Formulation

Using these two properties, we formulate our data-level fusion methodology as a quadratic programming problem:

$$obj = min_{\boldsymbol{w},\varepsilon_{i,j}}(1-r)\sum_{i=1}^{m}\sum_{j=1}^{n_i-1} c_{i,j}\varepsilon_{i,j} + r\boldsymbol{w}'\boldsymbol{Y}'\boldsymbol{D}\boldsymbol{Y}\boldsymbol{w},$$

$$s.t.\, \boldsymbol{w}'\boldsymbol{M}'\boldsymbol{1} = 1, \boldsymbol{M}\boldsymbol{w} \geq \boldsymbol{0}, \boldsymbol{E_i}\boldsymbol{\omega_i} \geq \boldsymbol{0}\,,$$

$$\varepsilon_{i,j} \geq 0, i = 1, \dots, m, j = 1, \dots, n_i - 1, \tag{5.1}$$

where $\varepsilon_{i,j}$ is the slack variable that measures the amount of violation in monotonicity of the composite health index for unit i and observation epoch j; $c_{i,j}$ is a weight coefficient for the slack variable $\varepsilon_{i,j}$; n_i is the number of available observation epochs in each unit i; m is the total number of training units; $\boldsymbol{w} \in R^{s\times 1}$ is the vector of weight coefficients used to combine multiple sensor data at each observation epoch for each unit, where s is the number of selected sensors; $\boldsymbol{Y} \in R^{m\times s}$ is the matrix recording the last observations before failure with the rows representing each training unit and the columns representing each selected sensor; $\boldsymbol{D} \in R^{m\times s}$ is a symmetric matrix of following form: $\boldsymbol{D} = \frac{\boldsymbol{I}-\boldsymbol{O}/m}{m-1}$, where $\boldsymbol{O}$ is a matrix of all ones and $\boldsymbol{I}$ is an identity matrix; $\boldsymbol{M} \in R^{s\times s}$ is a diagonal matrix denoting the degradation trend information with 1 (-1) on the diagonal entry if the corresponding sensor information shows an increasing (decreasing) trend; $\boldsymbol{\omega_i} = [\boldsymbol{w}', \varepsilon_{i,1}, \dots, \varepsilon_{i,n_i-1}]' \in R^{(s+n_i-1)\times 1}$ is a vector that needs to be determined for unit i such that the composite health index for unit i remains monotonic after adding the slack variables $\varepsilon_{i,1}, \dots, \varepsilon_{i,n_i-1}$ at each observation epoch; $\boldsymbol{E_i} \in R^{(n_i-1)\times(s+n_i-1)}$ is the matrix used to maximize the monotonicity for unit i and has the following form:

$$\boldsymbol{E_i} = \begin{bmatrix} x_{i,1,2} - x_{i,1,1} & \dots & x_{i,s,2} - x_{i,s,1} & \\ \dots & \dots & \dots & \boldsymbol{I} \\ x_{i,1,n_i} - x_{i,1,n_i-1} & \dots & x_{i,s,n_i} - x_{i,s,n_i-1} & \end{bmatrix},$$

where $x_{i,k,j}$ is the sensor data for unit i, sensor k and observation epoch j; r is a tuning

parameter controlling the relative importance of these two additive terms in the quadratic formulation. Discussions on determining the values of c_{ij} and $\boldsymbol{M}$ can be found in the next sub-section.

The formulation in equation (5.1) is inspired by the modeling efforts in linear support vector machines (SVM) for non-separable case (Hastie et al. 2003). The main idea of SVM is to select a hyperplane that creates the biggest margin between the training points for two different classes. In the case that a point is classified on the wrong side of the margin, which is called non-separable case of SVM, a slack variable is introduced to measure the distance of this point to the correct side of the margin. Similarly, the slack variable $\varepsilon_{i,j}$ is added in equation (5.1) to compensate for the violation in monotonicity. Thus, if we denote the composite health index for unit i and observation epoch j as $b_{i,j}$, then, $\varepsilon_{i,j} = max\left(b_{i,j} - b_{i,j+1}, 0\right)$ when solving equation (5.1).

The objective function in equation (5.1) is the summation of two parts: $\sum_{i=1}^{m}\sum_{j=1}^{n_i-1} c_{i,j}\varepsilon_{is,j}$ measures the total weighted amount of violation in monotonicity for Property 5.1 and $\boldsymbol{w'Y'DYw}$ measures the variance in the failure threshold for Property 5.2 (see Appendix A.9 for details). Therefore, equation (5.1) reflects a trade-off between maximizing the monotonic property and minimizing the variance in the failure threshold for prognostics.

To facilitate solving this optimization model, the formulation expressed in equation (5.1) can be simplified as follows:

$$obj = min_{\boldsymbol{\omega}}\ (1-r)\boldsymbol{l'\omega} + r\boldsymbol{\omega'H\omega},$$
$$s.t.\ \boldsymbol{\omega'N'1} = 1, \boldsymbol{F\omega} \geq \boldsymbol{0}, \tag{5.2}$$

where $\boldsymbol{l} \in R^{(s+\sum_{i=1}^{m}(n_i-1))\times 1}$ is the vector of weights for the selected sensors and all slack variables, and equals to $[\boldsymbol{Z}^{1\times s}, \boldsymbol{c'_{1,.}}, \ldots, \boldsymbol{c'_{m,.}}]'$, where the matrix $\boldsymbol{Z}^{a\times b}$ is an a-by-b matrix with all zero entries and $\boldsymbol{c_{i,.}} = [c_{i,1}, \ldots, c_{i,n_i-1}]'$; $\boldsymbol{H} = \boldsymbol{G'Y'DYG}$, where $\boldsymbol{G} \in R^{s\times(s+\sum_{i=1}^{m}(n_i-1))}$ and equals to $[\boldsymbol{I} \quad \boldsymbol{Z}^{s\times(\sum_{i=1}^{m}(n_i-1))}]$. Note that $\boldsymbol{D}$ is a positive

semidefinite (P.S.D) matrix, and therefore it can be shown that $\boldsymbol{H}$ is also P.S.D. (see Appendix A.10 for details). Thus, a global minimizer exists in equation (5.2) as long as there is a feasible vector $\boldsymbol{\omega} \in R^{(s+\sum_{i=1}^{m}(n_i-1))\times 1}$, where $\boldsymbol{\omega} = [\boldsymbol{w}', \boldsymbol{\varepsilon}'_{\boldsymbol{1},.}, \dots, \boldsymbol{\varepsilon}'_{\boldsymbol{m},.}]'$ and $\boldsymbol{\varepsilon_{i,.}} = [\varepsilon_{i,1}, \dots, \varepsilon_{i,n_i-1}]'$. Finally, $\boldsymbol{N} \in R^{s\times(s+\sum_{i=1}^{m}(n_i-1))}$ and is equal to $[\boldsymbol{M} \quad \boldsymbol{Z}^{s\times(\sum_{i=1}^{m}(n_i-1))}]$; $\boldsymbol{F} \in R^{(s+2*\sum_{i=1}^{m}(n_i-1))\times(s+\sum_{i=1}^{m}(n_i-1))}$ and has the following form:

$$\boldsymbol{F} = \begin{bmatrix} \boldsymbol{M} & \boldsymbol{Z}^{s\times(\sum_{i=1}^{m}(n_i-1))} \\ \boldsymbol{A} & \boldsymbol{I} \\ \boldsymbol{Z}^{(\sum_{i=1}^{m}(n_i-1))\times s} & \boldsymbol{I} \end{bmatrix},$$

where $\boldsymbol{A} \in R^{(\sum_{i=1}^{m}(n_i-1))\times s}$ and $\boldsymbol{A} = \begin{bmatrix} \boldsymbol{A_1} \\ \dots \\ \boldsymbol{A_m} \end{bmatrix}$; $\boldsymbol{A_i} \in R^{(n_i-1)\times s}$ and

$$\boldsymbol{A_i} = \begin{bmatrix} x_{i,1,2} - x_{i,1,1} & \dots & x_{i,s,2} - x_{i,s,1} \\ \dots & \dots & \dots \\ x_{i,1,n_i} - x_{i,1,n_i-1} & \dots & x_{i,s,n_i} - x_{i,s,n_i-1} \end{bmatrix}.$$

5.3.3 Model Settings and Parameter Selections

In this section, we discuss several key elements related to our model formulation. Specifically, we focus on data processing and sensor selection, algorithm robustness, setting weight coefficients for $c_{i,j}$, selection of data-fusion function, and tuning parameter setting.

5.3.3.1 Data Processing and Sensor Selection

Since multiple sensors are observed during operation, the first step is to determine which of these sensors should be selected as input to our data-level fusion model. As a preliminary criterion, we focus on sensors that generate signals that exhibit a characteristically increasing or decreasing trend. Thus, we will select a sensor if its last observation is relatively larger (increasing trend) or smaller (decreasing trend) than the initial observation for all the training units. Once the sensors have been selected and trend

information has been identified, then s and $\boldsymbol{M}$ can be determined. Without loss of generality, all sensor data will be standardized.

5.3.3.2 Algorithm Robustness

In many applications, sensor signals may exhibit a relatively stationary trend associated with the non-defective phase of a unit's operation. This may be followed by a defective phase where a unit is still operational but its degradation gradually worsens over time. This phenomenon can be reflected in the characteristics of the degradation signal. For example, in (Gebraeel and Lawley 2008), the authors identified two distinct phases for bearing applications. The first phase was referred to as the non-defective phase and extended from the point of new equipment installation until the very first onset of a fault. In this work, we refer to the time corresponding to the initial fault as the incipient fault time, which we denote as t_f. The second phase was referred to the defective phase. It started from the time of the incipient fault t_f and extended until the point of failure, i.e., when the signal crossed the designated failure threshold.

The dataset used in this chapter also exhibits similar characteristics. For example, Figure 5.4 illustrates these two phases in the degradation signals observed from two sensors "Ps30" and "phi". A vertical dashed line is used to distinguish these two phases. The horizontal dashed line is used to represent the respective failure thresholds. Since no degradation occurs in the non-defective phase, the sensor data observed during that phase does not show a significant trend. Consequently, from a prognostics perspective, it cannot be used to predict remaining lifetime. Thus, only the sensor data pertaining to the defective phase should be used to develop our composite health index. Specifically, we may replace the term $\sum_{i=1}^{m}\sum_{j=1}^{n_i-1} c_{i,j}\varepsilon_{i,j}$ with $\sum_{i=1}^{m}\sum_{j=\tilde{t}_f^i}^{n_i-1} c_{i,j}\varepsilon_{i,j}$ in equation (5.1), where $\tilde{t}_f^i$ is the estimated incipient fault time for unit i.

The key challenge now will be to automatically identify the incipient fault time.

Detection of incipient faults for automatic inspection and minimization of maintenance costs has been studied extensively (Demetriou and Polycarpou 1998). One approach is to build a time series model with moving time windows for each training unit. A CUSUM or exponentially weighted moving average (EWMA) control chart can then be used to monitor the changes in the model residuals (Mousavi and Butler-Purry 2010). Although some efforts have been made (Frank 1990; Zhang, Polycarpou, and Parisini 2002; Chow and Yee 1991), in numerous applications, the accurate identification of incipient fault time using in-situ sensor data is still an ongoing research area. In this chapter, we focus on how to assign the weight coefficients $c_{i,j}$ such that the resulting health index is robust with respect to the uncertainties in estimating the incipient fault time.

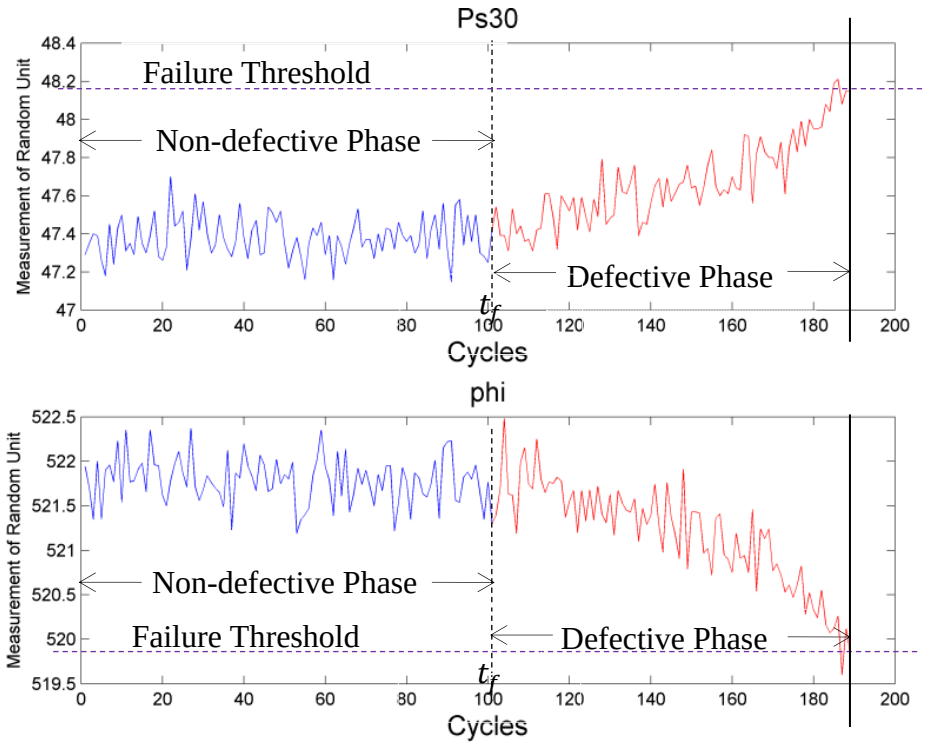

Figure 5.4: Illustration of two phases in degradation signals

5.3.3.3 Setting Weight Coefficients

Recall that $\boldsymbol{\varepsilon_{i,\cdot}}$ measures the amount of violation in monotonicity as unit i

degrades, and $\boldsymbol{c}'_{\boldsymbol{i},\cdot}\boldsymbol{\varepsilon}_{\boldsymbol{i},\cdot}$ is the total weighted sum of violations in monotonicity for unit i. As a unit degrades, the accuracy of predicting its remaining lifetime becomes increasingly sensitive to the amount of violations in monotonicity of the degradation signal. Therefore, we assign higher weights to the slack variables, $\varepsilon_{i,j}$ (see equation (5.1)), as j increases, where j is the observation epoch. Consequently, we define the following condition for $c_{i,j}$:

$$c_{i,j+1} \geq c_{i,j} \geq 0, i = 1, \dots, m, j = \tilde{t}_f^i, \dots, n_i - 2. \tag{5.3}$$

If we assume that each training unit is equally important, then the following constraint must be satisfied:

$$\sum_{j=\tilde{t}_f^i}^{n_i-1} c_{i,j} = 1,\ i = 1, \dots, m. \tag{5.4}$$

We can assume $\{c_{i,j}\}$ follows an arithmetic series ($2c_{i,j} = c_{i,j+1} + c_{i,j-1}$) or a geometric series ($c_{i,j}^2 = c_{i,j+1}c_{i,j-1}$) depending on the emphasis placed on the monotonicity. As a result, $c_{i,j}$ can be computed by initializing $c_{i,\tilde{t}_f^i} = 0$ and using one of the following expressions depending on which assumption is chosen:

- For an arithmetic series:

$$c_{i,j} = c_{i,\tilde{t}_f^i} + (j - \tilde{t}_f^i)\frac{2-2c_{i,\tilde{t}_f^i}(n_i - \tilde{t}_f^i)}{(n_i - \tilde{t}_f^i)(n_i - \tilde{t}_f^i - 1)}, j = \tilde{t}_f^i, \dots, n_i - 1. \tag{5.5}$$

- For a geometric series:

$$c_{i,j} = c_{i,\tilde{t}_f^i} * q^{j-\tilde{t}_f^i}, j = \tilde{t}_f^i, \dots, n_i - 1, \tag{5.6}$$

where q statisfies $c_{i,\tilde{t}_f^i} q^{n_i - \tilde{t}_f^i} - q + 1 - c_{i,\tilde{t}_f^i} = 0$.

Since more weights will be assigned to $\varepsilon_{i,j}$ as j increases, the estimated vector of weight coefficients, $\boldsymbol{w}$, becomes progressively dominated by the sensor data at observation epochs that are closer to the failure point. We will show in the case study section that our composite health index has the advantage that it will be robust with respect to the uncertainties in estimating the incipient fault time.

5.3.3.4 Selection of Data-Fusion Function

The formulation expressed in equation (5.2) uses a weighted average data-fusion function to combine the selected sensor data (i.e. $\boldsymbol{w}'\boldsymbol{M}'\mathbf{1} = 1$). The vector $\boldsymbol{w}$ measures the relative importance of each sensor, and thus the composite health index is a weighted average of the sensor data. It is worth noting that the linearity assumption may not be suitable in some applications, in which case non-linear functions may be used when developing the health index.

5.3.3.5 Tuning Parameter Setting

The tuning parameter r is used to control the relative importance given the two terms of the objective function, monotonicity and threshold variance, in equation (5.2). The optimal value of r can be obtained by cross-validation. For K-fold cross-validation, we can split the training data into K equal-sized groups. For a particular value of $r(0 < r < 1)$, we leave the kth group data out and train the model in equation (5.2) based on the $K - 1$ groups of data. Next, we calculate the amount of violation in the monotonic property, VM_k and the variance in the failure threshold, VF_k. We repeat the procedure for $k = 1, \dots, K$ and combine VM_k and VF_k for different k (e.g. $VM = \sum_{k=1}^{K} VM_k /K, VF = \sum_{k=1}^{K} VF_k /K$) and use it as the evaluation criterion for the chosen r value. Clearly, increasing r puts more emphasis on reducing the variance in the failure threshold on the expense of increasing the possibility of violating the monotonic property of the health index.

To solve a multi-objective optimization problem, one standard approach is to plot the efficient frontier with respect to the two terms of the objective function in equation (5.2). It is known that when moving from one solution to another on the efficient frontier, there is always a certain amount of sacrifice in one objective (e.g increased amount of violation in the monotonic property), in order to achieve a certain amount of gain in the

other (e.g. decreased variance in the failure threshold). In practice, the optimal value of r depends on the different emphasis we place on the two terms of the objective function.

5.3.4 Flow chart of the Data-Level Fusion Approach

Figure 5.5 illustrates the flow chart of our proposed data-level fusion approach based on multiple sensor data for degradation modeling and prognostics. Denote the optimal values of r and $\boldsymbol{\omega}$ as r^* and $\boldsymbol{\omega}^*$. Only the first s entries of $\boldsymbol{\omega}^*$, which are the optimal values of $\boldsymbol{w}$, $\boldsymbol{w}^*$, will be used to construct the health index for testing units.

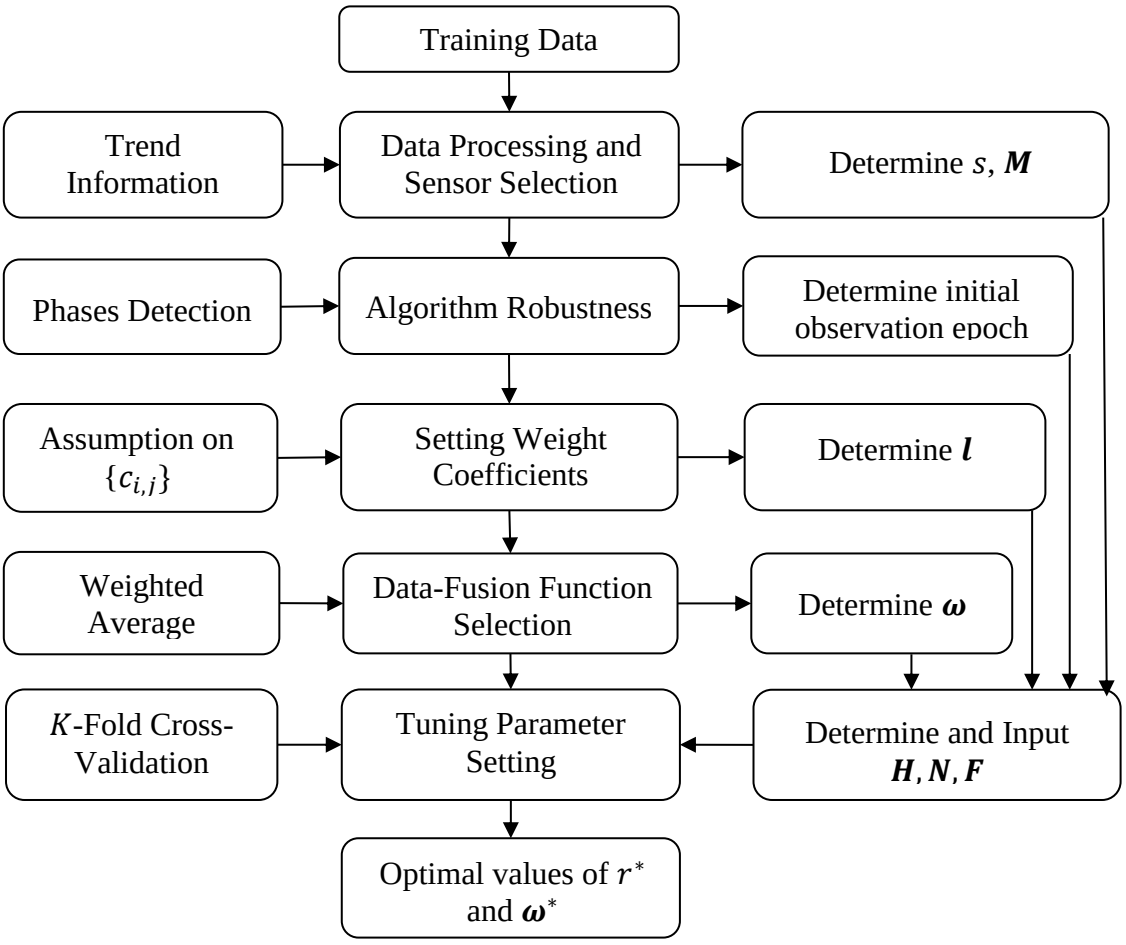

Figure 5.5: Flow chart of the proposed data-level fusion approach

5.4 Case Study

In this case study, we investigate the performance of our data-level fusion methodology using degradation-based sensor data pertaining to turbofan engines. The dataset consists of 100 training units (i.e. $m = 100$) with a total of 20631 observation epochs (i.e. $\sum_{i=1}^{m} n_i = 20631$), 100 testing units with a total of 13096 observation epochs, and a file recording the actual remaining lifetime of the 100 testing units. (Additional details pertaining to the experimental setup and simulation model used to generate the data have been discussed earlier in Section 5.2.) Detailed procedures for data processing and sensor selection, algorithm robustness, weight coefficients setting, data-fusion function selection, tuning parameter setting and computational complexity analysis are illustrated in this section.

To numerically evaluate the improved performance of the composite health index when it is used for model fitting and remaining life prediction, the stochastic degradation modeling framework (Gebraeel 2006) is adopted to compute and update the remaining life distribution (RLD) of each unit in real-time. We will compare the accuracy of predictions using the composite health index and that resulting from using each individual sensor based on the same stochastic degradation modeling framework (Gebraeel 2006). It is worth mentioning that the composite health index can be considered as another sensor data, which can be directly treated as an input for other feature-level or decision level fusion methods. Since the input data become more informative, the accuracy of predictions is expected to be improved by using both the composite health index and the original sensor data.

5.4.1 Data Processing and Selection

Among the 21 outputs listed in Table 5.1, 11 sensor data are selected. The selection is made on the basis that the data shows a consistent degradation trend for all training units. Those 11 (i.e. $s = 11$) sensors are T24, T50, P30, Nf, Ps30, phi, NRf, BPR,

htBleed, W31 and W32. Furthermore, the corresponding diagonal elements of $\boldsymbol{M}$ are identified as $[1, 1, -1, 1, 1, -1, 1, 1, 1, -1, -1]'$. Recall that 1 refers to an increasing trend, while -1 refers to a decreasing trend.

5.4.2 Algorithm Robustness

As mentioned before, since more weights will be assigned to $\varepsilon_{i,j}$ as j increases, the estimated vector of weight coefficients, $\boldsymbol{w}$, becomes progressively dominated by the sensor data at observation epochs that are closer to the failure point. To demonstrate this point, we consider the constraint: $n_i - \tilde{t}_f^i = p, \forall i$, where p represents the number of observation epochs in the defective phase. This constraint ensures that the number of observations (from the defective phase) used to construct the health index is the same for all training units. Since each unit has different values for n_i and $\tilde{t}_f^i$, there are no guarantees that the defective phases of all the training units will be equal to p. In what follows, we will show that even when last p observations before failure are used, the methodology still provides a reasonably robust estimation of the weight vector.

Figure 5.6 illustrates the relationship between the estimated optimal weights $\boldsymbol{w}^*$ and different values of p. It is clear from the graph that beyond specific values for p, the estimated $\boldsymbol{w}^*$ becomes relatively unaffected by changes of p. Furthermore, as p increases, the elements of $\boldsymbol{w}^*$ converge to constant values. Based on our experimental observations as shown in Figure 5.6, we use the last 100 observations (i.e. $p = 100$) of each unit when estimating $\boldsymbol{w}^*$ in equation (5.1).

In addition, a discrete random number has been added to $p = 100$ to simulate the estimation uncertainties of the defective phase in each unit. The experiments yield similar robust result, where $\boldsymbol{w}^*$ is also robust with respect to the uncertainties in estimating the defective phase in each unit. Results have been omitted due to the page limit restrictions. Thus, as long as sufficient observation epochs are selected to represent the defective

phase (i.e. p is sufficiently large), $\boldsymbol{w}^*$ will be relatively robust.

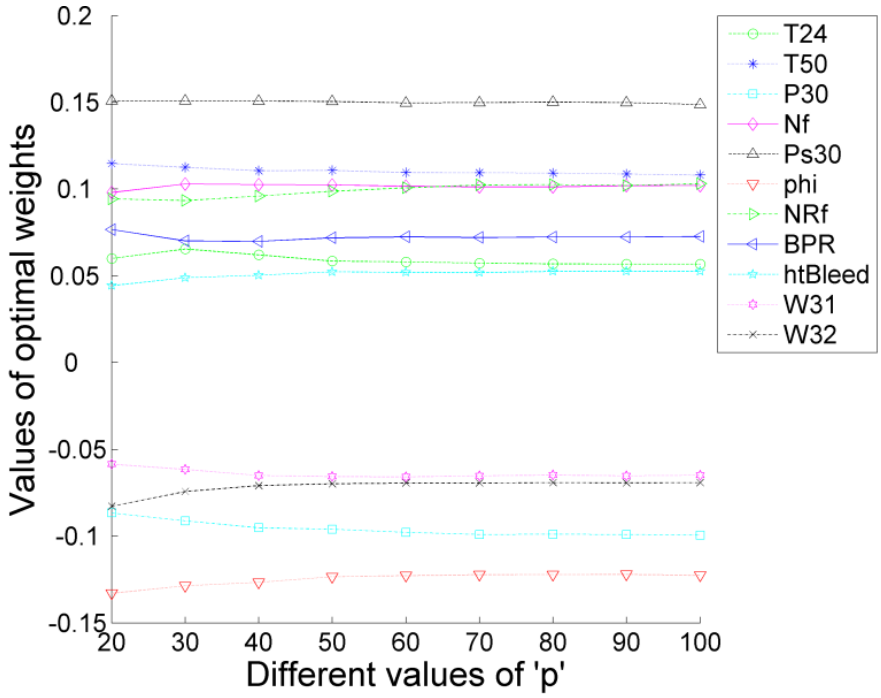

Figure 5.6: Changes in the optimal weights $\boldsymbol{w}^*$ at different values of p

5.4.3 Selecting Weight Coefficients and Data-Fusion Function

An arithmetic series for $\{c_{i,j}\}$ is adopted by assuming linearly increasing weight coefficients. Recall that these coefficients capture the violation in the monotonic property as unit i degrades. In addition, a weighted average data-fusion function is selected for demonstration.

5.4.4 Tuning Parameter Setting

As mentioned earlier, the optimal value of the tuning parameter, r^*, can be estimated using K-fold cross-validation. For the purpose of this study, K is chosen to be 5. Thus, in each fold validation, we train the model in equation (5.2) using 80 training units. For each selected r value, we calculate the average amount of violation in monotonicity,

VM, and the average variance of the failure threshold, VF, of the composite health index using 5-fold cross-validation.

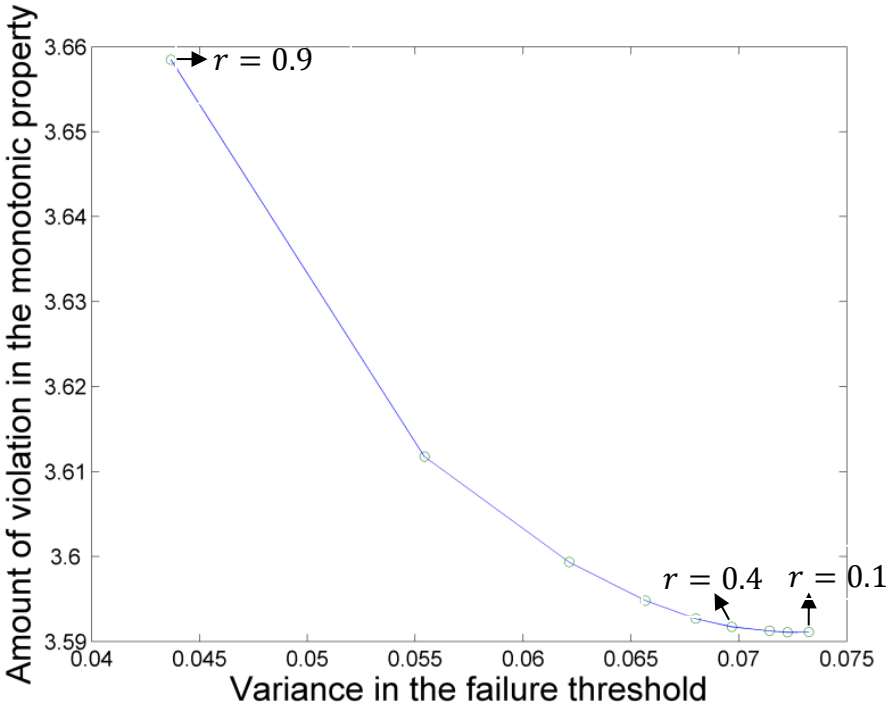

Figure 5.7: Efficient frontier of the amount of violation in the monotonic property V.S. the variance in the failure threshold of the health index

Figure 5.7 plots the relationship between the amount of violation in monotonicity versus the variance in the failure threshold for different r values. This efficient frontier plot demonstrates that as r becomes larger, the amount of violation in monotonicity trend increases and the variance in the failure threshold decreases.

In this case study, we choose $r = 0.4$ because the marginal reduction in the violation in monotonicity is small compared to the marginal increase in the variance of the failure threshold. In practice, the value of r can be chosen depending on how important each property is when developing the composite health index. Setting $r = 0.4$ and solving the quadratic formulation in equation (5.2) for the selected sensor data, we get the optimal weights $\boldsymbol{w}^*$, which are summarized below in Table 5.2.

Table 5.2: Optimal weights $\boldsymbol{w}^*$ to combine the selected sensor data

Name	T24	T50	P30	Nf	Ps30	phi	NRf	BPR	htBleed	W31	W32
Value	0.0568	0.1081	-0.0994	0.1021	0.1488	-0.1226	0.1030	0.0726	0.0526	-0.0649	-0.0691

5.4.5 Computational Complexity Analysis

All numerical experiments are performed using MATLAB V7.9 and TOMLAB V7.8 (Holmström et al. 2008) in Windows 7 operating system with two Intel Core i7-2820QM 2.30 GHz processors and 8 GB RAM. Most of the computational time was used for solving the optimization model expressed in equation (5.2) with $s + \sum_{i=1}^{80}(n_i - \tilde{t}_f^i) = 11 + 80 * 100 = 8011$ number of variables and $s + 2 * \sum_{i=1}^{80}(n_i - \tilde{t}_f^i) = 16011$ number of inequality constraints. Our experimental study shows that on average it takes about 6 seconds to solve the optimization problem using CPLEX solver in Tomlab (Holmström et al. 2008).

5.4.6 Stochastic Degradation Modeling

5.4.6.1 Degradation Model Development

Based on the scatter plot of the sensor data in Figure 5.8, degradation signals show exponential functional forms. The exponential functional form has been widely used to model cumulative damage processes (Gebraeel 2006; Gebraeel and Lawley 2008; Gebraeel 2010). In this case study, we use the stochastic degradation modeling approach proposed in (Gebraeel 2006) to evaluate the performance of the composite health index when used to predict remaining lifetime.

We begin by assuming that the sensor data $x_{i,k,j}$ satisfies:

$$x_{i,k,j} = \phi_k + \theta_{i,k} e^{\alpha_{i,k} * j + \beta_{i,k} * j^2 + \tau_{i,k}(j) - \frac{\sigma_k^2}{2}}, \tag{5.7}$$

where ϕ_k is a constant deterministic parameter for sensor k, $\theta_{i,k}$, $\alpha_{i,k}$ and $\beta_{i,k}$ are random variables, and $\tau_{i,k}(j)$ is normally distributed random error term with mean 0 and variance

σ_k^2. Since $E\left(e^{\tau_{i,k}(j)-\frac{\sigma_k^2}{2}}\right)=1$, then $E\left(x_{i,k,j}\middle|\theta_{i,k},\alpha_{i,k},\beta_{i,k}\right)=\phi_k+\theta_{i,k}e^{\alpha_{i,k}*j+\beta_{i,k}*j^2}$.

Similar to the work presented in (Gebraeel 2006) we use the log transformation, i.e., we define $L_{i,k,j}$ as:

$$L_{i,k,j}=ln\left(x_{i,k,j}-\phi_k\right)=\theta'_{i,k}+\alpha_{i,k}*j+\beta_{i,k}*j^2+\tau_{i,k}(j), \qquad (5.8)$$

where $\theta'_{i,k}=ln\theta_{i,k}-\frac{\sigma_k^2}{2}$. We further assume that the stochastic parameters $\theta'_{i,k}$, $\alpha_{i,k}$ and $\beta_{i,k}$ are jointly distributed and follow a multivariate normal distribution: $\boldsymbol{\Gamma_{i,k}}=\begin{pmatrix}\theta'_{i,k}\\ \alpha_{i,k}\\ \beta_{i,k}\end{pmatrix}\sim N_3(\boldsymbol{u_0^k},\boldsymbol{\Sigma_0^k})$.

5.4.6.2 Parameter Estimation

The prior distribution of the $\boldsymbol{\Gamma_{i,k}}$ can be estimated by fitting the degradation path of each training unit with the model defined in equation (5.8). σ_k^2 can be estimated by using the residual sum of square over the total number of degree of freedom in the training stage. Once the prior joint distribution of the stochastic parameters is estimated, it is updated using sensor data obtained from each individual testing unit. Next, the updated degradation model can be utilized to compute the RLD which is particular to this testing unit. This process emulates the utilization of in-situ sensor signals to update the remaining lifetime estimation based on the unique degradation characteristics of each unit.

Figure 5.8 shows the result of fitting the exponential model to each selected sensor data, and to the composite health index obtained for a random training unit. Table 5.3 summarizes the estimated σ_k^2 for all selected sensors and the health index. It clearly shows that the composite health index gives a much better fitting result.

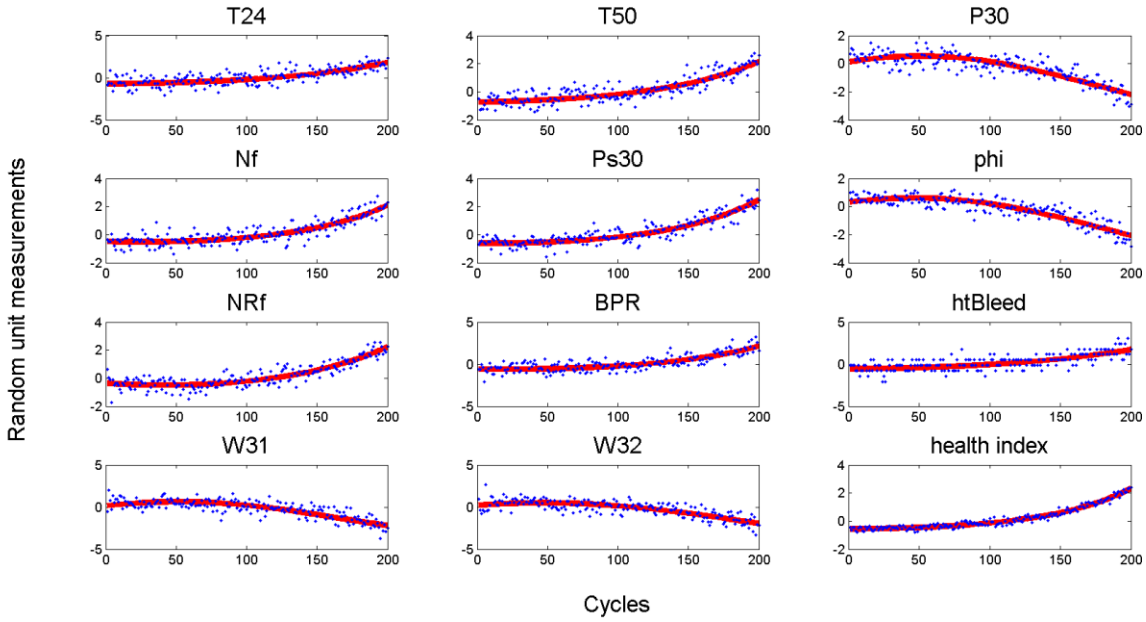

Figure 5.8: Degradation signals plot and model fittings for all selected sensor data and the health index in training unit #1

Table 5.3: Estimated σ_k^2 of all selected sensors and the health index

Name	T24	T50	P30	Nf	Ps30	phi
Value	0.0795	0.067	0.0676	0.0634	0.0574	0.0591
Name	NRf	BPR	htBleed	W31	W32	health index
Value	0.0615	0.0751	0.1052	0.081	0.0789	0.0189

Let $\boldsymbol{L}_{.,\boldsymbol{k},\boldsymbol{n}_.}$ be the sequence of the log transformed data, which records the last observations before failure in all training units for sensor k, and $\boldsymbol{L}_{.,\boldsymbol{k},\boldsymbol{n}_.} = [L_{1,k,n_1}, \dots, L_{m,k,n_m}]'$. Denote the mean of failure threshold for sensor k as u_d^k and the variance of failure threshold for sensor k as v_d^k. u_d^k and v_d^k can be estimated by calculating the mean and the variance of $\boldsymbol{L}_{.,\boldsymbol{k},\boldsymbol{n}_.}$, respectively. Table 5.4 summarizes the variance of the failure threshold for all selected sensors and the health index, respectively. It clearly shows that variance of the failure threshold in the composite health index is much smaller than the one in any other sensor data due to the formulation in equation (5.2).

Table 5.4: Variance in the failure threshold of all selected sensors and the health index

Name	T24	T50	P30	Nf	Ps30	phi
Var.	0.0274	0.0140	0.0264	0.0683	0.0154	0.0206
Name	NRf	BPR	htBleed	W31	W32	health index
Var.	0.0580	0.0225	0.0435	0.0220	0.0317	0.0101

5.4.6.3 Estimation of Updated Residual Life Distribution

Let $\boldsymbol{L_{i,k,.}}$ be the sequence of the log transformed data observed up to current observation epoch n_i for unit i and sensor k, such that $\boldsymbol{L_{i,k,.}} = [L_{i,k,1}, \dots, L_{i,k,n_i}]'$. The posterior distribution of $\boldsymbol{\Gamma_{i,k}}$ still follows a multivariate normal distribution: $\boldsymbol{\Gamma_{i,k}}|\boldsymbol{L_{i,k,.}} \sim N_3(\boldsymbol{u_p^{i,k}}, \boldsymbol{\Sigma_p^{i,k}})$, where $\boldsymbol{u_p^{i,k}} = \left(\frac{\boldsymbol{\Psi_i}'\boldsymbol{\Psi_i}}{\sigma_k^2} + (\boldsymbol{\Sigma_0^k})^{-1}\right)^{-1} (\frac{\boldsymbol{\Psi_i}'\boldsymbol{L_{i,k,.}}}{\sigma_k^2} + (\boldsymbol{\Sigma_0^k})^{-1}\boldsymbol{u_0^k})$, $\boldsymbol{\Sigma_p^{i,k}} = \left(\frac{\boldsymbol{\Psi_i}'\boldsymbol{\Psi_i}}{\sigma_k^2} + (\boldsymbol{\Sigma_0^k})^{-1}\right)^{-1}$ and $\boldsymbol{\Psi_i} \in R^{n_i \times 3} = \begin{bmatrix} 1 & 1 & 1 \\ \dots & \dots & \dots \\ 1 & j & j^2 \\ \dots & \dots & \dots \\ 1 & n_i & n_i^2 \end{bmatrix}$ (see Appendix A.11 for details).

Define $\tilde{T}_{i,k}$ as the estimated remaining lifetime of testing unit i based on the signal from sensor k. We are interested in deriving the RLD by evaluating the distribution of the time at which the sensor signal crosses the failure threshold. Since $L_{i,k,n_i+t} = \theta'_{i,k} + \alpha_{i,k} * (n_i + t) + \beta_{i,k} * (n_i + t)^2 + \tau_{i,k}(n_i + t)$, then L_{i,k,n_i+t} is normally distributed with mean $\tilde{u}_{i,k,n_i+t}$ and variance $\tilde{\sigma}^2_{i,k,n_i+t}$, where $\tilde{u}_{i,k,n_i+t} = [1, n_i + t, (n_i + t)^2]\boldsymbol{u_p^{i,k}}$ and $\tilde{\sigma}^2_{i,k,n_i+t} = [1, n_i + t, (n_i + t)^2]\boldsymbol{\Sigma_p^{i,k}}[1, n_i + t, (n_i + t)^2]' + \sigma_k^2$. Further, we assume that the failure thresholds for different units are independent. Thus, the conditional cumulative distribution function (cdf) of the estimated remaining lifetime $\tilde{T}_{i,k}$ given the historical data $\boldsymbol{L_{i,k,.}}$ is:

$$F_{\tilde{T}_{i,k}|\boldsymbol{L_{i,k,.}}}(t) = P\left(\tilde{T}_{i,k} \le t \middle| \boldsymbol{L_{i,k,.}}\right) = P\left(L_{i,k,n_i+t} \ge u_d^k \middle| \boldsymbol{L_{i,k,.}}\right) = 1 - P\left(L_{i,k,n_i+t} < u_d^k \middle| \boldsymbol{L_{i,k,.}}\right)$$

$$= \Phi\left(\frac{u_d^k - \tilde{u}_{i,k,n_i+t}}{\sqrt{\tilde{\sigma}_{i,k,n_i+t}^2 + v_d^k}}\right) = \Phi\left(g(t)\right)$$

, (5.9)

where $\Phi(\cdot)$ is the cdf of the standard normal distribution. Conditional on the fact that $\tilde{T}_{i,k} \ge 0$, the truncated cdf for $\tilde{T}_{i,k}$ can be written as:

$$P\left(\tilde{T}_{i,k} \le t \middle| \boldsymbol{L_{i,k,.}}, T_{i,k} \ge 0\right) = \frac{P\left(0 \le \tilde{T}_{i,k} \le t \middle| \boldsymbol{L_{i,k,.}}\right)}{P\left(\tilde{T}_{i,k} \ge 0 \middle| \boldsymbol{L_{i,k,.}}\right)} = \frac{\Phi\left(g(t)\right) - \Phi\left(g(0)\right)}{1 - \Phi\left(g(0)\right)}. \quad (5.10)$$

Since the RLD is skewed, it is preferable to utilize the median as the point estimator of the remaining lifetime. Numerically, this can be estimated by finding the observation epoch t where $P\left(\tilde{T}_{i,k} \le t \middle| \boldsymbol{L_{i,k,.}}, \tilde{T}_{i,k} \ge 0\right) = 0.5$.

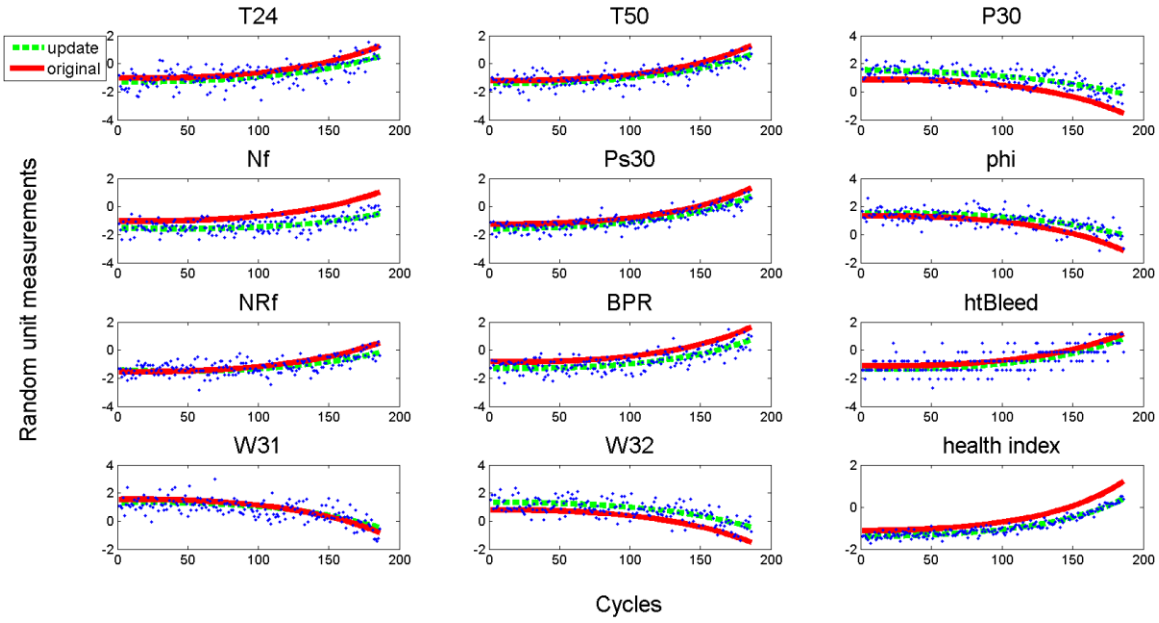

Figure 5.9: Degradation signals plot with original and updated model fitting for all selected sensor data and the health index in testing unit #24

Figure 5.9 illustrates the original and the updated degradation model of a random testing unit in all selected sensors and the health index. The solid line shows the original

model fitting based on the priors which are estimated from training units, whereas the dashed line presents the updated model fitting based on the collected sensor data for this particular testing unit. Similar to Figure 5.8, the composite health index shows a much better monotonic property and model fitting result.

5.4.6.4 Prediction Results

To evaluate the performance of the health index for remaining life prediction, we compute the percentage difference between the predicted and the actual failure time. We consider two cases for the predicted failure time: (1) when it is estimated based on the composite health index, and (2) when it is estimated based on each individual sensor signal. Specifically, we define the percentage error, $err_{i,k}$, as the relative difference between the predicted and the actual failure time for unit i and sensor k, which is expressed as:

$$err_{i,k} = \frac{(n_i+\tilde{T}_{i,k})-(n_i+T_i)}{n_i+T_i} = \frac{\tilde{T}_{i,k}-T_i}{n_i+T_i}, \quad (5.11)$$

where n_i is the number of available observation epochs of testing unit i when it stops further usage; T_i is the actual remaining lifetime for unit i and $\tilde{T}_{i,k}$ is the estimated remaining lifetime for unit i and sensor k.

Since different testing units stop further usage at different time, we compare the absolute value of the mean percentage error by using each selected sensor and the composite health index at different levels of actual remaining lifetime, as shown in Figure 5.10. For example, the points correspond to the "all" label are the comparison results based on all 100 testing units whereas the points correspond to the "80" label are the comparison results based on the testing units with equal to or less than 80 actual remaining observation epochs.

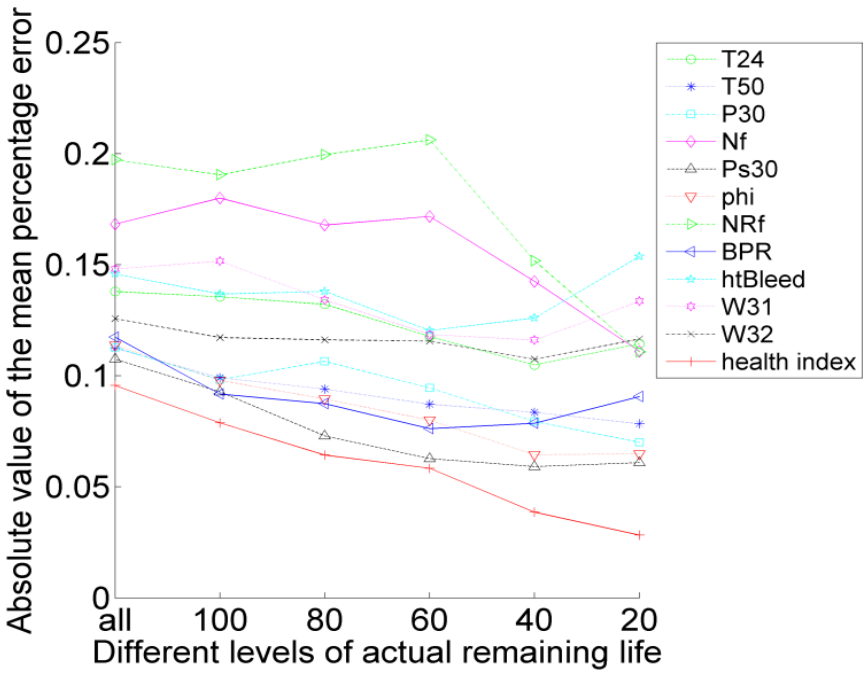

Figure 5.10: Comparison results of the absolute value of the mean percentage error by using each selected sensor and the health index at different levels of the actual remaining lifetime

Using the results in Figure 5.10, we can make the following observations:

i) The composite health index outperforms any single sensor data when it is used for remaining life prediction, which results from the controls on two terms in equation (5.2) when developing the composite health index: maximizing the monotonic property and minimizing the variance in the failure threshold.

ii) The advantages of the composite health index for remaining life prediction become more obvious when the unit approaches the actual failure time. For example, at label "40" or "20", the percentage error of remaining life prediction by using the composite health index is much smaller than the one by using any other sensor data. The first reason for this phenomenon is that as the actual remaining lifetime becomes smaller, our predictions are made for a shorter future time period, and therefore less uncertainty is involved. Second, less actual remaining lifetime usually indicates more historical data have been collected, and thus we are more confident about the updated fitting models.

The final possible explanation is since we assign higher weights to the slack variables, $\varepsilon_{i,j}$ as j increases, the remaining life prediction by using the composite health index becomes more accurate when we make the prediction at the observation epoch that is closer to the actual failure time. This unique characteristic of the composite health index has significant practical impact, especially with regards to safety.

Often practitioners are not only interested in point estimation of the remaining lifetime, but also interested in evaluating a confidence interval (CI) of the predicted remaining lifetime. Confidence intervals can be obtained by the truncated cdf of the estimated remaining lifetime $\tilde{T}_{i,k}$ in equation (5.10). Figure 5.11 shows the 95% CIs of the remaining life prediction for testing unit #24 for each selected sensor as well as the composite health index. The bars represent the 95% CIs of the remaining life prediction, and the dots represent the point estimates. The dashed horizontal line represents the actual value of the remaining lifetime.

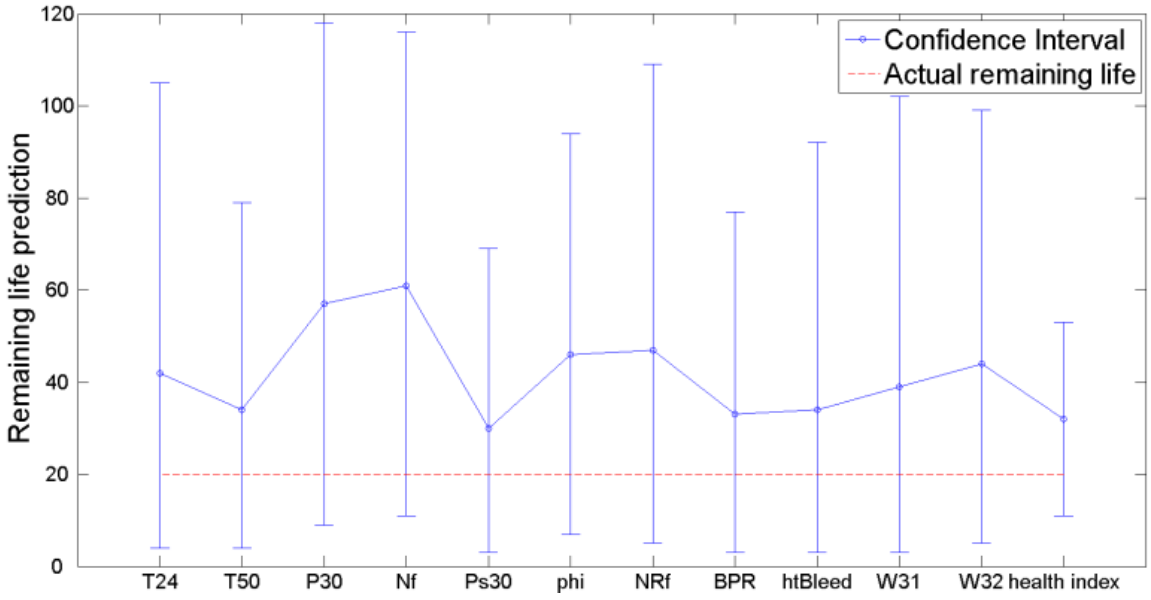

Figure 5.11: Confidence intervals of the remaining life prediction for the testing unit #24 by using each selected sensor and the health index

It is clear that using the composite health index to predict the remaining lifetime

provides the narrowest CI. Due to the goodness of model fitting and low variance of the failure threshold, the denominator in the $\Phi(\cdot)$ operation of equation (5.9) by using the composite health index is smaller than the one by using any other sensor data, which results in the narrowest CI in the health index. Table 5.5 summarizes the mean of the widths of the 95% CIs of the remaining life predictions for all testing units when evaluated using each selected sensor versus the composite health index. According to the results of Table 5.5, using the composite health index for remaining life prediction can reduce the widths of the 95% CIs by 37.5% (i.e. (157.0-98.2)/157.0). Thus, the composite health index can provide a more precise estimation of the remaining lifetime.

Table 5.5: Mean widths of the 95% CIs of the remaining life prediction in all testing units using all selected sensors and the health index

Name	T24	T50	P30	Nf	Ps30	phi
Width	195.8	168.6	178.7	195.2	160.03	157.0
Name	NRf	BPR	htBleed	W31	W32	health index
Width	190.0	183.7	212.3	202.8	190.4	98.2

5.5 Discussion and Conclusion

This chapter develops a systematic approach which includes data selection, data processing, and data fusion steps that lead to an improved degradation-based prognostic model. The novelty of this methodology lies in the development of a data-level fusion technique that combines signals from multiple sensors. By identifying the two essential properties that degradation signals should have for successful prognostic applications (i.e. maximizing the monotonic property and minimizing the variance in the failure threshold), a composite health index can be developed to better characterize the degradation performance of each system. Guidelines for several key elements related to the problem formulation, algorithm robustness, weight coefficients setting, selection of data-fusion function, and other important aspects are discussed and illustrated in the case study. One

advantage of this methodology is that the remaining life prediction becomes more accurate as the unit approaches failure compared with using each individual sensor. This property could have a great impact on deciding when to schedule maintenance or to stop operation in practice. Another advantage of this methodology is that the widths of the CI can be significantly reduced by using the composite health index for remaining life prediction, which indicates the composite health index can be a more efficient tool for prognostics.

The methodology was tested and validated using the degradation sensor data of aircraft gas turbine engine that were generated by C-MAPSS (Saxena, Goebel, Simon, and Eklund 2008). The stochastic degradation modeling framework (Gebraeel 2006) was adopted to numerically evaluate the performance of the composite health index by computing and updating the RLD of each unit in real-time. However, the methodology developed in this chapter is not limited to this type of modeling framework. In other words, the composite health index can be considered as another sensor data, which can be directly treated as an input for other feature-level or decision level fusion methods. Since the input data become more informative, the accuracy of predictions is expected to be improved by using both the composite health index and the original sensor data.

This research establishes a new direction in data fusion by proposing an appropriate data-level fusion technique that is specifically beneficial for degradation modeling and prognostic applications. There are several important topics for future research that are related to this work. First, further studies can be done to investigate the performance when non-linear features are created and the kernel methods are used to map *in-situ* sensor data into higher dimensional space. Second, although this chapter focuses on the degradation dataset with a single operation condition and a single failure mode, extensions to the cases that have more than one failure mode or operational condition are worthy of further exploration.

CHAPTER 6

CONCLUSIONS AND FUTURE RESEARCH

6.1 Summary of Original Contributions

This thesis contributes to the area of data fusion for effective employment of the underlying monitoring and data gathering capabilities for system modeling, performance assessment, diagnosis, and prognosis of the system behavior. The research has interdisciplinary nature, and developed new methodologies by integrating techniques in advanced statistics, engineering domain knowledge, and operation research. The proposed data fusion methodologies mainly focus on two topics: (1) sensor system design and (2) degradation modeling and prognostic analysis. The original contributions of this thesis include the following aspects:

- *An algorithm named as "Best Allocation Subsets by Intelligent Search" (BASIS) with optimality proof was developed to obtain the optimal fixed sensor allocation design in a Bayesian Network at minimum cost under different user specified detection requirements. In addition, a diagnosis ranking method was developed to identify the root cause based on a Bayesian Network.* This BASIS algorithm is developed based on integrating the analysis of multivariate T^2 control chart and causal structures when only partial observations are available. The proposed BASIS algorithm is conducted in a systematic and intelligent way, which does not require expensive Monte Carlo simulation studies when deriving the optimal sensor allocation solution. On the other hand, as an extension to the LASSO-based variable selection method (Wang and Jiang 2009), the diagnosis ranking algorithm is developed to find the root cause when only partial observations are available. The developed methodologies are

successfully demonstrated on a hot forming process and a cap alignment process. This study has revealed that a trade-off problem occurs when detection speed, fault diagnosis accuracy and cost saving are taken into consideration.

- *A novel approach to adaptively reallocate sensor resources in a Bayesian Network based on online observations was developed to enhance both monitoring and diagnosis capabilities.* This fundamental investigation establishes a new research question that focuses on adaptively reallocating sensors for abnormality detection during online monitoring. This study proposes a max-min criterion, which enables manage sensor reallocation and process change detection in an integrated manner. The methodology is tested and validated based on a hot forming process and a cap alignment process, which can significantly improve the detection delay and diagnosis accuracy compared with the work in Liu and Shi (2012).
- *A systematic Scalable-Efficient-Robust Adaptive (SERA) sensor allocation strategy for online high-dimensional process monitoring was proposed with the purpose of minimizing detection delay in a general DSN*. This methodology involves a novel monitoring scheme by using the sum of top-r local statistics for fast process change detection. The use of this framework has several advantages over other approaches, which include significant decreases in computational cost (i.e. the complexity is only linear in the number of variables), and extensive savings for physical sensors, data acquisition, transmission and processing time. Two properties of this algorithm are also investigated. The methodology is tested and validated on a hot forming process and a real solar flare process. Both studies have demonstrated the capabilities of the SERA algorithm to quickly detect and also localize the process changes.
- *A generic real-time sensor selection and data-level fusion algorithm was developed to construct a composite health index for better degradation modeling and prognostic analysis.* This methodology is proposed to achieve two essential properties that if present in a degradation signal can enhance the effectiveness for

degradation modeling and prognostics. Guidelines for several key elements related to the problem formulation, algorithm robustness, weight coefficients setting, selection of data-fusion function, and other important aspects are discussed in the methodology. The case study, which is based on the degradation signals of aircraft gas turbine engines, demonstrates that the proposed method can provide a much better prognostic result compared to relying solely on the data from any individual sensor.

6.2 Future Research

There are several important topics to be explored for further development of data fusion methodologies for sensor system design and prognostic analysis. Here are some examples:

- *Sensor System Design and Data Analytics:*
  - Improvement in the searching speed of the BASIS algorithm: The computation complexity of the current BASIS algorithm in Chapter 2 is exponential in the number of variables. Thus, when the manufacturing workstation has hundreds or thousands of variables, directly implementing the BASIS algorithm can be inefficient. In this situation, we suggest to sequentially decompose a large Bayesian network into clustered sub-graphs if the path coefficient between these sub-graphs is insignificantly small. Then, BASIS algorithm can be implemented separately within each clustered subsystem. If the number of variables within each cluster is still large, then it needs further improvement in the searching algorithm to find the optimal solution.
  - Theoretical analysis and assumption relaxation in the SERA algorithm: The current SERA algorithm in Chapter 4 assumes each variable follows a standard normal distribution and only focuses on mean shift detection. Future studies can be done to

relax these assumptions. In addition, there are three parameters, u_{min}, Δ, and r in the SERA algorithm, which are assumed to be all constant in the current formulation. Further studies can be done to investigate the adaptive value of these parameters based on online measurements and detection requirements to further improve the performance. Furthermore, the theoretical basis for the threshold selection, d in the SERA algorithm is a challenging, but important topic to study.

- *Prognostic Analytics from Multi-Stream Condition Monitoring:*
  - *Further investigation of the non-linear features and extension to the cases with more than one failure mode or operational condition:* The current data fusion function is selected and formulated as linear in Chapter 5. However, the linearity assumption may not be suitable in some applications, in which case non-linear functions may be used when developing the health index. Therefore, further studies can be done to investigate the performance when non-linear features are created and the kernel methods are used to map in-situ sensor data into higher dimensional space. Second, the proposed methodology assumes that the degradation occurs in a cumulative manner under a single operation condition, which results from a single failure mode. Extensions to the cases that have more than one failure mode or operational condition are worthy of further exploration.

APPENDIX A

PROOFS AND ADDITIONAL INFORMATION

A.1 Proof of Proposition 2.1

For any $\widetilde{\boldsymbol{\delta}} \in R_1$, there exists index i, so that $\widetilde{\boldsymbol{\delta}} = a\boldsymbol{\delta}(i)$, where $|a| \geq 1$. If $\boldsymbol{s}$ is a feasible solution from the BASIS algorithm, then $\Delta(\boldsymbol{s}) = (\boldsymbol{A^{-1}\delta}(i))_{\boldsymbol{s}}^{\boldsymbol{T}}\{[\boldsymbol{A^{-1}\Sigma_V}(\boldsymbol{A^{-1}})^{\boldsymbol{T}}]_{\boldsymbol{s}}\}^{-1}\ (\boldsymbol{A^{-1}\delta}(i))_{\boldsymbol{s}} \geq \tilde{\Delta}(card(\boldsymbol{s}))$ based on definition 2.2. $\Delta(\boldsymbol{s})$ can be rewritten as $\boldsymbol{\delta}(i)_{\boldsymbol{s}}^{\boldsymbol{T}}(\boldsymbol{A^{-1}})_{\boldsymbol{s}^r}^{\boldsymbol{T}}\{[\boldsymbol{A^{-1}\Sigma_V}(\boldsymbol{A^{-1}})^{\boldsymbol{T}}]_{\boldsymbol{s}}\}^{-1}(\boldsymbol{A^{-1}})_{\boldsymbol{s}^r}\boldsymbol{\delta}(i)_{\boldsymbol{s}}$, where $(\boldsymbol{A^{-1}})_{\boldsymbol{s}^r}$ is the matrix $\boldsymbol{A^{-1}}$ with only rows indexed by $\boldsymbol{s}$.

Thus, it remains to prove that $(\boldsymbol{A^{-1}})_{\boldsymbol{s}^r}^{\boldsymbol{T}}\{[\boldsymbol{A^{-1}\Sigma_V}(\boldsymbol{A^{-1}})^{\boldsymbol{T}}]_{\boldsymbol{s}}\}^{-1}(\boldsymbol{A^{-1}})_{\boldsymbol{s}^r}$ is a positive semidefinite (P.S.D) matrix, so that $(\boldsymbol{A^{-1}}\widetilde{\boldsymbol{\delta}})_{\boldsymbol{s}}^{\boldsymbol{T}}\{[\boldsymbol{A^{-1}\Sigma_V}(\boldsymbol{A^{-1}})^{\boldsymbol{T}}]_{\boldsymbol{s}}\}^{-1}(\boldsymbol{A^{-1}}\widetilde{\boldsymbol{\delta}})_{\boldsymbol{s}} \geq \Delta(\boldsymbol{s}) \geq \tilde{\Delta}(card(\boldsymbol{s}))$. Since $\boldsymbol{A}$ is a triangular matrix with positive diagonal elements, $\boldsymbol{A}$ and $\boldsymbol{A^{-1}}$ are positive definite (P.D.) matrices. Moreover, $\boldsymbol{\Sigma_V}$ is also P.D., since it is a diagonal covariance matrix for $\boldsymbol{V}$. Therefore, $\{[\boldsymbol{A^{-1}\Sigma_V}(\boldsymbol{A^{-1}})^{\boldsymbol{T}}]_{\boldsymbol{s}}\}^{-1}$ is a symmetric P.D. matrix. Furthermore, $\{[\boldsymbol{A^{-1}\Sigma_V}(\boldsymbol{A^{-1}})^{\boldsymbol{T}}]_{\boldsymbol{s}}\}^{-1}$ can be expressed by Cholesky decomposition as $\{[\boldsymbol{A^{-1}\Sigma_V}(\boldsymbol{A^{-1}})^{\boldsymbol{T}}]_{\boldsymbol{s}}\}^{-1} = \boldsymbol{LL^T}$, where $\boldsymbol{L}$ is a lower triangular matrix with strictly positive diagonal entries. Thus, $(\boldsymbol{L^T}(\boldsymbol{A^{-1}})_{\boldsymbol{s}^r})^{\boldsymbol{T}}(\boldsymbol{L^T}(\boldsymbol{A^{-1}})_{\boldsymbol{s}^r})$ is a symmetric P.S.D matrix. As a result, any $\widetilde{\boldsymbol{\delta}} \in R_1$ is detectable if $\boldsymbol{s}$ is a feasible solution obtained from the BASIS algorithm.

A.2 Proof of Proposition 2.2

Denote the row space of a matrix by $Row(\cdot)$ and the RREF of $(\boldsymbol{A^{-1}})_{\boldsymbol{s}^r}$ by $(\boldsymbol{A^{-1}})_{\boldsymbol{s}^r}^{rref}$. Noting that $(\boldsymbol{A^{-1}})_{\boldsymbol{s}^r}^{rref}$ is unique and $Row\left((\boldsymbol{A^{-1}})_{\boldsymbol{s}^r}^{rref}\right) = Row((\boldsymbol{A^{-1}})_{\boldsymbol{s}^r})$.

Therefore, if $\exists \boldsymbol{\delta}_1 \in R_p^{k_i}, \boldsymbol{\delta}_2 \in R_p^{k_j}$ (where $i \neq j$ and $i, j = 1,2, \dots, m$), and $(\boldsymbol{A^{-1}})_{s^r}^{rref} \boldsymbol{\delta}_1 = (\boldsymbol{A^{-1}})_{s^r}^{rref} \boldsymbol{\delta}_2 = \boldsymbol{b}$, where $\boldsymbol{b}$ is a constant vector, then $\exists \widetilde{\boldsymbol{\delta}}_1 \in R_p^{k_i}, \widetilde{\boldsymbol{\delta}}_2 \in R_p^{k_j}$, such that $(\boldsymbol{A^{-1}})_{s^r} \widetilde{\boldsymbol{\delta}}_1 = (\boldsymbol{A^{-1}})_{s^r} \widetilde{\boldsymbol{\delta}}_2 = \boldsymbol{b}$. In proposition 2.2, if $\boldsymbol{\tau}(i)$ can be expressed as $\boldsymbol{\tau}(i) = a\boldsymbol{\tau}(j)$ for $\forall v(i), v(j) \in \boldsymbol{\theta}[\boldsymbol{v}]$, then $\exists \boldsymbol{\delta}_1 \in R_p^{k_i}, \boldsymbol{\delta}_2 \in R_p^{k_j}$, where $a\boldsymbol{e}_{v(i)}^{\boldsymbol{T}} \boldsymbol{\delta}_1 = \boldsymbol{e}_{v(j)}^{\boldsymbol{T}} \boldsymbol{\delta}_2$ and $\boldsymbol{e}_i = [0 \ \dots 1 \ \dots 0]^T$ with the i th element equal to one, such that $(\boldsymbol{A^{-1}})_{s^r}^{rref} \boldsymbol{\delta}_1 = (\boldsymbol{A^{-1}})_{s^r}^{rref} \boldsymbol{\delta}_2$. Thus, from definition 2.5, $\boldsymbol{\theta}[\boldsymbol{v}]$ is a minimal diagnosable class.

A.3 Detailed Steps of estimating $F_{n(s)}(t)$

This appendix illustrates the details of estimating $F_{n(\boldsymbol{s})}(t)$, which include the following steps: (i) Generate sufficient samples ${}^{\boldsymbol{1}}\boldsymbol{X}, \dots, {}^{\boldsymbol{n}}\boldsymbol{X} \sim \boldsymbol{N_m}(\boldsymbol{0}, \boldsymbol{\Sigma_X})$. (ii) Calculate the statistics $C_{\boldsymbol{s}}$ for each sample i, which is denoted as ${}^{i}C_{\boldsymbol{s}}$, if $T^2 = {}^{\boldsymbol{i}}\boldsymbol{X}_{\boldsymbol{s}}^{\boldsymbol{T}} \boldsymbol{M}_{\boldsymbol{s}}^{\boldsymbol{-1}} {}^{\boldsymbol{i}}\boldsymbol{X}_{\boldsymbol{s}} \leq UCL = \mathcal{X}_{\alpha}^2\big(card(\boldsymbol{s})\big)$. (iii) Assume that we collect $n(\boldsymbol{s})$ points, where the expected value of $n(\boldsymbol{s})$ equals to $n * (1 - \alpha)$. (iv) Estimate the empirical distribution function of $F_{n(\boldsymbol{s})}(t)$ by using $\frac{1}{n(\boldsymbol{s})} \sum_{i=1}^{n(\boldsymbol{s})} I({}^{i}C_{\boldsymbol{s}} \leq t)$, where $I(\cdot)$ is an indicator function.

A.4 Details of the Simulation Steps for Tables 3.3, 3.4, and 3.5

This appendix elaborates the details of the simulation steps when comparing the performance between the adaptive and the fixed strategy.

1. Given the number of available sensors q and the value of $\hat{\alpha}$, the following substeps are performed for each single mean shift fault scenario i ($i = 1, \dots m$):
   (i) A dataset of $\boldsymbol{X} = [X_1, X_2, X_3, X_4, X_5]^T$ with M $(= 5000)$ samples is generated, in which a mean shift τ is introduced at the first sample of X_i.

(ii) Implement the WISD, where sensors are initially deployed on the variables that provide the smallest ${}^{i}\Delta(\boldsymbol{s})$ value based on Table 3.1. For each incoming sample, calculate the testing statistics $T^2 = \boldsymbol{X_s^T M_s^{-1} X_s}$ and plot it on a chi-square control chart with upper control limit $\mathcal{X}_{\alpha}^{2}(card(\boldsymbol{s}))$ and lower control limit 0. Conduct the adaptive sensor allocation strategy in Figure 3.2. In this case study, α is chosen as 0.01.

(iii) Index of the first out-of-control sample on the control chart is recorded as RL_i. In addition, conduct the fault diagnosis step in Figure 3.2. Set F_i equal to one if the diagnosis result is correct, and set UF_i equal to one if the diagnosis result is uniquely correct based on the definitions of 3.2 and 3.3, respectively. In addition, record the cardinality of the active adding set. Furthermore, record the number of times that sensor locations have been changed by implementing the adaptive strategy and denote as AS_i.

(iv) Repeat steps (i)-(iii) for N $(= 10000)$ times. The average of RL_i, $\overline{RL_i}$; the average of F_i divided by the average of the cardinality of the active adding set, $\bar{F}_i$; the average of UF_i, $\overline{UF_i}$; and the average of AS_i, $\overline{AS_i}$, are computed and recorded.

2. Calculate the maximum out-of-control ARL, $RL_{max} = max_i(\overline{RL_i})$ and the average out-of-control ARL, $\overline{\overline{RL}} = \sum_i \overline{RL_i}\,/m$. Similarly, calculate the minimum correct diagnosis rate, $F_{min} = min_i(\bar{F}_i)$; the minimum uniquely correct diagnosis rate, $UF_{min} = min_i(\overline{UF_i})$; the average of correct diagnosis rate, $\bar{\bar{F}} = \sum_i \bar{F}_i\,/m$; and the average of uniquely correct diagnosis rate, $\overline{\overline{UF}} = \sum_i \overline{UF_i}\,/m$. Furthermore, calculate the average number of times that sensor locations have been changed by implementing the adaptive strategy, $\overline{\overline{AS}} = \sum_i \overline{AS_i}\,/m$. These metrics RL_{max}, $\overline{\overline{RL}}$, F_{min}, UF_{min}, $\bar{\bar{F}}$, $\overline{\overline{UF}}$ and $\overline{\overline{AS}}$ will be used to thoroughly compare the performance of the adaptive and the fixed strategy.

3. Repeat steps 1 and 2 under different combinations of q values ($q = \{card(\boldsymbol{LF}) + 1, \dots, m-1\}$) and $\hat{\alpha}$ values ($\hat{\alpha} = \{0, 0.2, 0.4, 0.6, 0.8, 1\}$), and present the results in Tables 3.3, 3.4 and 3.5.

A.5 Proof of Property 4.1

This appendix proves the first property of the SERA algorithm, which is equivalent to show the following statement: Suppose sensor resources will never be redistributed to the set of variables $\boldsymbol{U}$ after time t_0, then $\boldsymbol{U}$ must be an empty set, $\emptyset$. Denote $\boldsymbol{M}\backslash\boldsymbol{U} = \{k \in \boldsymbol{M} | k \notin \boldsymbol{U}\}$. To prove the first property of the SERA algorithm, let us first consider the following lemma:

Lemma 1: $W_{k',t} \geq W_{k,t}$, for $\forall t > t_0$, $\forall k' \in \boldsymbol{M}\backslash\boldsymbol{U}$, and $\forall k \in \boldsymbol{U}$.

We can prove lemma 1 via contradiction. Assume $\exists t > t_0$, $\exists k' \in \boldsymbol{M}\backslash\boldsymbol{U}$, and $\exists k \in \boldsymbol{U}$, such that $W_{k,t} > W_{k',t}$. If $k' \in \boldsymbol{S_t}$, then the sensor on variable k' will be redistributed to other variables in $\boldsymbol{M}\backslash\boldsymbol{U}$ at time $t+1$. Since the incremental part of the local statistics for both variables $k'$and k is always Δ, sensor resources cannot be redistributed back to variable k' without first deployed on variable k. In this way, $k' \in \boldsymbol{U}$, which contradicts to the assumption. On the other hand, if $k' \notin \boldsymbol{S_t}$, then it follows the same logic that sensor resources cannot be redistributed to variable k' without first deployed on variable k, which also contradicts to the assumption. Therefore, we have proved lemma 1 and now we will use it to prove the first property of the SERA algorithm.

Since sensor resources will never be redistributed to the variables in $\boldsymbol{U}$ after time t_0, $\forall k' \in \boldsymbol{M}\backslash\boldsymbol{U}$ must have sensor deployed with infinite number of times as $d \to \infty$. Now, let us first prove the case when $\rho_{k'} < 0$. Without loss of generality, we assume $E(X_{k',t}) = u_{k'} \geq 0$. The incremental part of the local statistics for any variable without sensor deployed is always Δ, while the incremental part for any variable k' with sensor

deployed is either $u_{min}X_{k',t} - \frac{u_{min}^2}{2}$ or $-u_{min}X_{k',t} - \frac{u_{min}^2}{2}$ or 0. Since only one term (i.e. either $u_{min}X_{k',t} - \frac{u_{min}^2}{2}$ or $-u_{min}X_{k',t} - \frac{u_{min}^2}{2}$) can be positive at any moment and $X_{k',t}$ is an i.i.d. normal random variable, there must be a series of $X_{k',t}$ such that either $\sum_{t=1}^{\infty}\left(u_{min}X_{k',t} - \frac{u_{min}^2}{2}\right) \geq \Delta t$ or $\sum_{t=1}^{\infty}\left(-u_{min}X_{k',t} - \frac{u_{min}^2}{2}\right) \geq \Delta t$. Since $\rho_{k'} < 0$, $P\left(\sum_{t=1}^{\infty}\left(u_{min}X_{k',t} - \frac{u_{min}^2}{2}\right) \geq \Delta t\right) + P\left(\sum_{t=1}^{\infty}\left(-u_{min}X_{k',t'} - \frac{u_{min}^2}{2}\right) \geq \Delta t\right) = lim_{t\to\infty}\left(1 - \varphi\left(\frac{\Delta\sqrt{t}}{u_{min}} + \frac{\sqrt{t}u_{min}}{2} - u_{k'}\sqrt{t}\right)\right) + lim_{t\to\infty}\left(1 - \varphi\left(\frac{\Delta\sqrt{t}}{u_{min}} + \frac{\sqrt{t}u_{min}}{2} + u_{k'}\sqrt{t}\right)\right) = 0$. Thus, there is no such series of $X_{k',t}$. Second, let us consider the case when $\rho_{k'} = 0$. Define $Y_{k',n} = u_{min}X_{k',t_0+n} - \frac{u_{min}^2}{2} - \Delta$ and $H_{k',n} = \sum_{i=1}^{n} Y_{k',i}$. Then, $Y_{k',n}$ is an i.i.d. normal random variable with mean 0 and variance u_{min}^2. Consequently, $\{H_{k',n}: n \geq 1\}$ refers to the oscillating random walk process. Denote $D = min\{H_{k',n}: n \geq 1\}$. Thus, $D \xrightarrow{a.s.} -\infty$ as $n \to \infty$ (Gut 1988). In other words, there must exist a time t, such that $W_{k,t} > W_{k',t}$. Therefore, it is impossible that sensor resources are always reallocated among the variables that only belong to $\boldsymbol{M}\backslash\boldsymbol{U}$. In other words, $\boldsymbol{U}$ must be an empty set. In this way, we have finished the proof for property 4.1.

A.6 Proof of Property 4.2

This appendix proves the second property of the SERA algorithm. Considering the variable k, where $k \in \boldsymbol{S_t}$ and $k \in \boldsymbol{B}$, then $W_{k,t} \geq W_{k',t}$ for $\forall k' \notin \boldsymbol{S_t}$. Without loss of generality, let $E(X_{k,t}) = u_k \geq 0$. Define $Y_{k,n} = X_{k,t+n} - \frac{u_{min}}{2} - \frac{\Delta}{u_{min}}$ and $H_{k,n} = \sum_{i=1}^{n} Y_{k,i}$. Then, $Y_{k,n}$ is an i.i.d. normal random variable with mean $u_k - \frac{u_{min}}{2} - \frac{\Delta}{u_{min}}$ and variance 1. Consequently, $\{H_{k,n}: n \geq 0\}$ refers to the Guassian random walk process,

where $H_{k,0} = 0$. Denote $D = min\{H_{k,n}: n \geq 0\}$. We are interested to show that $P(D = 0)$ is nonzero if the stopping criteria $d \to \infty$. Since $P(D = 0) = P(H_{k,n} \geq 0, \forall n \geq 0)$, it is equivalent to show that there is a nonzero probability that once a sensor is deployed on the variable $k \in \boldsymbol{B}$ at time t, it will never be reallocated to other variables (i.e. $W_{k,t+n} \geq W_{k',t+n}$ for $\forall k' \notin \boldsymbol{S_t}$, $\forall n \geq 0$). According to (Chang and Peres 1997; Janssen and Van Leeuwaarden 2007), the probability that the minimum of the Gaussian random walk is zero satisfies:

$$P(D = 0) = \sqrt{2}\delta_k exp\{\frac{\delta_k}{\sqrt{2\pi}}\sum_{r=0}^{\infty}\frac{\zeta\left(\frac{1}{2}-r\right)}{r!(2r+1)}\left(-\frac{\delta_k^2}{2}\right)^r\} \text{ for } 0 < \delta_k < 2\sqrt{\pi},$$

where $\delta_k = u_k - \frac{u_{min}}{2} - \frac{\Delta}{u_{min}}$ and $\zeta(\cdot)$ is the Riemann zeta function. It is worth mentioning that $P(D = 0)$ is an increasing function as δ_k gets larger (i.e. even when $\delta_k \geq 2\sqrt{\pi}$), which means the random walk is less likely to go back to 0 as δ_k increases. Now, we use property 4.1 to prove property 4.2. According to property 4.1, we have already shown that sensor resources will not stick to the variables in $\boldsymbol{M}\backslash\boldsymbol{B}$, and thus they must be redistributed to the variables in $\boldsymbol{B}$ at some time. Since once the sensor is deployed on the variable in $\boldsymbol{B}$, there is always a nonzero probability $P(D = 0)$ such that the sensor will never be redistributed to other variables. Therefore, as $d \to \infty$, sensors will eventually stick to the variables that belong to $\boldsymbol{B}$. It worth mentioning when the number of sensors $q \geq card(\boldsymbol{B})$, all variables in $\boldsymbol{B}$ will eventually have sensor deployed and the remaining sensors are redistributed among the variables in $\boldsymbol{M}\backslash\boldsymbol{B}$.

A.7 Details of the Simulation Steps for Table 4.1

This appendix elaborates the details of the simulation steps when comparing the performance between the SERA algorithm and the CBA algorithm under different combinations of Δ ($\Delta = 0.01, 0.1, 0.5$), τ ($\tau = 1.5, 2, 2.5, 3$), and q ($q = 2,3,4$) values for single mean shift case.

1. Given each value of the number of available sensors q, the mean shift magnitude τ, and the incremental parameter Δ, the following substeps are performed for each single mean shift fault scenario i ($i = 1, \dots 5$):
   (i) A dataset of $\boldsymbol{X} = \{X_1, X_2, X_3, X_4, X_5\}$ with M $(= 5000)$ samples is generated, in which a mean shift τ is introduced at the first sample of X_i.
   (ii) Implement the WISD. For each incoming sample, calculate the local statistics and update sensor layout based on the SERA algorithm in Figure 4.1.
   (iii) Index of the first out-of-control sample is recorded as RL_i. In addition, set UF_i equal to one if the variable associated with the largest local statistic is the root cause variable, X_i.
   (iv) Repeat steps (1)-(3) for N $(= 10000)$ times. The average of RL_i, $\overline{RL_i}$ and the average of UF_i, $\overline{UF_i}$ are computed and recorded.
2. Calculate the maximum out-of-control ARL, $RL_{max} = max_i(\overline{RL_i})$ and the average out-of-control ARL, $\overline{\overline{RL}} = \sum_i \overline{RL_i}\,/5$. Similarly, calculate the minimum uniquely correct diagnosis rate, $UF_{min} = min_i(\overline{UF_i})$ and the average of uniquely correct diagnosis rate, $\overline{\overline{UF}} = \sum_i \overline{UF_i}\,/5$.
3. Repeat steps 1 and 2 for different combinations of Δ ($\Delta = 0.01, 0.1, 0.5$), τ ($\tau = 1.5, 2, 2.5, 3$), and q ($q = 2,3,4$) values, and present the results in Table 4.1.

A.8 Details of Finding the Threshold Value d

This appendix describes the detailed steps to estimate the threshold value d given any prescribed in-control ARL, ARL_U. Specially, we conduct the following evaluation processes:

1. Set d_{min} and d_{max} a small and a large values as the initial upper and the lower bounds of d, respectively. Let $d = \frac{d_{min}+d_{max}}{2}$.

2. Generate a bootstrap dataset with M $(= 5000)$ samples by randomly drawing the data with replacement from the first 100 frames.
3. Implement the RISD approach. Record the index of the first out-of-control sample, RL, based on the proposed SERA algorithm.
4. Repeat steps 2-3 for N $(= 10000)$ times (i.e. producing N bootstrap datasets). Calculate the average of RL, $\overline{RL}$.
5. If the $\overline{RL}$ is larger than ARL_U, let $d_{max} = d$; Otherwise, let $d_{min} = d$. Then update $d = \frac{d_{min}+d_{max}}{2}$.
6. Repeat steps 2-5 until there is only small difference between $\overline{RL}$ and ARL_U.

A.9 Proof of the expression of the variance in the failure threshold of the composite health index in equation (5.1)

This appendix shows that the variance in the failure threshold of the composite health index can be expressed as the quadratic term: $\boldsymbol{w'Y'DYw}$. The unbiased sample variance can be estimated by: $\frac{(\boldsymbol{Yw})'(\boldsymbol{Yw})-m\left(\frac{\boldsymbol{1'Yw}}{m}\right)^2}{m-1} = \frac{\boldsymbol{w'Y'Yw}-\frac{\boldsymbol{w'Y'11'Yw}}{m}}{m-1} = \boldsymbol{w'Y'}\left(\frac{\boldsymbol{I}-\frac{\boldsymbol{11'}}{m}}{m-1}\right)\boldsymbol{Yw} = \boldsymbol{w'Y'DYw}$.

A.10 Proof of H is positive semidefinite (P.S.D) in equation (5.2)

This appendix proves that $\boldsymbol{H}$ is positive semidefinite (P.S.D) matrix. First, it is straightforward to show that $\boldsymbol{D} = \frac{\boldsymbol{I}-\boldsymbol{O}/m}{m-1}$ is a symmetric P.S.D matrix. Then, $\boldsymbol{D}$ can be decomposed as: $\boldsymbol{D} = \boldsymbol{LL'}$ by Cholesky decomposition, where $\boldsymbol{L}$ is a lower triangular matrix. Next, $\boldsymbol{H}$ can be written as: $\boldsymbol{H} = \boldsymbol{G'Y'DYG} = (\boldsymbol{L'YG})'\boldsymbol{L'YG}$. Thus, $\boldsymbol{H}$ is P.S.D.

A.11 Proof of the posterior distribution of $\boldsymbol{\Gamma_{i,k}}$ follows a multivariate normal distribution

This appendix derives the posterior distribution of $\boldsymbol{\Gamma_{i,k}}$ still follows a multivariate normal distribution with mean $\boldsymbol{u_p^{i,k}} = \left(\frac{\boldsymbol{\Psi_i}'\boldsymbol{\Psi_i}}{\sigma_k^2} + (\boldsymbol{\Sigma_0^k})^{-1}\right)^{-1} (\frac{\boldsymbol{\Psi_i}'\boldsymbol{L_{i,k,.}}}{\sigma_k^2} + (\boldsymbol{\Sigma_0^k})^{-1}\boldsymbol{u_0^k})$ and variance $\boldsymbol{\Sigma_p^{i,k}} = \left(\frac{\boldsymbol{\Psi_i}'\boldsymbol{\Psi_i}}{\sigma_k^2} + (\boldsymbol{\Sigma_0^k})^{-1}\right)^{-1}$. The multivariate normal distribution can be expressed as $P(\boldsymbol{\Gamma_{i,k}}) = \frac{1}{(2\pi)^{3/2}|\boldsymbol{\Sigma_0^k}|^{1/2}} e^{-\frac{1}{2}(\boldsymbol{\Gamma_{i,k}}-\boldsymbol{u_0^k})'(\boldsymbol{\Sigma_0^k})^{-1}(\boldsymbol{\Gamma_{i,k}}-\boldsymbol{u_0^k})}$. Thus,

$$
\begin{aligned}
P(\boldsymbol{\Gamma_{i,k}}|\boldsymbol{L_{i,k,.}}) &\propto P(\boldsymbol{L_{i,k,.}}|\boldsymbol{\Gamma_{i,k}})P(\boldsymbol{\Gamma_{i,k}}) \\
&\propto e^{-\frac{1}{2\sigma_k^2}(\boldsymbol{L_{i,k,.}}-\boldsymbol{\Psi_i}\boldsymbol{\Gamma_{i,k}})'(\boldsymbol{L_{i,k,.}}-\boldsymbol{\Psi_i}\boldsymbol{\Gamma_{i,k}})} e^{-\frac{1}{2}(\boldsymbol{\Gamma_{i,k}}-\boldsymbol{u_0^k})'(\boldsymbol{\Sigma_0^k})^{-1}(\boldsymbol{\Gamma_{i,k}}-\boldsymbol{u_0^k})} \\
&\propto e^{\boldsymbol{\Gamma_{i,k}'}\left(\frac{\boldsymbol{\Psi_i}'\boldsymbol{\Psi_i}}{\sigma_k^2}+(\boldsymbol{\Sigma_0^k})^{-1}\right)\boldsymbol{\Gamma_{i,k}}-2\left(\frac{\boldsymbol{L_{i,k,.}'}\boldsymbol{\Psi_i}}{\sigma_k^2}+(\boldsymbol{u_0^k})'(\boldsymbol{\Sigma_0^k})^{-1}\right)\boldsymbol{\Gamma_{i,k}}}.
\end{aligned}
\tag{5.12}
$$

It is known that if $P(\boldsymbol{L_{i,k,.}}|\boldsymbol{\Gamma_{i,k}})$ follows normal distribution and $P(\boldsymbol{\Gamma_{i,k}})$ follows multivariate normal distribution, the posterior will also follow multivariate normal distributions. As a result, $\boldsymbol{\Gamma_{i,k}}|\boldsymbol{L_{i,k,.}} \sim N_3(\boldsymbol{u_p^{i,k}}, \boldsymbol{\Sigma_p^{i,k}})$ and $P(\boldsymbol{\Gamma_{i,k}}|\boldsymbol{L_{i,k,.}}) \propto e^{-\frac{1}{2}(\boldsymbol{\Gamma_{i,k}}-\boldsymbol{u_p^{i,k}})'(\boldsymbol{\Sigma_p^{i,k}})^{-1}(\boldsymbol{\Gamma_{i,k}}-\boldsymbol{u_p^{i,k}})}$.

Comparing (5.12) with $(\boldsymbol{\Gamma_{i,k}}-\boldsymbol{u_p^{i,k}})'(\boldsymbol{\Sigma_p^{i,k}})^{-1}(\boldsymbol{\Gamma_{i,k}}-\boldsymbol{u_p^{i,k}}) = \boldsymbol{\Gamma_{i,k}'}(\boldsymbol{\Sigma_p^{i,k}})^{-1}\boldsymbol{\Gamma_{i,k}} - \boldsymbol{2}(\boldsymbol{u_p^{i,k}})'(\boldsymbol{\Sigma_p^{i,k}})^{-1}\boldsymbol{\Gamma_{i,k}} + (\boldsymbol{u_p^{i,k}})'(\boldsymbol{\Sigma_p^{i,k}})^{-1}\boldsymbol{u_p^{i,k}}$, we get the equations $(\boldsymbol{\Sigma_p^{i,k}})^{-1} = \left(\frac{\boldsymbol{\Psi_i}'\boldsymbol{\Psi_i}}{\sigma_k^2} + \left(\boldsymbol{\Sigma_0^k}\right)^{-1}\right)$ and $(\boldsymbol{u_p^{i,k}})'(\boldsymbol{\Sigma_p^{i,k}})^{-1} = \left(\frac{\boldsymbol{L_{i,k,.}'}\boldsymbol{\Psi_i}}{\sigma_k^2} + (\boldsymbol{u_0^k})'\left(\boldsymbol{\Sigma_0^k}\right)^{-1}\right)$. This finishes the proof that $\boldsymbol{\Gamma_{i,k}}|\boldsymbol{L_{i,k,.}} \sim N_3(\boldsymbol{u_p^{i,k}}, \boldsymbol{\Sigma_p^{i,k}})$, where $\boldsymbol{\Sigma_p^{i,k}} = \left(\frac{\boldsymbol{\Psi_i}'\boldsymbol{\Psi_i}}{\sigma_k^2} + \left(\boldsymbol{\Sigma_0^k}\right)^{-1}\right)^{-1}$ and $\boldsymbol{u_p^{i,k}} = \left(\frac{\boldsymbol{\Psi_i}'\boldsymbol{\Psi_i}}{\sigma_k^2} + \left(\boldsymbol{\Sigma_0^k}\right)^{-1}\right)^{-1} (\frac{\boldsymbol{\Psi_i}'\boldsymbol{L_{i,k,.}}}{\sigma_k^2} + \left(\boldsymbol{\Sigma_0^k}\right)^{-1}\boldsymbol{u_0^k})$.

REFERENCES

Azarbayejani, M., El-Osery, A. I., Choi, K. K., and Taha, M. M. R. (2008), "A Probabilistic Approach for Optimal Sensor Allocation in Structural Health Monitoring," *Smart Materials and Structures*, 17, 055019.

Bakshi, B. R. (1998), "Multiscale PCA With Application to Multivariate Statistical Process Monitoring," *AIChE journal*, 44, 7, 1596-1610.

Buntine, W.L. (1994), "Operations for Learning With Graphical Models," *Journal of Artificial Intelligence Research*, 2, 159-225.

Byington, C. S., Brewer, R. C., Meyer, T., and Amin, S. R. (2007), "Gearbox Corrosion Prediction Via Oil Condition Sensing and Model Fusion," *STLE 62nd Annual Meeting and Exhibition*, Philadelphia, PA.

Camci, F., and Chinnam, R. B. (2010), "Health-State Estimation and Prognostics in Machining Processes," *IEEE Transactions on Automation Science and Engineering*, 7, 3, 581-597.

Chan, L. K., and Zhang, J. (2001), "Cumulative Sum Control Charts for the Covariance Matrix," *Statistica Sinica*, 11, 767-790.

Chang, J. T., and Peres, Y. (1997), "Ladder Heights, Gaussian Random Walks, and the Riemann Zeta Function," *The Annals of Probability*, 25, 787-802.

Chatterjee, S., and Qiu, P. (2009), "Distribution-Free Cumulative Sum Control Charts Using Bootstrap Based Control Limits," *Annals of Applied Statistics*, 3, 349-369.

Cheng, S. W., and Thaga, K. (2005a), "Max-CUSUM Chart for Autocorrelated Processes," *Statistica Sinica*, 15, 527-546.

—(2005b), "Multivariate Max-CUSUM Chart," *Quality Technology and Quantitative Management*, 2, 221-235.

Chow, M. Y., and Yee, S. O. (1991), "Methodology for On-line Incipient Fault Detection in Single Phase Squirrel Cage Induction Motors Using Artificial Neural Networks," *IEEE Transactions on Energy Conversion*, 6, 536-545.

Crosier, R. B. (1986), "A New Two-Sided Cumulative Sum Quality Control Scheme," *Technometrics*, 28, 187-194.

—(1988), "Multivariate Generalizations of Cumulative Sum Quality-Control Schemes," *Technometrics*, 30, 291-303.

Demetriou, A., and Polycarpou, M. M. (1998), "Incipient Fault Diagnosis of Dynamical Systems Using Online Approximators," *IEEE Transactions on Automatic Control*, 43, 11, 1612-1617.

Ding, Y., Elsayed, E. A., Kumara, S., Lu, J. C., Niu, F., and Shi, J. (2006), "Distributed Sensing for Quality and Productivity Improvements," *IEEE Transactions on Automation Science and Engineering*, 3, 344-359.

Ding, Y., Kim, P., Ceglarek, D., and Jin, J. (2003), "Optimal Sensor Distribution for Variation Diagnosis in Multistation Assembly Processes," *IEEE Transactions on Robotics and Automation*, 19, 543-556.

Duda, R. O., Hart, P. E., and Stork, D. G. (2000) *Pattern Classification* (2nd ed.). Wiley, New York.

Edan, Y., and Nof, S. Y. (2000), "Sensor Economy Principles and Selection Procedures," *IIE Transactions*, 32, 3, 195-203.

Efron, B., and Tibshirani, R. J. (1993), *An Introduction to the Bootstrap*. Chapman and Hall, Boca Raton, FL.

Fiorelli, E., Leonard, N. E., Bhatta, P., Paley, D., Bachmayer, R., and Fratantoni, D. M. (2006), "Multi-AUV Control and Adaptive Sampling in Monterey Bay," *IEEE Journal of Oceanic Engineering*, 31, 4, 935-948.

Frank, P. M. (1990), "Fault Diagnosis in Dynamic Systems Using Analytical and Knowledge-Based Redundancy – A Survey and Some New Results," *Automatica*, 26, 3, 459-474.

Gebraeel, N. (2006), "Sensory-Updated Residual Life Distributions for Components With Exponential Degradation Patterns," *IEEE Transactions on Automation Science and Engineering*, 3, 382-393.

Gebraeel, N. (2010), "Prognostics-Based Identification of the Top-k Units in a Fleet," *IEEE Transactions on Automation Science and Engineering*, 7, 1, 37-48.

Gebraeel, N., and Lawley, M. (2008), "A Neural Network Degradation Model for Computing and Updating Residual Life Distributions," *IEEE Transactions on Automaction Science Engineering*, 5, 1, 154-163.

Goebel, K., and Bonissone, P. (2005), "Prognostic Information Fusion for Constant Load Systems," *Proceedings of the 8th International Conference on Information Fusion*, 2, 1247-1255.

Gut, A. (1988), *Stopped Random Walks, Limit Theory and Applications*. Springer, Berlin.

Hall, D. L., and Llinas, J. (1997), "An Introduction to Multisensor Data Fusion," *Proceedings of the IEEE*, 85, 6-23.

Hawkins D. M. (1993), "Regression Adjustment for Variables in Multivariate Quality Control," *Journal of Quality Technology*, 25, 170-182.

Healy, J. D. (1987), "A Note on Multivariate CUSUM Procedures," *Technometrics*, 29, 409-412.

Heckerman, D. (1995), "A Tutorial on Learning With Bayesian Networks," in *Learning in Graphical Models*. Jordan, M. (eds), MIT Press, Cambridge, MA.

Heger, T., and Pandit, M. (2004),"Optical Wear Assessment System for Grinding Tools," *Journal of Electronic Imaging*, 13, 450-461.

Hitchings, D., and Castañón, D. A. (2010), "Adaptive Sensing for Search With Continuous Actions and Observations," *Proceedings of IEEE Conference on Decision and Control*, 7443-7448.

Hocking, R. R., and Leslie, R. N. (1967) "Selection of the Best Subset in Regression Analysis," *Technometrics*, 9, 4, 531-540.

Holmström, K., Göran, A. O., and Edvall, M. M. (2008), *User's Guide for TOMLAB*. Tomlab Optimization Inc, San Diego, CA.

Hotelling, H. (1947), "Multivariate Quality Control", *Techniques of Statistical Analysi*. Eisenhart, C., Hastay, M. and Wallis, W.A. (eds), McGraw-Hill, New York, 111-184.

Hu, C., Youn, B. D., and Wang, P. (2010), "Ensemble of Data-Driven Prognostic Algorithms With Weight Optimization and K-Fold Cross Validation," *Proceedings of the ASME 2010 International Design Engineering Technical Conferences and Computers and Information in Engineering Conference*, 3, 1023-1032.

Janssen, A. J. E. M., and Van Leeuwaarden, J. S. H. (2007), "On Lerch's Transcendent and the Gaussian Random Walk," *The Annals of Applied Probability*, 17, 421-439.

Jardine, A. K. S., Lin, D., and Banjevic, D. (2006), "A Review on Machinery Diagnostics and Prognostics Implementing Condition-Based Maintenance," *Mechanical Systems and Signal Processing*, 20, 7, 1483-1510.

Katenka, N., Levina, E., and Michailidis, G. (2008), "Robust Target Localization From Binary Decisions in Wireless Sensor Networks," *Technometrics*, 50, 448-461.

Khan, A., and Ceglarek, D. (2000), "Sensor Optimization for Fault Diagnosis in Multi-Fixture Assembly Systems With Distributed Sensing," *ASME Journal of Manufacturing Science and Engineering*, 122, 215-226.

Khan, A., Ceglarek, D., and Ni, J. (1998), "Sensor Location Optimization for Fault Diagnosis in Multi-fixture Assembly Systems," *ASME Journal of Manufacturing Science and Engineering*, 120, 781-791.

Kobayashi, T., and Simon, D. L. (2007), "Hybrid Kalman Filter Approach for Aircraft Engine In-flight Diagnostics: Sensor Fault Detection Case," *ASME Journal of Engineering for Gas Turbines and Power*, 129, 3, 746-754.

Koller, D. and Friedman, N. (2009), *Probabilistic Graphical Models principles and techniques (Adaptive Computation and Machine Learning)*. The MIT Press, USA.

Lauritzen, S. L., and Wermuth, N. (1989), "Graphical Models for Associations between Variables, Some of Which are Qualitative and Some Quantitative," *Annals of Statistics*, 17, 1, 31-57.

Li, J., and Jin, J. (2010), "Optimal Sensor Allocation by Integrating Causal Models and Set-Covering Algorithms," *IIE Transaction*, 42, 564-576.

Li, J. and Meerkov, S. M. (2009), *Production Systems Engineering*. Springer, New York, NY.

Li, J. and Shi, J. (2007), "Knowledge Discovery from Observational Data for Process Control using Causal Bayesian," *IIE Transactions*, 39, 6, 681-690.

Li, J., Blumenfeld, D. E., and Marin, S. P. (2007), "Manufacturing System Design to Improve Quality Buy Rate: An Automotive Paint Shop Application Study," *IEEE Transactions on Automation Science and Engineering*, 4, 1, 75-79.

—(2008), "Production System Design for Quality Robustness," *IIE Transactions*, 40, 3, 162-176.

Li, J., Jin, J. and Shi, J. (2008), "Causation-based T2 Decomposition for Multivariate Process Monitoring and Diagnosis," *Journal of Quality Technology*, 40, 1, 46-58.

Lim, H. B., Lam, V. T., Foo, M. C., and Zeng, Y. (2006), "Adaptive Distributed Resource Allocation in Wireless Sensor Networks," *In Proceedings of the 2nd International Conference on Mobile Ad-hoc and Sensor Networks*, Hong Kong, China.

Limongelli, M. P. (2003), "Optimal Location of Sensors for Reconstruction of Seismic Response through Spline Function Interpolation," *Earthquake Engineering and Structural Dynamics*, 32, 1055-1074.

Liu, K. and Shi, J. (2012), "Objective-Oriented Optimal Sensor Allocation Strategy for Process Monitoring and Diagnosis by Multivariate Analysis in a Bayesian Network", *IIE Transactions*, 45, 630–643.

Liu, C., Ding, Y., and Chen, Y. (2005), "Optimal Coordinate Sensor Placements for Estimating Mean and Variance Components of Variation Sources," *IIE Transactions*, 37, 9, 877-889.

Liu, K., Gebraeel, N., and Shi, J. (2012), "A Data-Level Fusion Model for Developing Composite Health Indices for Degradation Modeling and Prognostic Analysis," accepted, *IEEE Transactions on Automation Science and Engineering*.

Liu, K., Mei, Y., and Shi, J., "Scalable-Robust-Efficient Adaptive (SERA) Sensor Allocation Strategy for Process Control," manuscript.

Liu, K., Zhang, X., and Shi, J. (2013), "Adaptive Sensor Allocation Strategy for Process Monitoring and Diagnosis in a Bayesian Network," conditionally accepted, *IEEE Transactions on Automation Science and Engineering*.

Lorden, G. (1971), "Procedures for Reacting to a Change in Distribution," *Annals of Mathematical Statistics*, 42, 1897–1908.

Lowry, C. A., Woodall, W. H., Champ, C. W., and Rigdon, S. E. (1992), "A Multivariate EWMA Control Chart," *Technometrics*, 34, 1, 46-53.

Mandroli, S. S., Shrivastava, A., and Ding, Y. (2006), "A Survey of Inspection Strategy and Sensor Distribution Studies in Discrete-Part Manufacturing Processes," *IIE Transactions*, 38, 309-328.

Mason, R., Tracy, N., and Young, J. (1997), "A Practical Approach for Interpreting Multivariate T^2 Control Chart Signals," *Journal of Quality Technology*, 29, 4, 396-406.

Meeker, W. Q., and Escobar, L. A. (1998), *Statistical Methods for Reliability Data*. Wiley, New York.

Mei, Y. J. (2010), "Efficient Scalable Schemes for Monitoring a Large Number of Data Streams," *Biometrika*, 97, 419-433.

—(2011), "Quickest Detection in Censoring Sensor Networks," *In Proceedings of IEEE International Symposium on Information Theory*, 2148-2152.

Mobley, R. K. (2002), *An Introduction to Predictive Maintenance*. Elsevier Butterworth-Heinemann, Burlington, MA.

Montgomery, D. C. (2009), *Introduction to Statistical Quality Control*. John Wiley & Sons, New York.

Mousavi, M. J., and Butler-Purry, K. L. (2010), "Detecting Incipient Faults via Numerical Modeling and Statistical Change Detection," *IEEE Transactions on Power* Delivery, 25, 1275-1283.

Nelson, W. (1990), *Accelerated Testing Statistical Models, Test Plans, and Data Analysis*. Wiley, New York.

Ngai, H. M., and Zhang, J. (2001), "Multivariate Cumulative Sum Control Charts Based on Projection Pursuit," *Statistica Sinica*, 11, 747-766.

Page, E. S. (1954), "Continuous Inspection Schemes," *Biometrika*, 41, 100-114.

Pearl, J., and Verma, T. S. (1991), "A Theory of Inferred Causation," *Studies in Logic and the Foundations of Mathematics*, 134, 789-811.

Pignatiello, J. J., and Runger, G. C. (1990), "Comparisons of Multivariate CUSUM Charts," *Journal of Quality Technology*, 22, 173-186.

Popa, D. O., Mysorewala, M. F., and Lewis, F. L. (2006), "EKF-Based Adaptive Sampling With Mobile Robotic Sensor Nodes," *Proceedings of IEEE/RSJ International Conference on Intelligent Robots and Systems*, 2451-2456.

Qiu, P., and Hawkins, D. M. (2001), "A Rank-Based Multivariate CUSUM Procedure," *Technometrics*, 43, 120-132.

—(2003), "A Nonparametric Multivariate Cumulative Sum Procedure for Detecting Shifts in all Directions," *Journal of the Royal Statistical Society Series D—The Statistician*, 52, 151-164.

Rahimi, M. H., Kaiser, W., Sukhatme, G. S., and Estrin, D. (2005), "Adaptive Sampling for Environmental Field Estimation Using Robotic Sensors," *Proceedings of IEEE/RSJ International Conference on Intelligent Robots and Systems*, 3692-3698.

Salahshoor, K., Mosallaei, M., and Bayat, M. (2008), "Centralized and Decentralized Process and Sensor Fault Monitoring Using Data Fusion Based on Adaptive Extended Kalman Filter algorithm," *Measurement*, 41, 1059-1076.

Sarkar, S., Jin, X., and Ray, A. (2011), "Data-Driven Fault Detection in Aircraft Engines With Noisy Sensor Measurements," *ASME Journal of Engineering for Gas Turbines*, 133, 081602.

Saxena, A., Celaya, J., Balaban, E., Goebel, K., Saha, B., Saha, S., and Schwabacher, M. (2008), "Metrics for Evaluating Performance of Prognostics Techniques," *Proceedings of the 1st International Conference* on *Prognostics and Health Management*, 1-17.

Saxena, A., Goebel, K., Simon, D., and Eklund, N. (2008), "Damage Propagation Modeling for Aircraft Engine Run-to-Failure Simulation," *Proceedings of the 1st International Conference* on *Prognostics and Health Management*, 1-9.

Shewhart, W. A. (1931), *Economic Control of Quality of Manufactured Product*. American Society for Quality, New York.

Shi, J. (2006), *Stream of Variation Modeling and Analysis for Multistage Manufacturing Processes*. CRC Press, Boca Raton, FL.

Siegmund, D., and Venkatraman, E. S. (1995), "Using the Generalized Likelihood Ratio Statistic for Sequential Detection of a Change-Point," *Annals of Statistics*, 23, 1, 255-271.

Simon, D., and Simon, D. L. (2005), "Aircraft Turbofan Engine Health Estimation Using Constrained Kalman Filtering," *ASME Journal of Engineering for Gas Turbines and Power*, 127, 323-328.

Sun, Q. (2002), "Sensor Fusion for Vehicle Health Monitoring and Degradation Detection," *Proceedings of the 5th International Conference on Information Fusion*, 1422-1427.

Tan, R., Xing G., Chen, J., Song W., and Huang, R., (2012), "Fusion-Based Volcanic Earthquake Detection and Timing in Wireless Sensor Networks," *ACM Transaction on Sensor Networks (ACM TOSN)*, 9, 2, 17:1-25.

Tarabanis, K. A., Allen, P. K., and Tsai, R. Y. (1995), "A Survey of Sensor Planning in Computer Vision," *IEEE Transactions on Robotics and Automation*, 11, 1, 86-104.

Tartakovsky, A. G., Rozovskii, B. L., Blazek, R. B., and Kim, H. (2006), "Detection of Intrusions in Information Systems by Sequential Change-Point Methods (With Discussion)," *Statistical Methodology*, 3, 252-340.

Hastie, T., Tibshirani, R., and Friedman, J. H. (2003), *The Elements of Statistical Learning: Data Mining, Inference, and Prediction*. Springer, New York.

Tsui, K-L, Han, S. W., Jiang, W., and Woodall, W. H. (2012), "A Review and Comparison of Likelihood Based Charting Methods," *IIE Transactions*, 44, 724-743.

Tsung, F., and Wang, K. (2010), "Adaptive Charting Techniques: Literature Review and Extensions," *Frontiers in Statistical Quality Control 9*. Physica-Verlag, Berlin, 19-36.

Vapnik, V. N. (1999), *The Nature of Statistical Learning Theory* (2nd ed.). Springer-Verlag, New York.

Verron, S., Tiplica, T., and Kobi, A. (2008), "Fault Detection and Identification With a New Feature Selection Based on Mutual Information," *Journal of Process Control*, 18, 5, 479-490.

Volponi, A. J., Brotherton, T., Luppold, R., and Simon, D. L. (2004), *Development of an Information Fusion System for Engine Diagnostics and Health Management*. Cleveland, OH: NASA.

Wang, K. and Jiang, W. (2009), "High-Dimensional Process Monitoring and Fault Isolation via Variable Selection," *Journal of Quality Technology*, 41, 3, 247-258.

Willett, R., Martin, A., and Nowak, R. (2004), "Backcasting: Adaptive Sampling for Sensor Networks," *In Proceedings of the International Symposium on Information Processing in Sensor Networks*, 124-133.

Wolbrecht, E., D'Ambrosio, B., Paasch, R., and Kirby, D. (2000), "Monitoring and Diagnosis of a Multistage Manufacturing Process Using Bayesian Networks,"

Artificial Intelligence for Engineering Design, Analysis and Manufacturing, 14, 1, 53-67.

Woodall, W. H., and Ncube, M. M. (1985), "Multivariate CUSUM Quality Control Procedures," *Technometrics*, 27, 3, 285-292.

Xie, Y., Huang, J., and Willett, R. (2013), "Changepoint Detection for High-Dimensional Time Series With Missing Data," *IEEE Journal of Selected Topics in Signal Processing*, 7, 1, 12-27.

Zhang, X., Polycarpou, M. M., and Parisini, T. (2002), "A Robust Detection and Isolation Scheme for Abrupt and Incipient Faults in Nonlinear Systems," *IEEE Transactions on Automatic Control*, 47, 4, 576–593.

Zhou, S., Ding, Y., Chen, Y., and Shi, J. (2003), "Diagnosability Study of Multistage Manufacturing Processes Based on Linear Mixed-effects Models," *Technometrics*, 45, 4, 312-325.

Zhu, Y., and Jiang, W. (2009), "An Adaptive T2 Chart for Multivariate Process Monitoring and Diagnosis," *IIE Transactions*, 41, 11, 1007-1018.

Zoghi, M., and Kahaei, M. H. (2010), "Adaptive Sensor Selection in Wireless Sensor Networks for Target Tracking," *IET Signal Processing*, 4, 5, 530-536.